Division of Pharmaceutical Chemistry and Technology
Faculty of Pharmacy
University of Helsinki
Finland

# INSIGHTS INTO PARTICLE FORMATION AND ANALYSIS

by

Jenni Pessi

ACADEMIC DISSERTATION

To be presented, with the permission of the Faculty of Pharmacy of the University of Helsinki, for public examination in Auditorium 2, Infocenter Korona (Viikinkaari 11), on November 3rd 2017, at 12:00 noon.

Helsinki 2017

Supervisors

Professor Jouko Yliruusi
Division of Pharmaceutical Chemistry and Technology
Faculty of Pharmacy
University of Helsinki
Finland

Professor Edward Hæggström
Division of Material Physics
Department of Physics
University of Helsinki
Finland

Professor Anne Juppo
Division of Pharmaceutical Chemistry and Technology
Faculty of Pharmacy
University of Helsinki
Finland

Reviewers

Professor Jukka Rantanen
Department of Pharmaceutics and Analytical Chemistry
University of Copenhagen
Denmark

Ph.D. (Pharm.) Juha Kiesvaara
Orion Pharma
Finland

Opponent

Professor João Pinto
The Department of Galenic Pharmacy and
Pharmaceutical Technology
Faculty of Pharmacy
University of Lisbon
Portugal


ISBN 978-951-51-3679-4 (Paperback)
ISBN 978-951-51-3680-0 (PDF)
ISSN 2342-3161 (Print)
ISSN 2342-317X (Online)

Hansaprint Oy
Turenki 2017

# ABSTRACT

Pessi J., 2017, **Insights into particle formation and analysis.**

Dissertationes Scholae Doctoralis Ad Sanitem Investigandam Universitatis Helsinkiensis, 52/2017, pp. 78
ISBN 978-951-51-3679-4 (Paperback), ISBN 978-951-51-3680-0 (PDF, http://ethesis.helsinki.fi),
ISSN 2342-3161 (Print), ISSN 2342-317X (Online)

This thesis consists of two parts, particle formation and analysis. In the first part, particle formation in microfluidic devices and in devices employing supercritical fluids is investigated, and in the second part, essential issues in analytical methods for determining drug release and solid-state properties are addressed.

Microfluidic technology was employed to produce microcapsules for protein formulations. The microcapsules were produced with a biphasic flow to create water-oil-water double emulsion droplets with ultrathin shells. All the particles were found to be intact and with a particle size of 23 - 47 μm. The encapsulation efficiency of bovine serum albumin in the microcapsules was 84%. This study demonstrates that microfluidics is a powerful technique for engineering formulations for therapeutic proteins.

A new, robust, stable, and reproducible method based on expansion of supercritical solutions using carbon dioxide as a solvent was developed to produce nanoparticles. The method, Controlled Expansion of Supercritical Solution (CESS), uses controlled mass transfer, flow, pressure reduction, and particle collection in dry ice. CESS offers control over the crystallization process as the pressure in the system is reduced according to a specific profile. Controlled pressure reduction keeps the particle growth and production process stable. With CESS, we produced piroxicam nanoparticles, 60 mg/h, featuring narrow size distribution (176 ± 53 nm).

The Lyophilic Matrix (LM) method was developed for investigating dissolution rates of nanoparticles, powders, and particulate systems. The LM method is based on its ability to discriminate between non-dissolved particles and the dissolved species. In the LM method, the test substance is embedded in a thin lyophilic core-shell matrix. This permits rapid contact with the dissolution medium while inhibiting dispersion of non-dissolved particles without presenting a substantial diffusion barrier. By minimizing method-induced effects on the dissolution profile of nanopowders, the LM method overcomes shortcomings associated with current dissolution tests.

Time-gated Raman spectroscopy was applied for solid-state analysis of fluorescent powder mixtures. A setup with a 128 × (2) × 4 CMOS SPAD detector was used for the quantitative analysis of solid-state forms of piroxicam. Time-gating provides an instrumental method for rejecting the fluorescence signal. This study demonstrated that traditional PLS analysis of time-gated Raman spectra resulted in mean RMSE of 4.1%. The time-gated Raman spectroscopy method shows potential for relatively routine quantitative solid-state analysis of photoluminescent pharmaceuticals.

# ACKNOWLEDGEMENTS

I would like to express my gratitude to all who have contributed to this thesis. This work would not have been possible without the help, encouragement, and guidance of several people.

The research presented in this thesis was carried out at the Division of Pharmaceutical Chemistry and Technology and at the Division of Material Physics at the University of Helsinki and at the School of Engineering and Applied Sciences at Harvard University during the years 2013-2017. I would like to acknowledge the founding sources, the Finnish Funding Agency for Innovation (Tekes) and the University of Helsinki Doctoral Programme in Drug Research.

I am immensely grateful to my supervisors, Professor Jouko Yliruusi, Professor Edward Hæggström, and Professor Anne Juppo. I feel fortunate to have been supervised by three inspiring professors. Furthermore, I would like to thank Associate Professor Clare Strachan for the chance to work with Raman spectroscopy and for the language revision of this thesis.

I am indebted to the preliminary examiners of this dissertation, Professor Jukka Rantanen and Doctor Juha Kiesvaara, for taking the time to review my thesis, and to Professor João Pinto for agreeing to be the opponent.

Moreover, I would like to express my gratitude to all my co-authors for sharing their knowledge and expertise with me. It has been a privilege to work with such talented people. I wish to extend my gratitude to all my colleagues at the Division of Pharmaceutical Chemistry and Technology, at the Electronics Research Laboratory, at Weitz lab, and at Nanoform Finland Ltd.

Finally, I would like to thank my friends, my family, for all the support and raucous laughter.

Helsinki, September 2017

Jenni Pessi

# CONTENTS

# LIST OF ORIGINAL PUBLICATIONS

This thesis is based on the following publications:

I **Pessi J**, Santos HA, Miroshnyk I, Weitz DA, Mirza S. Microfluidics-assisted engineering of polymeric microcapsules with high encapsulation efficiency for protein drug delivery. *International Journal of Pharmaceutics*. 2014; 472(1): 82-87.

II **Pessi J**, Lassila I, Meriläinen A, Räikkönen H, Hæggström E, Yliruusi J. Controlled Expansion of Supercritical Solution: a robust method to produce pure drug nanoparticles with narrow size-distribution. *Journal of Pharmaceutical Sciences*. 2016; 105(8): 2293-2297.

III **Pessi J***, Svanbäck S*, Lassila I, Hæggström E, Yliruusi J. Lyophilic matrix method for dissolution and release studies of nanoscale particles. *Journal of Pharmaceutical and Biomedical Analysis*. 2017; 145: 549-554.

IV Lipiäinen T*, **Pessi J***, Movahedi P, Koivistoinen J, Kurki L, Tenhunen M, Yliruusi J, Juppo AM, Heikkonen J, Pahikkala T, Strachan CJ. Time-gated Raman spectroscopy and quantitative determination of solid-state forms of fluorescent pharmaceuticals. Manuscript.

The publications are referred to by their roman numerals. Papers I-III are reprinted with the kind permission of Elsevier. In publications III and IV, the first two authors contributed equally to the work (*).

In addition, unpublished material regarding dissolution rate and crystal form evaluation of the nanoparticles produced with CESS, referred as new data in the text, is presented.

# ABBREVIATIONS AND SYMBOLS

| | |
|---|---|
| A | Surface area |
| $A_1$ | Flow area |
| $\alpha_C$ | Condensation coefficient |
| ACN | Acetonitrile |
| API | Active pharmaceutical ingredient |
| ASES | Aerosol Solvent Extraction System |
| a.u. | Arbitrary unit |
| β | Differential Raman cross section |
| β1 | Coagulation coefficient |
| BCS | Biopharmaceutical Classification System |
| BSA | Bovine serum albumin |
| C | Concentration |
| $C_s$ | Saturation solubility |
| CAN-BD | Carbon dioxide Assisted Nebulization with a Bubble Dryer |
| CESS | Controlled Expansion of Supercritical Solution |
| $CHF_3$ | Fluoroform |
| CMOS SPAD | Complementary metal-oxide semiconductor single-photon avalanche diode |
| $CO_2$ | Carbon dioxide |
| d | Diffusion layer thickness |
| D | Diffusion coefficient |
| $D_0$ | Number of molecules per $cm^3$ |
| δ | Delta function (accounting for the particle formation by homogenous nucleation) |
| DSC | Differential scanning calorimetry |
| EE | Encapsulation efficiency |
| e.g. | *exempli gratia* (for example) |
| FITC | Fluorescein isothiocyanate |
| FTIR | Fourier transform infrared spectroscopy |
| $\Delta G_{crit}(kT)^{-1}$ | Reduced Gibbs energy |
| Δpv | Pressure drop |
| GAS | Gas Anti-Solvent |
| $G_n$ | Condensation rate |
| h | Specific enthalpy |
| i.e. | *id est* (that is) |
| Θ | Non-isothermal factor |
| $H_3PO_4$ | Ortophosphoric acid |
| HPLC | High performance liquid chromatography |
| HPMC | (Hydroxypropyl)methyl cellulose |

| | |
|---|---|
| J | Nucleation rate |
| k | Boltzmann's constant |
| $k_1$ | A constant |
| K | Geometric factor |
| l | Characteristic length |
| L | Specific intensity of the Raman scattering |
| LM | Lyophilic matrix |
| m | Mass |
| $m_2$ | Molecular mass |
| μ | Dynamic viscosity |
| MH | Monohydrate |
| n | Particle distribution function |
| o/w/o/w | Oil - in water - in oil - in water |
| p | Pressure |
| $p_2$ | Partial pressure of the solute |
| $p_{2,\,sub}$ | Saturation vapor pressure of the solute |
| PCA | Precipitation with Compressed Anti-solvents |
| PCL | Polycaprolactone |
| $P_D$ | Power density of the incident laser light |
| PDMS | Polydimethylsiloxane |
| PEG | Polyethylene glycol |
| PEI | Poly(ethyleneimine) |
| PGSS | Particles from Gas-Saturated Solutions |
| Ph.Eur. | European Pharmacopoeia |
| PLGA | Poly(lactic-co-glycolic acid) |
| PLS | Partial least squares regression |
| PVA | Poly(vinyl alcohol) |
| PVP | Poly(vinylpyrrolidinone) |
| q | Specific heat |
| $Q^2$ | Predictive ability of the model |
| $R^2$ | Correlation coefficient |
| ρ | Density |
| RESS | Rapid Expansion of Supercritical Solutions |
| RESAS(S) | Rapid Expansion of Supercritical Solutions to Aqueous Solution |
| RESOLV | Rapid Expansion of Supercritical Solutions into a liquid solvent |
| RESS-N | Rapid Expansion of Supercritical Solutions with a Non-solvent |
| RESS-SC | Rapid Expansion of Supercritical Solutions with Solid Co-solvent |
| RMSE | Relative root mean square error |
| RMSEE | Relative root mean square error of estimation |
| RMSECV | Relative root mean square error of cross validation |

| | |
|---|---|
| RMSEP | Relative root mean square error prediction |
| S | Supersaturation |
| $\sigma$ | Surface tension |
| $\sigma_1$ | Interfacial tension of the solute |
| SA | Sodium alginate |
| SAA | Supercritical Assisted Atomization |
| SAILA | Supercritical Assisted Injection in a Liquid Anti-solvent |
| SAS | Supercritical Anti-Solvent |
| $scCO_2$ | Supercritical carbon dioxide |
| SDS | Sodium dodecyl sulfate |
| SEDS | Solution Enhanced Dispersion by Supercritical Fluids |
| SEM | Electron scanning microscopy |
| SFEE | Supercritical Fluid Extraction of Emulsions |
| SNV | Standard normal variate |
| t | Time |
| T | Temperature |
| TFA | Trifluoroacetic acid |
| u | Speed |
| USP | United States Pharmacopoeia |
| $\Phi_2$ | Solute fugacity coefficient |
| $v_2$ | Number concentration of solved molecules |
| $v_{2,s}$ | Molecular volume of the solid phase |
| V | Particle volume |
| $V^*$ | Any other particle volume |
| $V_2$ | Molecular volume |
| $V_{crit}$ | Volume of the critical nucleus |
| $y_{2,E}(T_E,p_E)$ | Mole fraction of the solute at post-expansion temperature and pressure |
| $y^*_2(T, p)$ | Equilibrium mole fraction of the solute at the extraction temperature and pressure |
| w/o/w | Water - in oil - in water |
| w | Weight |
| x | Length |
| XRPD | X-ray powder diffractometry |

# 1 INTRODUCTION

Particle technologies are used to increase bioavailability of active pharmaceutical ingredients (APIs) in drug formulations and to enhance the properties of the formulations. For example, compounds with poor water-solubility or protein structures require sophisticated formulations to provide adequate bioavailability and therapeutic effect (Zhou, 1994, Merisko-Liversidge *et al.*, 2003). Analyzing these kinds of formulations is often challenging due to limitations of current analytical methods.

This thesis consists of two parts, particle formation and analysis. In the first part particle formation in microfluidic devices and in devices employing supercritical fluids is investigated. In the microfluidic devices, the particles are formed drop-by-drop, whereas in the supercritical devices the aim is to form large quantities of particles at once by homogeneous nucleation (Martín and Cocero, 2008, Utada *et al.*, 2007b).

Development of protein-based formulations requires particle technologies for producing drug carrier systems (Langer, 1998). Polymeric microcapsules hold great potential as delivery systems for oral protein delivery (Freiberg and Zhu, 2004). Microfluidics has advantages for the preparation of polymeric microcapsules since the technology allows precise control of the fabrication process (Umbanhowar *et al.*, 2000, Utada *et al.*, 2005).

Poorly water-soluble APIs in group II of the Biopharmaceutical Classification System (BCS) benefit from particle technologies that reduce particle size and increase the active surface area (Amidon *et al.*, 1995). Decreasing particle size is an effective way to improve dissolution rate, solubility, and consequently the bioavailability of poorly water-soluble APIs (Merisko-Liversidge and Liversidge, 2008). Many (40-70%) new potential drug molecules belong to BCS group II, and thus there is a demand in the pharmaceutical industry for efficient particle technologies capable of particle size reduction (Cooper, 2010, Lipinski, 2002).

Particle technologies based on supercritical carbon dioxide ($scCO_2$) offer efficient, inexpensive, and ecological methods for production of small particles (Fages *et al.*, 2004). Particle preparation methods based on $scCO_2$ are bottom-up methods and the particles are formed by recrystallization (Sun, 2002). The production is possible with a one-step preparation process and the particles are pure, and the obtained polymorph can be controlled assuming adequate energy differences between crystal forms of an API (York, 1999, Pasquali *et al.*, 2008).

In the second part of this thesis, essential issues in analytical methods for determining drug release and solid-state properties of particles are addressed. The dissolution rate and the solid-state form of an API are primary physicochemical properties to be determined and modified during drug discovery and development (Vippagunta *et al.*, 2001, Dokoumetzidis and Macheras, 2006).

The dissolution rates of the nanoscale particles reflect the performance and quality of the formulation especially in formulations where nanoparticles are used (Merisko-Liversidge and Liversidge 2008). Thus, to assess the impact of nanosizing, it is vital to produce reliable dissolution rate data of the nanoparticulate system. Dissolution testing became an essential tool for formulation research and development, manufacturing, and storing as the correlation between *in vitro* dissolution and bioavailability was established (Brown *et al.*, 2004, Edwards, 1951, Nelson, 1957). Dissolution rate data produced with reliable test methods agrees with *in vivo* data, facilitates adjustment of doses for animal experiments, and provides means for quality control (Cohen, Hubert *et al.* 1990, Jünemann and Dressman 2012). Current methods for investigating dissolution rates were not designed for dissolution studies of nanoparticles, powders, and particulate systems and thus produce results that do not predict the dissolution behaviour *in vivo* (Heng, Cutler *et al.* 2008).

Most (90%) APIs crystallize as solid particles, in which particular inter- and intra-molecular bonding results in different solid-state forms having different physicochemical properties (Vippagunta *et al.*, 2001, Haleblian and McCrone, 1969, Gupta and Kompella, 2006). Dissolution rate, equilibrium solubility, stability, and bioavailability among other properties depend on the solid-state of the API. Effective methods for evaluating possible alterations in the solid-state of polymorphic and solvate systems during research and development, manufacturing, and storage are needed (Brittain, 1997, Wartewig and Neubert, 2005). Raman spectroscopy permits qualitative and quantitative analysis of APIs exhibiting different solid-state forms (Strachan *et al.*, 2004, Das and Agrawal, 2011). One of the main issues encountered especially in the quantitative analysis of APIs and excipients with Raman spectroscopy is photoluminescence. While the other issues can generally be addressed with suitable data analysis, complete subtraction of fluorescence without any instrument-based means is difficult even with sophisticated algorithms (Jestel 2005). Subtracting the fluorescence signal from the Raman signal is possible with time-resolved techniques (Fishburn 2012). The ability to detect the arrival time and energy of each photon allows assessing the lifetime of both the fluorescence and Raman signals (Patounakis, Shepard *et al.* 2006).

# 2 REVIEW OF THE LITERATURE

## 2.1 PARTICLE PRODUCTION WITH MICROFLUIDICS

### 2.1.1 DROPLET-BASED MICROFLUIDICS

Microfluidic techniques permit mixing of immiscible fluids with precise control to form single, double, and multiple emulsions through a single-step emulsification (Squires and Quake, 2005). The microfluidic approach allows production of three-dimensional flows (Utada *et al.*, 2005). This makes precise manufacturing possible and gives control over droplet formation. Specifically, monodisperse droplets of desired structure and size can be created by adjusting the process and formulation variables (Whitesides and Stroock, 2001). To create polymeric microcapsules, emulsions containing polymers in organic solvents as the oil phase of the droplets are produced as templates for microcapsule formation (Datta *et al.*, 2014).

### 2.1.2 MICROFLUIDIC DEVICES

Different geometries have been employed to create the flows used in the microfluidic devices: T-junctions, cross-junctions, flow-focusing, and co-flowing systems (Zhang and Liu, 2012). The glass capillary devices employ the latter two (Utada *et al.*, 2007a). Microfluidic devices can be manually manufactured out of glass capillaries (Duncanson *et al.*, 2012a, Chu *et al.*, 2007, Shum *et al.*, 2011, Kim *et al.*, 2011) or be machine-manufactured (e.g. by lithography of polydimethylsiloxane (PDMS) (Xia and Whitesides, 1998). This literature review concentrates on the glass capillary devices as polymer particle production requires use of volatile organic solvents as the oil phase and for example, PDMS devices swell if such an oil phase is used (Lee *et al.*, 2003).

Glass capillary devices consist of square and circular shaped capillaries (Utada *et al.*, 2007a). The tips of the circular capillaries are heated, pulled and sanded into tapered tips with desired diameter. The devices for multiple emulsions contain two or more circular capillaries that can be placed one within another or facing each other with the tips carefully aligned. Microfluidic devices can employ coaxial flow, hydrodynamic flow focusing, or a combination of these two (**Figure 1**). With the simplest co-flow design one fluid flows on the outside of the circular capillary through the square capillary, whereas the other flows through the inner circular capillary (Umbanhowar *et al.*, 2000). The resulting coaxial flow of the two fluids easily forms drops. The alternative to co-flow is flow-focusing of the inner fluid by the outer fluid (Gañán-Calvo and Gordillo, 2001). The outer fluid is introduced into the

device as in the co-flow device, yet the inner fluid is introduced from the opposite side, and both fluids are collected, and exit through the cylindrical capillary. The process resembles the co-flow device design, but one fluid flows in the opposite direction and is hydrodynamically focused through the narrow orifice by the outer fluid. This method produces a stream that is narrower than the diameter of the orifice. By combining co-flow and flow-focusing, the preparation of complex materials is possible (Utada *et al.*, 2005). The designs of these devices are more complicated and accurate alignment of the tapered capillaries is required. Furthermore, the desired number of layers can be added to the procedure by repeating the flow-focusing and co-flow parts to the devices (Chu *et al.*, 2007, Wang *et al.*, 2011). However, the more complex the emulsion structure, the more control is needed for the process to succeed (Utada *et al.*, 2007b).

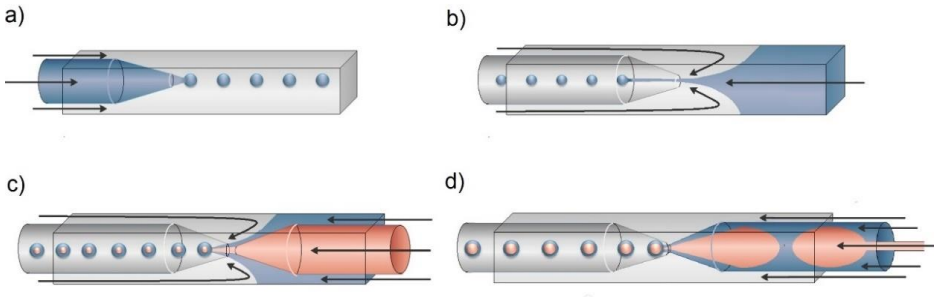


**Figure 1** a) Co-flow microcapillary device for producing single emulsion droplets, b) a flow-focusing microcapillary device for making single emulsion droplets, c) device that combines co-flow and flow-focusing creating double emulsion droplets, and d) biphasic flow for production of double emulsion droplets with thin shells (adapted from Shah *et al.*, 2008 and Kim *et al.*, 2011).

### 2.1.3 DROPLET FORMATION IN MICROFLUIDIC DEVICES

As one liquid is introduced into another liquid and these two liquids are immiscible, a jet and ultimately drops of a certain diameter are formed (Scheele and Meister, 1968, Tyler, 1933, Meister and Scheele, 1969). Jetting transforming into dripping is caused by the Rayleigh–Plateau instability (Rayleigh, 1879, Plateau, 1873). When perturbations in a jet occur, thinner regions are formed and the internal pressure in these regions is increased (Plateau, 1873, Rayleigh, 1879, Tyler, 1933). The consequent differential pressure of a curved surface on the jet causes thin parts of the jets to become thinner. This differential pressure, the Laplace pressure, causes the fluid within the jet to push to regions of lower pressure and eventually, the jet turns into drops separated by a certain interval (Tyler, 1933). Droplet formation in glass capillary microfluidic devices is based on this jetting to dripping transition caused by hydrodynamic instability (Powers *et al.*, 1998).

In microfluidic devices, droplet formation is influenced by the viscous drag of the coaxial fluid and by surface tension forces (Scheele and Meister, 1968, Umbanhowar *et al.*, 2000). Surface tension drives the forming droplet away from the thinner region of the jet and viscous drag of the fluid that resists this flow. At the break-off point of the jet, the forming droplet is pulled further downstream by the coaxial outer fluid. The location of the break-off point in the jet depends on the Laplace pressure and on the downstream velocity of the interface; how fast the droplet is filled up and how fast it is pulled further downstream (Meister and Scheele, 1969, Scheele and Meister, 1968).

Two classes of jetting-to-dripping phenomena exist (Umbanhowar *et al.*, 2000). The first phenomenon depends on the drop being pulled further downstream. The coaxial outer fluid can thus be used to chop the droplet from the jet. The second phenomenon depends more on the filling of the droplet. The droplet is filled as the inner fluid flows significantly faster than the outer fluid and the viscous drag is small. The inertial force of the fluid must overcome the surface tension forces and thus droplets are formed. A simple model for predicting droplet formation in a co-flowing system applicable to droplet formation in glass capillary devices is presented by Utada *et al.* (2007b). The following principles of droplet formation apply to immiscible, Newtonian fluids, in laminar flow, where the effect of gravity is negligible. The relevant dimensionless numbers for droplet formation in immiscible liquids with low Reynolds numbers are the capillary number and the Weber number (Zhang and Liu, 2012, Utada *et al.*, 2007b).

The break-off of the droplet occurs when the sum of the capillary number of the outer fluid and the Weber number of inner fluid is approximately equal to 1 (Utada *et al.*, 2007b). This does not apply when the capillary number of the outer fluid is small. The capillary number is the balance between the drag of the outer fluid and the surface tension forces (**Equation 1**) (Zhang and Liu, 2012).

(**1**) $$Ca = \frac{\mu u}{\sigma}$$

Here, $\mu$ is the dynamic viscosity, $u$ is speed and $\sigma$ is the surface tension. The Weber number is the balance between inertial and surface tension forces (**Equation 2**) (Zhang and Liu, 2012).

(**2**) $$We = \frac{\rho u^2 l}{\sigma}$$

Here, $l$ is the characteristic length and $\rho$ is the density.

When manufacturing complex droplets, polymeric capsules, and structures based on multiple emulsions, the process contains several droplet formation occurrences each of which can be either dripping or jetting. By adjusting these occurrences individually, different droplet structures can be created (Shah *et al.*, 2008). Control of and knowledge about the dripping-to-jetting transition

in microfluidic devices allow control over the droplet formation and permits creation of different kinds of structures (Utada *et al.*, 2007a). Drop formation in microfluidic devices has also been modeled numerically, and the results agreed with the experiments (Vladisavljević *et al.*, 2014)

### 2.1.4 PRODUCTION OF POLYMERIC MICROCAPSULES WITH MICROFLUIDICS

Preparation of polymeric microcapsules requires at least a water-in-oil-in water (w/o/w) double emulsion, where the substance to be encapsulated in the microcapsule is in the inner phase and the polymer forming the capsule shell is the middle phase (Datta *et al.*, 2014). A microfluidic device can introduce the middle phase from the opposite site as flow-focusing in the square capillary or as biphasic co-flow together with the inner phase from a circular capillary (Utada *et al.*, 2005, Kim *et al.*, 2011). The latter approach permits production of ultra-thin polymer shells (Kim *et al.*, 2011). The surfaces of the capillaries in double emulsion production are often coated with a hydrophilic coating to prevent wetting of the middle oil phase on the capillary wall (Datta *et al.*, 2014). Droplet formation in multiple emulsions occurs as described earlier and the droplet properties are determined by the manner of introducing the phases into the microfluidic device, by the content of the phases, and by the flow rates (Shah *et al.*, 2008, Datta *et al.*, 2014). The microfluidic technology permits the chemical compositions and structures of the prepared particles to be chosen independently (Duncanson *et al.*, 2012b).

The composition of the phases in polymeric microparticle production is as follows; the inner aqueous phase carries the substance to be encapsulated and any surface-active agent necessary to prevent the liquid interfaces from coalescing, as well as a thickener necessary to increase the viscosity of the phase. The mid phase, an organic solvent, carries the shell material whereas the outer aqueous phase contains a surfactant (Datta *et al.*, 2014). The droplet size and the shell thickness are controlled by adjusting the viscosities of the phases and the flow rates used in the preparation process (Vladisavljevic´ *et al.*, 2012). Furthermore, balancing the densities and viscosities of the inner and mid phase is essential for production of even polymeric shells (Datta *et al.*, 2012). Evaporation the organic solvent out of the middle phase from the collected droplets causes the formation of the polymeric shells and shrinking of the particles (Vladisavljevic´ *et al.*, 2012).

A specific microfluidic application for producing thin-shelled microcapsules is a device employing biphasic flow of the inner and the middle phase (Kim *et al.*, 2011). The middle phase is evenly distributed along the inner phase, and the thickness of the phase can be on a submicron scale. Additionally, this is a beneficial approach when viscous phases are used, since disruption of the flow of the middle phase is reduced. With this application, middle phases containing for example 1 wt% sorbitan oleate hexadecane (Kim

*et al.*, 2011), 1 - 5% of sorbitan oleate in hexane or hexadecane (Zhao *et al.*, 2017), 4.6 mg/mL of 1,2-dioleyl-sn-glycero-3-phosphocholine in a mix of chloroform and hexane (1 : 1.8) (Herranz-Blanco *et al.*, 2014), 5 wt% tetraglycerin-condensed ricinoleic acid ester in decane (Saeki *et al.*, 2010), 35 mol% 1,2-dioleyl-sn-glycero-3-phosphocholine, 35 mol%, 1,2-dipalmitoyl-sn-glycero-3-phosphocholine and 30 mol% cholesterol, in a mix of chloroform and hexane (1 : 1.8) (Arriaga *et al.*, 2014), and the middle oil phase, a solution of 20 wt% Krytox-polyethylene glycol-Krytox dissolved in a perfluorinated oil (Arriaga *et al.*, 2015), have been used. Thin shells can be manufactured with oils in the PDMS devices (Saeki *et al.*, 2010, Arriaga *et al.*, 2015). Thin shell formation has been successfully modeled with the volume of fluid - continuum surface force numerical model (Nabavi *et al.*, 2015).

Production of an oil-in water-in oil-in water (o/w/o/w) triple emulsion drop system with a thin water layer under the polymeric capsule shell is possible by adding a flow-focusing element to a device employing co-flowing biphasic flow (Choi *et al.*, 2016). Polymer particles with more complex structures can be manufactured with microfluidic devices. The quantity of the inner phases and co-encapsulation of different droplets has been varied with numerous applications to produce controllable multicomponent multiple emulsions (Wang *et al.*, 2014, Adams *et al.*, 2012). Besides repeating the structures of the device to obtain multiple emulsions, it is possible to fabricate one-step emulsification of multiple concentric shells capillary microfluidic devices (Kim and Weitz, 2011). Moreover, hollow polymer capsules have been prepared (Liu *et al.*, 2009). Additional elements such as size-tunable pores and tunable active release mechanisms can be added to the microparticles prepared as emulsion droplets by microfluidics (Duncanson *et al.*, 2012c, Abbaspourrad *et al.*, 2013). Stimuli-responsive microcapsules that selectively release their contents through head-to-tail depolymerization of poly(phthalaldehyde) have been prepared (DiLauro *et al.*, 2013) and double emulsion drops for acoustically-triggered release with perfluorohexane shells have been produced (Duncanson *et al.*, 2014). A variety of polymersomes, vesicles with a membrane composed of a bilayer of amphiphilic block-co-polymers (Discher *et al.*, 1999), have been prepared with the glass capillary devices: multi-compartment polymersomes for both storing multiple drugs in a single carrier and enabling simultaneous release of two active agents (Zhao *et al.*, 2011), polymersomes with hydrogel cores and induced UV-polymerization (Kim *et al.*, 2013) and polymersomes for triggered release using photo- and thermo-sensitive polymers (Amstad *et al.*, 2012).

## 2.2 PARTICLE PRODUCTION WITH SUPERCRITICAL CARBON DIOXIDE

### 2.2.1 SUPERCRITICAL FLUIDS

A supercritical fluid is a substance that exists above its critical point. The critical point of a pure substance, defined by pressure and temperature, is the point after which the vapour phase and the liquid phase merge to form a single homogeneous phase (Smith *et al.*, 2013). It is the termination point of the vapour-liquid equilibrium meaning that it is the highest possible temperature and pressure defined condition where vapour and liquid can coexist. The matter at the critical point is opalescent indicating the phase transition; infinitely high compressibility and density fluctuations cause the opalescence (Poliakoff and King, 2001). The exact pressure and temperature values of the critical point depend on the substance in question (Pereda *et al.*, 2008).

The supercritical phase has liquid-like density and solvent properties, gas-like viscosity, diffusivity, and compressibility, and low surface tension (McHugh and Krukonis, 1986). These properties enable particle formation with supercritical fluids. The ability of matter to solute solids above its critical point was discovered in 1879 (Hannay and Hogarth, 1879). The solvent power of the supercritical phase depends on its density, which is a function of temperature and pressure (McHugh and Krukonis, 1986). In the supercritical region, especially near the critical point, small changes in pressure or temperature significantly affect the density and thus the solvent properties of the phase.

Carbon dioxide ($CO_2$) is the most common solvent in supercritical processes since its critical temperature and pressure are relatively low, 73.9 bar and 31.1°C (McHugh and Krukonis, 1986) (**Figure 2**). The density of $CO_2$ at the critical point is 0.467 g/cm$^3$ (Smith *et al.*, 2013). $CO_2$ is an attractive alternative as a supercritical fluid since it is non-toxic, non-flammable, and 'Generally Recognized As Safe' (GRAS) by the FDA (Panza and Beckman, 2004, Pereda *et al.*, 2008). Additionally, $CO_2$ is environmentally benign when compared to organic solvents, and thus technologies using $CO_2$ can be considered 'green chemistry' (Panza and Beckman, 2004).

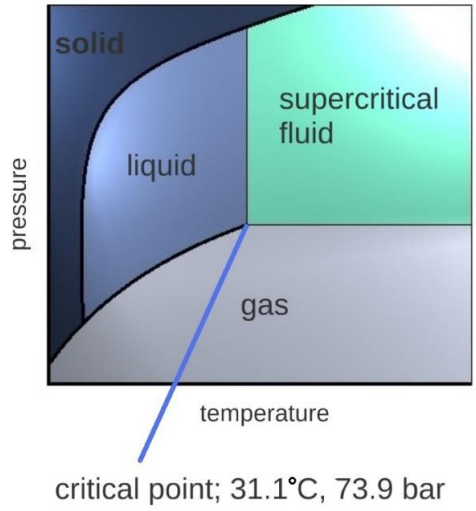


**Figure 2** Phase diagram of carbon dioxide.

### 2.2.2 PARTICLE PRODUCTION TECHNIQUES BASED ON SUPERCRITICAL CARBON DIOXIDE

Supercritical fluids were initially used for particle formation in the 1980s (Matson *et al.*, 1987, Smith and Wash, 1986). Nowadays supercritical fluid technology is important for particle manufacturing of micron and submicron particles (Gupta, 2006). Particle technologies based on supercritical fluids are bottom-up techniques meaning that the particles form by recrystallization (Meziani *et al.*, 2008). Particle formation is possible due to enhanced mass transfer caused by the high diffusivity of the solute in the supercritical fluid and by the ability to alter the solubility of the solute even with small changes in the density of the supercritical fluid (McHugh and Krukonis, 1986).

Several techniques employing $scCO_2$ have been developed. Particle production techniques employ $scCO_2$ as a solvent, as a solute, as anti-solvent, and as a propellant (Pasquali *et al.*, 2008, Türk, 2014) (**Table 1**). Technologies can be used to produce pure drug particles, cocrystals, polymer particles, and polymeric microcapsules (Yeo and Kiran, 2005, Türk, 2014, Meziani *et al.*, 2008).

**Table 1** *Particle production based on $scCO_2$, abbreviation, name of the method, and the role of $scCO_2$ in the process. Patented technologies are marked with an asterisk (*).*

| Abbreviation | Method | Role of $scCO_2$ | Reference |
|---|---|---|---|
| RESS * | Rapid Expansion of Supercritical Solutions | solvent | (Matson *et al*., 1987, Smith and Wash, 1986) |
| RESOLV/ RES(S)AS | Rapid Expansion of Supercritical Solutions into a liquid SOLVent / to Aqueous Solution | solvent | (Chang and Randolph, 1989) |
| RESS-SC | Rapid Expansion of Supercritical Solutions with Solid Co-solvent | solvent | (Thakur and Gupta, 2005) |
| RESS-N | Rapid Expansion of Supercritical Solutions with a Non-solvent | solvent | (Matsuyama *et al*., 2001) |
| SAS * | Supercritical Anti-Solvent | anti-solvent | (Fischer and Muller, 1991) |
| GAS * | Gas Anti-Solvent | anti-solvent | (Krukonis *et al*., 1994) |
| ASES * | Aerosol Solvent Extraction System | anti-solvent | (Bleich *et al*., 1993, Debenedetti *et al*., 2000) |
| SEDS * | Solution Enhanced Dispersion by Supercritical Fluids | anti-solvent | (Hanna and York, 2000) |
| PCA | Precipitation with Compressed Anti-solvents | anti-solvent | (Dixon *et al*., 1993) |
| SFEE | Supercritical Fluid Extraction of Emulsions | anti-solvent | (Chattopadhyay *et al*., 2006) |
| PGSS * | Particles from Gas-Saturated Solutions | solute | (Graser and Wickenhaeuser, 1984) |
| CAN-BD * | Carbon dioxide Assisted Nebulization with a Bubble Dryer | solute | (Sievers and Karst, 1997) |
| DELOS | Depressurization of an Expanded Liquid Organic Solution | co-solvent / solute | (Ventosa *et al*., 2001) |
| SAA * | Supercritical Assisted Atomization | propellant | (Reverchon and Della Porta, 2014, Reverchon, 2002) |
| SAILA | Supercritical Assisted Injection in a Liquid Anti-solvent | propellant | (Campardelli *et al*., 2012) |

Rapid Expansion of Supercritical Solutions (RESS) and its modifications use $scCO_2$ as a solvent; particles are formed as the supercritical fluid expands through a nozzle, solvent power is decreased, and precipitation occurs (Matson *et al*., 1987, Smith and Wash, 1986, Hanna and York, 1993). With techniques employing $scCO_2$ as an anti-solvent, Supercritical Anti-Solvent (SAS) (Fischer and Muller, 1991), Gas Anti-Solvent (GAS) (Krukonis *et al*.,

1994), Aerosol Solvent Extraction System (ASES) (Bleich *et al.*, 1993, Debenedetti *et al.*, 2000), Solution Enhanced Dispersion by Supercritical Fluids (SEDS) (Hanna and York, 2000), Precipitation with Compressed Anti-solvents (PCA) (Dixon *et al.*, 1993), and Supercritical Fluid Extraction of Emulsions (SFEE) (Chattopadhyay *et al.*, 2006) the solvent phase is an organic solvent, and $scCO_2$ is mixed with the solvent/solute mixture to decrease the solubility of the solute and cause precipitation.

Especially with techniques using $scCO_2$ as anti-solvent, the categorization of the techniques varies greatly between review articles. The categorization depends on the emphasis of the essential feature of the device used. For example, GAS and SAS can considered one technique, and ASES and SEDS as similar techniques that have been patented separately on the basis of the devices containing different nozzles (Jung and Perrut, 2001). Furthermore, GAS and SAS can be perceived as different techniques: GAS as a batch process and SAS as a continuous spraying process. SAS, ASES, and PCA can be perceived to be variations of the same technique (Yeo and Kiran, 2005), and other authors define GAS as a general term encompassing SAS, ASES, and PCA (York, 1999).

$ScCO_2$ can also be utilized as a solute. Particles produced by the Gas-Saturated Solutions (PGSS) technique uses rapid depressurization of $scCO_2$ dissolved in molten polymer or in liquid-suspended solutions through a nozzle to form particles by precipitation (Graser and Wickenhaeuser, 1984). In a similar technique, Carbon dioxide Assisted Nebulization with a Bubble Dryer (CAN-BD) $scCO_2$ is used both as a solute and a co-solvent (Sievers and Karst, 1997). The solute is dissolved in water and/or ethanol and mixed with $scCO_2$, and the mixture is then pumped through a small volume and microbubbles are generated. The bubbles are then decompressed into a low temperature drying chamber where the aerosol dries and particles are formed (Sievers *et al.*, 2003).

Furthermore, $scCO_2$ can be used to assist particle preparation processes as a propellant. The Supercritical Assisted Atomization (SAA) process is based on the solubilization of a controlled amount of $scCO_2$ in a liquid solvent/solute mixture; this solution is then atomized through a nozzle to produce particles. (Reverchon and Della Porta, 2014, Reverchon, 2002). Supercritical Assisted Injection in a Liquid Anti-solvent (SAILA) works similarly, except that the solution is depressurized into a water solution that acts as an anti-solvent (Campardelli *et al.*, 2012).

These particle production techniques based on $scCO_2$ are either patented as such or are derived from the existing techniques. For example, of techniques using $scCO_2$ as a solvent only RESS has been granted a patent. Rapid Expansion of Supercritical Solutions into a liquid SOLVent (RESOLV) or Rapid Expansion of Supercritical Solutions to Aqueous Solution (RESAS or RESSAS) are the same modification of RESS, where the $CO_2$ is expanded into liquid (Chang and Randolph, 1989), Rapid Expansion of Supercritical Solutions with Solid Co-solvent (RESS-SC) is a process using a solid co-solvent

in the crystallization process (Thakur and Gupta, 2005) , and Rapid Expansion of Supercritical Solutions with a Non-solvent (RESS-N) is used for coating particles with polymers (Matsuyama *et al.*, 2001). Then again, SEDS, even though derived from the ASES process, is patented as a separate technology (Hanna and York, 2000).

### 2.2.3 PARTICLE PRODUCTION WITH RESS

RESS is a solvent- and excipient-free production method (Matson *et al.*, 1987, Smith and Wash, 1986, Hanna and York, 1993). It has been used to micronize pharmaceutics and to produce nano- and submicron-size drug particles (Yasuji *et al.*, 2008, York, 1999, Fages *et al.*, 2004, Knez and Weidner, 2003).

The processes using $scCO_2$ as a solvent have been modified by changing process parameters (e.g. ultra-high pressure (Cortopassi *et al.*, 2008), nozzle construction (Domingo *et al.*, 1997, Huang and Moriyoshi, 2006), and by expanding the $scCO_2$ into a liquid environment (Chang and Randolph, 1989)). Nevertheless, since its invention, the essence of the technique is to rapidly decrease the pressure (Türk, 2014).

Since the RESS process utilizes supercritical fluid as a solvent, the process is free from organic solvents, the prepared particles are pure and contaminant-free, the obtained crystal form can be controlled and the polymorphic purity of the end-product can be assured (York, 1999, Pasquali *et al.*, 2008, Moribe *et al.*, 2008). Particle production based on $scCO_2$ as the solvent is efficient, inexpensive, and ecological. (Fages *et al.*, 2004). Additionally, RESS enables processing of heat-sensitive, thermolabile molecules. Supercritical particle production allows a one-step preparation process to be employed, which facilitates downstream processing (Fages *et al.*, 2004).

Limitations of RESS include poor solubility of some drug molecules in $scCO_2$ and lack of precise control over particle properties especially in nanoparticle production (Gupta and Shim, 2006, Türk, 2014). Solubility issues have been addressed by using a co-solvent (Meziani *et al.*, 2008). However, then the process may not be contaminant-free, and often complete removal of the co-solvent from the end-product is problematic. Added cost for particle production is caused by the elevated pressure required, high maintenance cost, and cleaning requirement of the equipment (Girotra *et al.*, 2013).

#### *2.2.3.1 Particle formation in supercritical carbon dioxide*

In RESS, the supercritical solution is expanded through a nozzle (Matson *et al.*, 1987, Smith and Wash, 1986) and the subsequent rapid decrease in solvent density reduces the solvent power causing supersaturation and particle

formation via homogeneous nucleation (Debenedetti, 1990, Martín and Cocero, 2008). The article by Helfgen *et al.*, 2003, also used as basis for outlining the particle formation in RESS in Türk 2014, describes the modeling of the flow field, as well as particle formation and growth. The study in Helfgen *et al.*, (2013) continues the research conducted in several studies Helfgen *et al.*, (2000), Helfgen *et al.*, (2001), Türk, (1999) and follows the theory in Tom and Debenedetti, (1991), Debenedetti *et al.*, (1993), Kwauk and Debenedetti, (1993). The aim of modeling the RESS process is to examine numerically the effect of process parameters (i.e. temperature, pressure, composition, flow rate and chamber dimensions) on the end-product, and to study the fluid hydrodynamic as well as the transport and growth of the formed particles. However, the numeric calculations lack accuracy, and the complete flow field is yet to be simulated (Moussa and Ksibi, 2010, Yamamoto and Furusawa, 2015).

To numerically model particle formation and growth, the flow field must be determined. The flow field has been simulated with one-dimensional (Lele and Shine, 1992, Türk, 1999, Helfgen *et al.*, 2003, Reverchon and Pallado, 1996, Weber and Thies, 2007) and two-dimensional (Liu *et al.*, 2014, Yamamoto and Furusawa, 2015, Moussa *et al.*, 2008, Franklin *et al.*, 2001, Khalil and Miller, 2004) models. The one-dimensional model describes a steady-state flow in one direction along the centerline in a capillary nozzle (Türk, 2000, Debenedetti *et al.*, 1993, Helfgen *et al.*, 2003) (**Equations 3-5**).

(**3**) $$\rho \frac{\mathrm{d}u}{\mathrm{d}x} + u\frac{\mathrm{d}\rho}{\mathrm{d}x} + \frac{\mathrm{d}A_1}{\mathrm{d}x} = 0$$

(**4**) $$u \frac{\mathrm{d}u}{\mathrm{d}x} + \frac{1}{\rho}\frac{\mathrm{d}p}{\mathrm{d}x} = -\Delta pv$$

(**5**) $$u \frac{\mathrm{d}u}{\mathrm{d}x} + \frac{\mathrm{d}h}{\mathrm{d}x} = \frac{\mathrm{d}q}{\mathrm{d}x}$$

The equations are the differential mass, momentum, and energy balance. Here, $\rho$ is density, $u$ is speed, $x$ is length, $A_1$ is flow area, $p$ is pressure, $\Delta pv$ is pressure drop, $h$ is specific enthalpy, and $q$ is specific heat. The term $\mathrm{d}A_1/\mathrm{d}x$ is zero, since $A_1$ is constant. Friction is included via the pressure drop $\Delta pV$ in the momentum and balance heat $q$, transmitted to the capillary nozzle, in the energy balance.

A more complex model of the flow field was developed using axisymmetric Navier-Stokes that takes into account more dimensions and captures changes off-axis (for example, the gradient of the thermal conditions at the nozzle exit) that were not described in 1D simulation (Yamamoto and Furusawa, 2015, Liu *et al.*, 2014). Modification of the equation of state is used to bind together

enthalpy, density, and pressure in the flow field modeling. The thermodynamic properties of the fluid flow and particle formation can be predicted, for example with the Peng–Robinson equation of state (Peng and Robinson, 1976) or Span–Wagner equation of state (Span and Wagner, 1996). Helfgen *et al.*, 2003 used a modified Peng–Robinson equation of state in their flow field model. Particle formation is modeled with a general dynamic equation (Helfgen *et al.*, 2003, Pratsinis, 1988) (**Equation 6**).

(**6**) $$\frac{\partial n}{\partial t} = J(V_{crit})\delta(V - V_{crit}) - \frac{\partial(Gn)}{\partial V} + \frac{1}{2}\int_0^V \beta(V - V^*, V)n(V - V^*, t)n(V^*, t)\mathrm{d}V^* - n(V, t)\int_0^\infty \beta(V, V^*)n(V^*, t)\mathrm{d}V^*$$

Here, $n$ is the particle distribution function, $t$ is time, $J$ is nucleation rate, $V_{crit}$ is the volume of the critical nucleus, $\delta$ is the delta function (accounting for the particle formation by homogenous nucleation), $V$ is particle volume, $V^*$ is any other particle volume, $G_n$ is the condensation rate, and $\beta_1$ is the coagulation coefficient. Nucleation is described as $J(V_{crit})\delta(V - V_{crit})$, condensation as $\partial(Gn)/\partial V$ and coagulation as $\frac{1}{2}\int_0^V \beta_1(V - V^*, V)n(V - V^*, t)n(V^*, t)\mathrm{d}V^* - n(V, t)\int_0^\infty \beta_1(V, V^*)n\ (V^*, t)\mathrm{d}V^*$. The equation can be solved with a sectional model (Moussa *et al.*, 2008) or with the method of moments (Pratsinis, 1988) as in Helfgen *et al.*, (2003) for the simulations.

The homogeneous nucleation and nucleation rate, $J$, can be calculated with **Equation 7**.

(**7**) $$J = \Theta\alpha_C V_2 v_2^2 \sqrt{\frac{2\sigma_1}{\pi m_2}} \exp\left(-\frac{\Delta G_{crit}}{k \cdot T}\right)$$

Here $\Theta$ is the non-isothermal factor (1 in dilute solutions), $\alpha_C$ is the condensation coefficient (0.1 in dilute solutions), $V_2$ is the molecular volume, $v_2$ is number concentration of solved molecules, $\sigma_1$ is the interfacial tension of the solute, $m_2$ is the molecular mass, $\Delta G_{crit}(kT)^{-1}$ is the reduced Gibbs energy, $k$ is the Bolzmann's constant, and $T$ is temperature. Particles are generated as solute precipitates and the particle formation, the creation of a single spherical particle of radius $r$, can be understood using the reduced Gibbs energy in a closed system (**Equation 8**) (Springer, 1978).

(**8**) $$\frac{\Delta G_{crit}}{k \cdot T} = \frac{4 \cdot \pi \cdot \sigma_1 \cdot r^2}{k \cdot T} - \frac{4 \cdot \pi \cdot r^3}{3 \cdot v_{2,s}}(\ln S - v_{2,s}(p - p_{2,sub})/(k \cdot T))$$

Here, $v_{2,s}$ is the molecular volume of the solid phase, $S$ the supersaturation, $p_2$ the partial pressure of the solute, and $p_{2,sub}$ the saturation vapor pressure of the solute.

$\Delta G_{crit}$ has two parts; volume free energy of the nucleus forming (decrease in chemical potential) and surface free energy (increase in chemical potential) (Springer, 1978). The variation of $\Delta G_{crit}$ and radius of the nucleus $r$ can be plotted as shown in **Figure 3** and $r$ reaches its maximum value when $\Delta G_{crit}$ = 0.

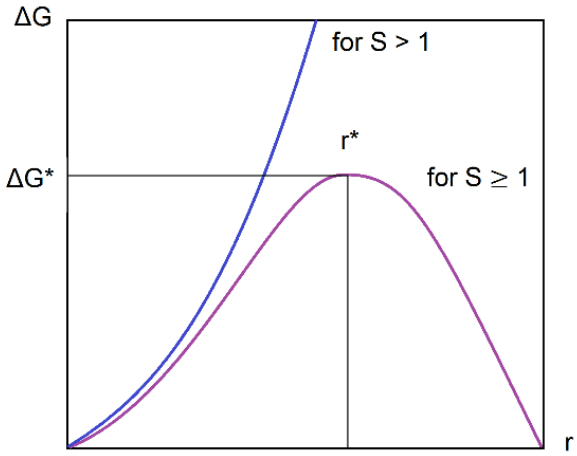


**Figure 3** Variation of the Gibbs free energy $\Delta G_{crit}$ changes with radius r at a constant degree of supersaturation and temperature. The maximum radius and corresponding variation in Gibbs free energy are marked with an asterisk (*) (adapted from Springer, 1978).

The parameter to alter in the expansion of a supercritical process is the supersaturation (**Equation 9**) (Debenedetti and Kumar, 1986).

(**9**) $$S = \frac{y_{2,E}(T_E,p_E)\cdot\phi_2(y_{2,E}(T_E,p_E))}{y_{*2}(T,p)\cdot\phi_2(y_{*2}(T,p))}$$

Here $y_{2,E}(T_E,p_E)$ is the mole fraction of the solute at post-expansion temperature and pressure, $y_{*2}(T, p)$ is the equilibrium mole fraction of the solute at the extraction temperature and pressure, and $\Phi_2$ is the solute fugacity coefficient relating the ideal gas pressure and the effective pressure of a real gas. The molar ratios determining the degree of supersaturation depend on the pre- and post-expansion pressure and temperature. A steep drop in pressure and temperature decreases the density and solvent power of $CO_2$ significantly and results in a high degree of supersaturation. The higher the degree of supersaturation, the more numerous and smaller are the formed nuclei (Debenedetti, 1990).

After nuclei formation, particles grow by two mechanisms: condensation as free molecules are deposited onto the nuclei surface, and coagulation as particles grow by colliding (Martín and Cocero, 2008, Türk, 2000). In RESS, the time available for particle growth by condensation is limited to microseconds (Weber and Thies, 2007).

The key RESS parameters that affect the end product are nozzle geometry, pre-expansion temperature and pressure, as well as the post-expansion pressure and temperature (Martín and Cocero, 2008, Palakodaty and York, 1999). In RESS, the ratio of pre-expansion to post-expansion pressures exceeds 10, the ejection velocity is sonic at the nozzle, and later supersonic (Helfgen *et al.*, 2003). The supersonic free jet ends with a Mach disk beyond which the velocities again are subsonic (Helfgen *et al.*, 2003, Türk, 2000).

Particle precipitation in the RESS process mainly takes place after the nozzle exit and in the shear layer of the jet (Liu *et al.*, 2014). The inlet pressure determines the exact location at which the particle formation begins (Yamamoto and Furusawa, 2015). The particle concentration is highest at the Mach disk and the main mechanism for particle growth is coagulation in the subsonic free jet (Helfgen *et al.*, 2001). The flow in the collection chamber of a RESS system is often complicated due to varying thermal and hydrodynamic conditions and changing density, temperature, pressure, and flow velocity. This velocity can reach 700 m/s before the Mach disk (Liu *et al.*, 2014). Particle growth is accelerated beyond the shock in the expansion jet, and thus theoretical predictions of particle size often deviate from the size of the actual particles (Yamamoto and Furusawa, 2015). The initial particle size in the RESS process has been calculated to be 5 nm - 25 nm (Weber *et al.*, 2002, Helfgen *et al.*, 2003) to 50 nm (Weber and Thies, 2007) at the nozzle. Online measurements conducted by Hermsdorf *et al.*, 2007 indicate that agglomeration and coagulation start in the Mach disc during the expansion and continue in the aerosol phase after the end of the expansion pulse.

#### *2.2.3.2 Particles produced with RESS*

Due to the conditions of the particle formation, especially particle growth by coagulation, the RESS process has been widely applied to microparticle production (Jung and Perrut, 2001). Microparticles produced with RESS have been fabricated since the 1980s and are still being produced (Müllers *et al.*, 2015, Jung and Perrut, 2001). More recently, the RESS process and its modifications have been used to produce nanoparticles (Türk *et al.*, 2002, Pathak *et al.*, 2004, Huang *et al.*, 2005, Huang and Moriyoshi, 2006, Hermsdorf *et al.*, 2007, Türk and Lietzow, 2008, Atila *et al.*, 2010, Hezave *et al.*, 2010, Kim *et al.*, 2010, Türk and Bolten, 2010, Asghari and Esmaeilzadeh, 2012, Bolten and Türk, 2012, Keshavarz *et al.*, 2012, Sabet *et al.*, 2012, Baseri and Lotfollahi, 2013, Montes *et al.*, 2013, Huang *et al.*, 2014, Paisana *et al.*, 2016, Sharma and Jagannathan, 2016). Nanoparticles have also been produced with RESS-SC (Thakur and Gupta, 2005, Thakur and Gupta, 2006, Pourasghar *et al.*, 2012, Samei *et al.*, 2012, Keshmiri *et al.*, 2015, Uchida *et al.*, 2015) and followed by collection into liquid media (RESOLV/RES(S)AS) (Dalvi *et al.*, 2013, Pathak *et al.*, 2004, Paisana *et al.*, 2016, Zabihi *et al.*, 2011, Young *et al.*, 2000, Pathak *et al.*, 2006, Pathak *et al.*, 2007).

**Table 2** introduces nanoparticles with a mean diameter of less than or equal to 500 nm produced with RESS and its modifications. The information provided about process parameters and the device has varied significantly in the literature. Nanoparticle production with RESS is not robust, repetitions on the production runs were often not performed and often the results strongly depend on small variations in the process parameters. As a result, no clear trends can be seen in the effect of the parameters on the end-product. For example, the most commonly investigated parameters: extraction pressure and extraction temperature give contradictory results. Higher extraction pressure lead to formation of larger particles in some studies (Huang *et al.*, 2014, Kim *et al.*, 2010, Pourasghar *et al.*, 2012, Sabet *et al.*, 2012) and to formation of smaller particles in others (Keshmiri *et al.*, 2015, Asghari and Esmaeilzadeh, 2012, Bolten and Türk, 2012, Dalvi *et al.*, 2013, Hezave *et al.*, 2010, Montes *et al.*, 2013, Samei *et al.*, 2012). Also, cases where both the highest and lowest extraction pressures investigated lead to formation of larger particles can be found (Zabihi *et al.*, 2011, Hirunsit *et al.*, 2005). The higher the extraction pressure, the steeper is the pressure drop and consequent higher degree of supersaturation, which leads to smaller nuclei formation (Türk, 2014). However, the extraction pressure also contributes to the concentration: a higher concentration increases the frequency of collisions and thus the particle growth by coagulation. Similarly, any increase in extraction temperature could lead to formation of larger (Hezave *et al.*, 2010, Huang *et al.*, 2014, Pourasghar *et al.*, 2012) or smaller (Asghari and Esmaeilzadeh, 2012, Bolten and Türk, 2012, Keshmiri *et al.*, 2015, Kim *et al.*, 2010, Montes *et al.*, 2013, Sabet *et al.*, 2012, Samei *et al.*, 2012) particles. The extraction temperature can imply two different effects on particle size via concentration pressure chamber; an increase in temperature decreases the density and thus the concentration, however, it also increases the solute's vapour pressure which increases the concentration (Smith *et al.*, 2013, Florence and Attwood, 2006). Contradictory results regarding the effect of nozzle diameter (decrease in particle size with wider nozzles (Asghari and Esmaeilzadeh, 2012, Huang *et al.*, 2014) and increase in particle size with wider nozzles (Kim *et al.*, 2010, Hezave *et al.*, 2010, Dalvi *et al.*, 2013)), collection distance (decrease in particle size with increased collection distance (Atila *et al.*, 2010) and increase in particle size with increased collection distance (Hezave *et al.*, 2010)), and co-solvent effect (decrease in particle size with more co-solvent (Pourasghar *et al.*, 2012) and with less co-solvent (Keshmiri *et al.*, 2015)) have also been observed.

The contradiction is not explained by any single factor caused by the parameters, for example, $CO_2$ density, and solute concentration. Issues in assessing the effect of the process parameters are most likely caused by differences in the devices used in the process. Conditions for particle growth vary, and the entire process is sensitive to flow and mass transfer dependent variation of the end-product.

Even though the RESS process is promising for nanoparticle production, the results have not always been satisfactory regarding particle size and product uniformity (Reverchon and Adami, 2006). Production rate, the quantities produced and yields are often not discussed. Many studies present results with some significantly larger (Dalvi *et al.*, 2013) or agglomerated particles (Hermsdorf *et al.*, 2007). Additionally, issues with the nanoparticle production publications include poor quality of SEM images (Huang and Moriyoshi, 2006, Huang *et al.*, 2014, Kim *et al.*, 2010, Baseri and Lotfollahi, 2013, Sabet *et al.*, 2012, Hezave *et al.*, 2010, Thakur and Gupta, 2006), questionable references (Baseri and Lotfollahi, 2013), apparently wrong XRD data, and misinterpreted Raman data (Sharma and Jagannathan, 2016) as well as presentation of the same image as two different end-products (Uchida *et al.*, 2015).

**Table 2** *Drug nanoparticles produced with RESS, RESOLV, RES(S)S, and RESS-SC. Extraction temperature (T(e)), extraction pressure (p(e)), nozzle diameter (nozzle ø), effect of co-solvent added (co-solvent), flow rate, spray distance, nozzle length, expansion temperature/nozzle temperature (T(exp), %=as%wt unless otherwise mentioned). The table first introduces the parameters the effects of which are investigated and parameters remaining constant during experiments are listed last. Abbreviations of the chemicals in the table are: bovine serum albumin (BSA), (hydroxypropyl)methyl cellulose (HPMC), polyethylene glycol (PEG), poly(ethyleneimine) (PEI), poly(lactic-co-glycolic acid) (PLGA), poly(vinyl alcohol) (PVA), poly(vinylpyrrolidone) (PVP), sodium dodecyl sulfate (SDS), sodium alginate (SA), and trifluoromethane ($CHF_3$).*

| Technique | Year | Model drug | Mean particle size | Parameters | Parameter effect on mean particle size | To be noted | Reference |
|---|---|---|---|---|---|---|---|
| RESS | 2012 | deferasirox | 0.05 µm - 5 µm | p(e): 140 bar / 170 bar / 200 bar<br>T(e): 30°C / 40°C / 45°C<br>nozzle ø: 500 µm / 900 µm / 1200 µm<br>co-solvent: none / acetone / isopropanol | p(e) ↑ size ↓<br>T(e) ↑ size ↓<br>nozzle ø ↑ size ↓<br>co-solvent added size ↓ | Clearance nozzle used | (Asghari and Esmaeilzadeh, 2012) |
| RESS | 2010 | digitoxin | 0.07 µm - 0.46 µm | T(exp): 83.18°C / 90°C / 100°C / 110°C / 116.82 °C<br>flow rate: 0.8 $mLmin^{-1}$ / 2.5 $mLmin^{-1}$ /<br>5.0 $mLmin^{-1}$ / 7.5 $mLmin^{-1}$ / 9.0 $mLmin^{-1}$<br>collection distance: 1.64 cm / 3 cm / 5 cm /<br>7 cm / 8.36 cm<br>(p(e): 100 bar; T(e): 45°C; co-solvent: 5%) | T(exp) ↑ size ↑<br>flow rate ↑ size ↓<br>collection distance ↑ size ↓ | Ethanol used as co-solvent | (Atila et al., 2010) |
| RESS | 2012 | carbamazepin | 0.43 µm - 0.9 µm | p(e): 150 bar/ 200 bar/ 250 bar/ 300 bar<br>T(e): 59.85°C/ 89.85°C/ 109.85°C | p(e) ↑ size ↓<br>T(e) ↑ size ↓ | | (Bolten and Türk, 2012) |
| RESOLV | 2013 | fenofibrate | 0.5 µm - 5 µm | p(e): 100 bar/ 200 bar<br>nozzle ø: 127 µm/ 254 µm/ 508 µm/<br>762 µm<br>nozzle length: 3 cm/ 6 cm<br>surfactants: Tween 80 / SDS (+PLGA)/ Pluronic F68 / HPMC / SA<br>(T(e): 59.85°C) | p(e) ↑ size ↓<br>nozzle ø ↓ size ↓<br>nozzle length ↓ size ↓<br>SDS (+PLGA); smallest particles | PLGA used as coprecipitate | (Dalvi et al., 2013) |
| Pulsed RESS | 2007 | ibuprofen | 0.1 µm - 0.5 µm | p(e): 200 bar/ 400 bar<br>T(e): 24.85°C/ 86.85°C<br>(nozzle ø: 150 µm) | T(e): 24.85°C and<br>p(e): 200 bar; smallest particles | Aggregated particles | (Hermsdorf et al., 2007) |
| RESS | 2010 | ketoprofen | 0.35 µm - 7.03 µm | p(e): 140 bar/ 160 bar/ 180 bar/ 200 bar/<br>220 bar<br>T(e): 34.85°C/ 44.85°C/ 54.85°C/ 64.85°C<br>nozzle ø: 450 mm/ 650 mm/ 1000 mm/<br>1200 mm/ 1700 mm<br>nozzle length: 2 mm/ 5 mm/ 8 mm/<br>11 mm/ 15 mm<br>collection distance:1cm/ 5cm/ 7cm/ 10cm | p(e) ↑ size ↓<br>T(e) ↑ size ↑<br>nozzle ø ↓ size ↓<br>nozzle length ↓ size ↓<br>collection distance ↑ size ↑ | | (Hezave et al., 2010) |
| RESS | 2005 | aspirin | 0.1 µm - 0.3 µm | p(e): 160 bar/ 170 bar/ 180 bar/ 190 bar/ 200 bar/ 210 bar<br>T(e): 50 °C/ 70°C/ 80°C/ 90°C<br>T(exp): 81°C/ 98°C/ 99°C/ 100°C/ 101°C/ 119°C / 14 °C<br>nozzle ø: 60 µm/ 350 µm | p(e) high/low size ↑, middle ↓<br>T(e) high/low size ↑, middle ↓<br>T(exp) no effect<br>Nozzle ø no effect | T(e) < T(exp) | (Huang et al., 2005) |

| Technique | Year | Model drug | Mean particle size | Parameters | Parameter effect on mean particle size | To be noted | Reference |
|---|---|---|---|---|---|---|---|
| RESS | 2006 | loperamide HCl | 0.3 µm - 0.5 µm | nozzle ø: 5 µm/ 100 µm/ 200 µm<br>(p(e): 150 bar; T(e): 49.85°C ; co-solvent: 1%) | nozzle ø ↓ size ↓ | Clearance nozzle, chloroform as co-solvent | (Huang and Moriyoshi, 2006) |
| RESS | 2014 | progesterone | 0.11 µm - 3.22 µm | p(e):120 bar/ 150 bar/ 180 bar/ 210 bar/ 260bar<br>T(e): 40°C/ 50°C/ 65°C<br>nozzle ø: 60 µm/ 350 µm | p(e) ↑ size ↑<br>T(e) ↑ size ↑<br>nozzle ø ↑ size ↓ | | (Huang et al., 2014) |
| RESS | 2012 | raloxifene | 0.019 µm - 0.137 µm | p(e): 100 bar/ 140 bar/ 180 bar<br>T(e): 40°C/ 60°C/ 80 C°C<br>collection distance: 5 cm/ 7 cm/ 10 cm | p(e) no effect<br>T(e) high/low size ↑, middle ↓<br>collection distance ↑ size ↓ | | (Keshavarz et al., 2012) |
| RESS-SC | 2015 | clobetasol propionate | 0.095 µm - 0.319 µm | p(e): 200 bar/ 220bar/ 260 bar<br>T(e): 70°C/ 90°C/ 110°C/<br>co-solvent: 3%/ 5%/ 7% | p(e) ↑ size ↓<br>T(e) ↑ size ↓<br>co-solvent ↑ size ↑ | Menthol as solid co-solvent | (Keshmiri et al., 2015) |
| RESS | 2010 | lidocaine | 0.1 µm - 0.3 µm | p(e): 150 bar/ 200 bar/ 250 bar/ 300 bar/ 350 bar<br>T(e): 40°C/ 50°C / 60°C/ 70°C<br>T(exp): 40°C/ 50°C / 60°C/ 70°C/ 80°C<br>nozzle ø: 30 µm/ 100 µm / 150 µm<br>nozzle (L/ø): 200/ 300/ 400/ 500 | p(e) ↑ size ↑<br>T(e) ↑ size ↓<br>T(exp) ↑ size ↓<br>nozzle ø ↑ size ↑<br>nozzle (L/ø) ↑ size ↑ | | (Kim et al., 2010) |
| RESS | 2013 | naproxen | 0.06 µm - 0.92 µm | p(e): 150 bar/ 200 bar/ 250 bar/ 300 bar<br>T(e): 45°C/ 60°C/ 100°C<br>co-solvent: 0%/ 5%/ 10% | p(e) ↑ size ↓<br>T(e) ↑ size ↓<br>co-solvent; 5% successful | Methanol as co-solvent | (Montes et al., 2013) |
| RESS<br>RESAS | 2016 | olanzapine | 0.15 µm - 0.35 µm | surfactant: 2% HPMC/ 2% PEG/ 2% PEG + 1% SLS / 0.1% Tween 80<br>(p(e): 200 bar; T(e): 50°C; nozzle ø: 150 µm) | Tween 80: smallest particles<br>PEG+SLS: most stable | | (Paisana et al., 2016) |
| RESOLV | 2004 and 2006 | ibuprofen and naproxen | Ibuprofen: 0.03 µm - 0.276 µm<br><br>Naproxen: 0.064 µm | surfactants:<br>Ibuprofen: $PVP_{40K}$ 0.5 $mgmL^{-1}$/ $PVP_{40K}$ 2 $mgmL^{-1}$/ $PVP_{360K}$ 0.5 $mgmL^{-1}$/ $PEG_{6K}$ 2 $mgmL^{-1}$/ $PEG_{35K}$ 2 mg/mL/ PVA 2 $mgmL^{-1}$/ BSA 2 $mgmL^{-1}$/ SDS3.3 $mgmL^{-1}$<br>Naproxen: $PVP_{40K}$ 0.5 mg/mL<br>(p(e): 200 bar;T(e): 40°C nozzle ø: 50 µm; naproxen: co-solvent: 2%) | Ibuprofen<br>$PVP_{360K:}$ smallest particles | Methanol as co-solvent for naproxen | (Pathak et al., 2004, Pathak et al., 2006) |

| Technique | Year | Model drug | Mean particle size | Parameters | Parameter effect on mean particle size | To be noted | Reference |
|---|---|---|---|---|---|---|---|
| RESOLV | 2007 | paclitaxel | 0.038 µm - 0.53 µm | surfactant: $PVP_{40K}$ 0.33 $mgmL^{-1}$/ $PVP_{40K}$ 1 $mgmL^{-1}$/ $PVP_{360K}$ 0.33 $mgmL^{-1}$ (p(e): 310 bar;T(e): 40 °C;nozzle ø: 50µm) | surfactant concentration ↑ size ↓ surfactant Mw ↑ size ↓ | | (Pathak et al., 2007) |
| RESS, RESS-SC | 2012 | lynestrenol | 0.058 µm - 0.326 µm | p(e): 150 bar/ 225 bar/ 300 bar T(e): 45°C/ 52.5°C/ 60°C co-solvent: 0%/ 2.5%/ 5% (nozzle ø: 600 µm) | p(e) ↑ size ↑ T(e) ↑ size ↑ co-solvent ↑ size ↓ | Menthol as solid co-solvent | (Pourasghar et al., 2012) |
| RESS | 2012 | paracetamol | 0.015 µm - 0.855 µm | p(e): 100 bar/ 140 bar/ 180 bar T(e): 39.85°C/ 59.85°C/ 79.85°C T(exp): 89.85°C/ 109.85°C/ 129.85°C T(chamber): -0.15°C/ 24.85°C/ 49.85°C collection distance: 50 mm /90 mm (nozzle ø: 60 µm) | T(e) ↑ size ↓ p(e) ↑ size ↑ T(exp) no effect T(chamber) ↑ size ↓ collection distance ↑ size ↑ | | (Sabet et al., 2012) |
| RESS-SC | 2012 | megestrol acetate | 0.103 µm - 0.516 µm | p(e): 150 bar/ 200 bar/ 250 bar T(e): 40 °C/ 50 °C/ 60°C co-solvent: 2%/ 4%/ 6% | p(e) ↑ size ↓ T(e) ↑ size ↓ co-solvent ↑ size ↑ (lowest p(e)); ↑ size ↓ (highest p(e)) | Menthol as solid co-solvent | (Samei et al., 2012) |
| RESS | 2016 | ibuprofen | 0.007 µm - 0.25 µm | surfactant: 0.25%/ 0.5%/ 0.75%/ 1% $PEI_{750000Da}$ 0.25%/ 0.5%/ 0.75%/ 1% $PEI_{1300Da}$ 0.25%/ 0.5%/ 0.75%/ 1% $PVP_{40000Da}$ 0.25%/ 0.5%/ 0.75%/ 1% Tween $40_{1283Da}$ (p(e): 325 bar; T(e): 40°C) | 1% $PEI_{750000Da}$: smallest particles | Particles collected in dry ice, sublimation into polymer solution | (Sharma and Jagannatha n, 2016) |
| RESS-SC | 2005 | griseofulvin | 0.05 µm - 0.25 µm | (p(e): 196 bar; T(e): 40°C) | | Menthol as solid co-solvent | (Thakur and Gupta, 2005) |
| RESS-SC | 2006 | phenytoin | 0.075 µm | (p(e): 196 bar; T(e): 45°C) | | Menthol as solid co-solvent | (Thakur and Gupta, 2006) |
| RESS | 2002 | griseofulvin | 0.15 µm - 0.2 µm | T(e): 74.85°C/ 114.85°C/ 144.85°C T(exp): 74.85°C /114.85°C/ 144.85°C (p(e): 200 bar, nozzle ø: 50 µm) | T(e) no effect T(exp) no effect | $CHF_3$ as solvent | (Türk et al., 2002, Helfgen et al., 2001) |

| Technique | Year | Model drug | Mean particle size | Parameters | Parameter effect on mean particle size | To be noted | Reference |
|---|---|---|---|---|---|---|---|
| RESS, RES | 2008 | salicylic acid and ibuprofen | RESS: salisylic acid 0.13 µm - 0.23 µm<br><br>RESSAS: salisylic acid 0.1 µm - 0.26 µm ibuprofen 0.08 µm | RESS: salisylic acid T(exp): 54.85°C/ 74.85°C/ 114.85°C (p(e): 200 bar; T(e): 49.85°C; ibuprofen (p(e): 150 bar; T(e): 34.85°C; T(exp): 34.85°C)<br>RESSAS: surfactant: 0.1%/ 0.5%/ 1% Tween 80 salisylic acid: (p(e): 200 bar; T(e): 34.85°C; T(exp): 54.85°C) ibuprofen: (p(e): 150 bar; T(e): 34.85°C; T(exp): 34.85°C)<br>(all experiments: nozzle ø: 50 µm; nozzle (L/ø): 1) | RESS: salisylic acid T(exp) ↑ size ↑<br><br>RESSAS: salisylic acid surfactant no effect ibuprofen surfactant ↑ size ↓ | Salicylic acid: 4.6 g/dm$^3$ in 1% Tween 80<br><br>Ibuprofen: 2.4 g/dm$^3$ in 1% Tween 80 | (Türk and Lietzow, 2008) |
| RESS, RESSAS | 2010 | naproxen | RESS: 0.56 µm - 0.82 µm<br><br>RESSAS: 0.3 µm - 8 µm | RESS: p(e): 200 bar/ 250 bar/ 300 bar T(exp): 49.85°C/ 69.85°C/ 89.85°C (collection distance: 300 mm)<br>RESAS: surfactant: 0.4% PVP / 0.4% Tween 80 (p(e): 200 bar; T(exp): 69.85°C)<br>(all experiments: T(e): 39.85°C; nozzle ø:75 µm) | RESS: p(e): 200 bar; T(exp): 49.85°C: smallest particles<br>RESAS: surfactant: 0.4% PVP: smallest particles | RESSAS: 1 g/dm$^3$ in 0.4% PVP | (Türk and Bolten, 2010) |
| RESS-SC | 2015 | theophylline | 0.085 µm - 0.09 µm | T(chamber) -7.95°C/ 30.05°C/ 110.05°C collection distance: 3 cm/ 5 cm/ 7 cm (p(e): 140 bar; T(e): 65.05°C; nozzle ø: 50µm) | T(chamber) no effect collection distance no effect | Vanillin as solid co-solvent | (Uchida et al., 2015) |
| RESAS | 2000 | cyclosporine | 0.4 µm - 0.7 µm | surfactant: 1.0%/ 5.0% Tween 80 (p(e): 345 bar; T(e): 30°C; T(exp): 60°C) | surfactant ↑ size ↓ | 38 mg/mL in 5.0% Tween 80 | (Young et al., 2000) |
| RESS, RESOLV | 2011 | ibuprofen | RESS: 0.04 µm - 0.18 µm<br><br>RESOLV: 0.08 µm - 0.4 µm | RESS: p(e): 80 bar/ 90 bar/ / 95 bar/ 100 bar/ 110 bar T(exp): 80°C/ 85°C/ 90°C/ 95°C/ 100°C<br>RESOLV: surfactant: 10% / 25% / 50% (v/v) PEG (p(e): 90 bar; T(exp): 80°C) | RESS: p(e): high/low size ↑, middle ↓ T(exp) ↑ size ↑, except with 110 bar; high/low size ↑, middle ↓<br>RESOLV: surfactant no effect | | (Zabihi et al., 2011) |

## 2.3 DISSOLUTION TESTING OF PARTICULATE SYSTEMS

### 2.3.1 BASIS FOR DISSOLUTION TESTING

The basis for *in vitro* dissolution testing was established in 1897 by Noyes and Whitney as they studied the rate of solution of solid substances in their own solutions (**Equation 10**) (Noyes and Whitney, 1897).

(**10**) $$\frac{dC}{dt} = k_1(C_s - C)$$

Here, $C_s$ is the saturation solubility of the drug, $C$ is the concentration at the expiration of time $t$, and $k_1$ is a constant. This equation was modified by Nernst and Brunner with the diffusion layer concept and Fick's second law to describe a proportional increase in dissolution rate with an increase of the surface area (**Equation 11**) (Nernst, 1904, Brunner, 1904).

(**11**) $$\frac{dm}{dt} = A\frac{D}{d}(C_s - C)$$

Here, $m$ is the mass of dissolved material, $A$ is the surface area, $D$ is the diffusion coefficient of the drug, and $d$ is the diffusion layer thickness. An increase in active surface area increases the rate of dissolution. Any decrease in particle size increases the active surface area, and thus the dissolution rate can be enhanced by reducing particle size. Furthermore, the saturation solubility of nanoscale particles is increased by the curvature of the surface as stated in the Ostwald-Freundlich equation derived from the Gibbs-Kelvin equation (Thomson, 1871, von Helmholtz, 1886).

Since accurate assessment of the diffusion layer thickness and the effect of the surface curvature is often impossible, the *in vitro* dissolution rates are obtained experimentally (Jünemann and Dressman, 2012). The first dissolution test method added to the United States Pharmacopeia (USP), the basket method, was developed in 1968 (Pernarowski *et al*., 1968). As the need to evaluate dissolution as a part of determining the bioavailability of a drug, dissolution procedures were added to the USP in 1970 (Cohen *et al*., 1990).

### 2.3.2 CURRENT METHODS FOR DISSOLUTION TESTING OF POWDERS, NANOPARTICLES, AND PARTICULATE SYSTEMS

The USP does not offer standardized methods for *in vitro* dissolution testing of powders, nanoparticles, and particulate systems (Azarmi *et al*., 2007, Shen and Burgess, 2013). Realistic results are often difficult to obtain when

characterizing these complex systems. Dissolution rates of powders, nanoparticles, and particulate systems have been investigated using the USP I (basket), II (paddle), and IV (flow-through) methods and modifications thereof (USP, 2015, Pillay and Fassihi, 1999, Cohen *et al.*, 1990, Azarmi *et al.*, 2007, Bhattachar *et al.*, 2002, Siewert *et al.*, 2003). For example, the USP I method was adapted for dissolution studies of powders by sealing the basket with molten paraffin (Shaw *et al.*, 2002). The USP IV flow-through apparatus has been found to be the most applicable of the compendial methods for nanoparticle dissolution studies (Heng *et al.*, 2008). Also, the flow-through method has been modified, for example by developing an open-loop system (Gao, 2009).

The most commonly used methods for *in vitro* dissolution testing of nanoparticulate systems are membrane diffusion methods (Shen and Burgess, 2013, Modi and Anderson, 2013). For example, in dialysis methods, the dissolving material is released in a dialysis bag and diffused across a dialysis membrane into the receiver compartment (Cho *et al.*, 2013). This system has been improved for example by using a bulk equilibrium reverse dialysis bag technique maximizing the driving force of drug release and automated microdialysis systems to facilitate the test procedure (Chidambaram and Burgess, 1999, Michalowski *et al.*, 2004).

Filtration, centrifugation, centrifugal filtration, and similar sample and separate methods have been used in dissolution testing of nanoparticles and particulate systems (Shen and Burgess, 2013, Cho *et al.*, 2013). Here the dissolved substance is separated from the particles, and non-dissolved particles are incubated in fresh medium until the next sampling (Cho *et al.*, 2013). Furthermore, dissolution rates of nanoparticles and particulate systems have been determined from tablets and admixtures with gel matrices and with techniques employing ion-selective electrodes (Sarnes *et al.*, 2013, Peschka *et al.*, 1998, Mitsana-Papazoglou *et al.*, 1987). Optical light scattering methods have been used in dissolution testing of powders and particulate systems (Anhalt *et al.*, 2012). Dynamic light scattering has been used to detect the disappearance of dissolving particles. Dynamic light scattering and similar *in situ* techniques are often combined with offline methods in dissolution studies of particulate systems (Xie *et al.*, 2015, Kuentz, 2015, Anhalt *et al.*, 2012).

### 2.3.3 DRAWBACKS AND SOURCES OF ERROR WITH CURRENT METHODS

The main issues encountered with current methods include: dispersion of non-dissolved particles, hydrodynamics-induced variability, membrane effects caused by diffusion barriers (e.g. gelatin, filters, or dialysis membranes), clogging and breaking of filters, sensitivity to flow and location in the dissolution vessel, as well as migration of nanoparticles to interfaces (e.g. wetting issues, floating, or adhesion) (Heng *et al.*, 2008, Qureshi and

Shabnam, 2001, Abouelmagd *et al.*, 2015, Washington, 1990, Baxter *et al.*, 2005, D'Arcy *et al.*, 2005, Zhang *et al.*, 1994).

The USP methods, originally developed for tablets, were not designed for dissolution studies of nanoscale particles, and thus produce results that do not predict the dissolution behaviour *in vivo* (Heng *et al.*, 2008, Shen and Burgess, 2013). Often, the measured values reflect features of the dissolution test device, equipment, and method, rather than the particle properties.

Dispersion and the consequent overestimation of nanoparticle dissolution rates in the USP I and II methods occur when the location of the particles is not fixed (Chauhan *et al.*, 2005, Shimpi *et al.*, 2005, Shaw *et al.*, 2002). Issues with the USP I apparatus are caused by the complex hydrodynamic conditions in the dissolution vessel and by inadequate mixing especially within the basket (D'Arcy *et al.*, 2006). Small particles are dispersed into the medium and large particles are deposited at the base of the basket (Morihara *et al.*, 2002). Wetting issues often occur due to lack of flow of the medium past the surface of the particles, aggregates are easily formed causing a delay in dissolution, and aggregate adhesion to the basket walls clogs of the mesh (Nicklasson *et al.*, 1991, Wennergren *et al.*, 1989).

Similar issues rise with the USP II apparatus and thus the results of USP II are often inconsistent and difficult to reproduce (Siewert *et al.*, 2002, Cox and Furman, 1984, Cox *et al.*, 1982). Variations in the flow field in the vessel has been investigated experimentally and computationally (Baxter *et al.*, 2005, D'Arcy *et al.*, 2005). Exposure of the dissolving material to different shear environments cause significant variation in the dissolution rate (Baxter *et al.*, 2005, Qureshi and Shabnam, 2001). Fluid velocities differ depending on location in the dissolution vessel size and the shape of the dissolution vessel affects the dissolution rate (Underwood and Cadwallader, 1976, Bocanegra *et al.*, 1990). The dissolution rate increases at off-center positions in the vessel with tablets (D'Arcy *et al.*, 2005). Disintegrated powders and particles are more likely to disperse within the dissolution vessel along the fluid flow patterns (Healy *et al.*, 2002). The agitation rate affects the dissolution rate, the thickness of the diffusional layer, and the microenvironment surrounding powder particles (Hamlin *et al.*, 1962, Levy *et al.*, 1965, Valizadeh *et al.*, 2004, Sheng *et al.*, 2008). These issues limit the ability to distinguish the different dissolution rates of different sized particles. The dissolution rates are reduced in a UPS II apparatus as the particulate systems form aggregates that float on the surface of the dissolution medium due to wetting issues (Heng *et al.*, 2008).

The USP IV apparatus requires careful selection of the pore size for the filter: too large a pore size permits particles to escape and consequently the dissolution rate is overestimated, whereas too small a pore size may result in clogging and even breaking of the filter (Jünemann and Dressman, 2012, Heng *et al.*, 2008). Both the flow rate and the position of test substance affect the dissolution rates (Zhang *et al.*, 1994). Even though apparatus IV has specific sample cells for dissolution testing of powders, the system has issues with poor

wettability (Siewert *et al.*, 2003). These issues have been addressed with the use of glass beads or surfactants. However, use of these often leads to loss of the discriminatory ability for different sized particles. Additionally, the compendial methods require large amounts of the test substance and medium, tedious sample preparation, and separation steps before analysis.

The dissolution rate of particulate systems determined with membrane diffusion methods is often underestimated (Heng *et al.*, 2008, Abouelmagd *et al.*, 2015). A dialysis membrane introduces a diffusion barrier (Heng *et al.*, 2008, Cho *et al.*, 2013). The diffusion of the test substance through the membrane can be slow and the dissolution method is likely to reflect the quality of the membrane rather than the dissolution rate of the test substance (Chidambaram and Burgess, 1999, Jünemann and Dressman, 2012).

Selecting a suitable membrane or dialysis bag is demanding; ideally the pores of the membrane should be 100 times the size of the dissolved test substance, yet small enough to prevent the nanoparticles from passing through, while the volume of the dissolution medium inside the membrane should ideally be 6–10 fold less than that of the outer release medium (Xu *et al.*, 2012, D'souza and DeLuca, 2006, Moreno-Bautista and Tam, 2011, Chidambaram and Burgess, 1999). The membrane material may also affect the drug release (Xie *et al.*, 2015).

Loss of sink condition is often inevitable and dilution of the particulate systems in the medium causes loss of the discriminatory ability with the membrane diffusion methods (Bhardwaj and Burgess, 2010, Calvo *et al.*, 1996, Abdel-Mottaleb and Lamprecht, 2011). Insufficient understanding of the driving force for test substance transport across the membrane leads to misinterpretation of the dissolution data (Modi and Anderson, 2013, Moreno-Bautista and Tam, 2011). Partitioning of the test substance between the inner and the outer phase affects the driving force across the dialysis membrane (Zambito *et al.*, 2012, Washington, 1990). The test substance is at risk of precipitation after dissolution inside the dialysis bag and the membrane may act as an adsorptive surface (Abouelmagd *et al.*, 2015, Cho *et al.*, 2013). Furthermore, surfactants cause issues especially with microdialysis (Shen and Burgess, 2013).

Separation methods face issues especially with nanoparticulate systems (Wallace *et al.*, 2012). Due to their small size, it is difficult to separate the particles from the dissolution medium in an efficient and rapid manner without influencing the dissolution profile. External energy, such as centrifugal force, agitation, pressurization, or shear stress, applied to the dissolution system causes accelerated drug release and consequently overestimation of the dissolution rate (Henriksen *et al.*, 1995, Wallace *et al.*, 2012, Cho *et al.*, 2013). On the other hand, incomplete separation or test substance precipitation in the medium result in underestimation of the dissolution rate (Henriksen *et al.*, 1995, Wallace *et al.*, 2012, Abouelmagd *et al.*, 2015).

When determining dissolution rates of nanoparticles from tablets and admixtures with gel matrices, the physical form of the test substance during the tableting or mixing processes may change, and particles may detach from the tablet surface during the dissolution process. The current methods also suffer from the diffusional barrier induced by the matrix (Sarnes *et al.*, 2013, Peschka *et al.*, 1998). The gel matrix is unrepresentative of the actual dissolution process since it is a representation of diffusion of a particular drug in a particular matrix.

Optical methods often work in narrow concentration regions (Jünemann and Dressman, 2012, Shen and Burgess, 2013). The intensity of light scattering is a function of particle size and concentration and is not easily interpreted. (Anhalt *et al.*, 2012, Jünemann and Dressman, 2012). Often in such cases, the particles are also wetted and kept dispersed by surfactants (Jünemann and Dressman, 2012). These change the dissolution kinetics and equilibrium dynamics of the system and surfactant systems are therefore often not representative of the actual dissolution environment. Fibre optics are rarely used for turbid systems in pharmaceutical dissolution testing (Jünemann and Dressman, 2012). Optical methods face the same wettability and dispersion issues as the traditional methods.

Ion-selective electrodes are unsuitable for non-electroactive test substances (Mitsana-Papazoglou *et al.*, 1987). Additionally, with dissolution testing, one needs to take into account the effect of dissolution media, the potential adsorption of the test substance to the equipment, the particle-medium ratio, and the handling of the samples, all of which can substantially affect the observed dissolution rate (Abouelmagd *et al.*, 2015).

## 2.4 SOLID-STATE QUANTIFICATION WITH RAMAN SPECTROSCOPY

### 2.4.1 PRINCIPLE OF RAMAN SPECTROSCOPY

The existence of scattered radiation with altered frequency compared to incident light was theorized in 1923 and experimentally proven in 1928 (Smekal, 1923, Raman and Krishnan, 1928). This inelastic light scattering, Raman scattering, is caused by energy transfer between light and the molecule(s) it interacts with (Smith and Dent, 2013). Most commonly, in situations involving spontaneous Raman scattering, light is scattered at slightly lower wavenumbers (Stokes scattering) or, less often, at higher wavenumbers (anti-Stokes scattering) than the incident light (Colthup *et al.*, 1990). The Raman phenomenon is generally rare, with only 1 to $10^6$-$10^8$ photons undergoing the energy exchange when encountering a molecule (Smith and Dent, 2013). Most scattering occurs as elastic scattering known as

Rayleigh scattering, where no energy is transferred overall between the scattering system and the incident radiation (**Figure 4**).

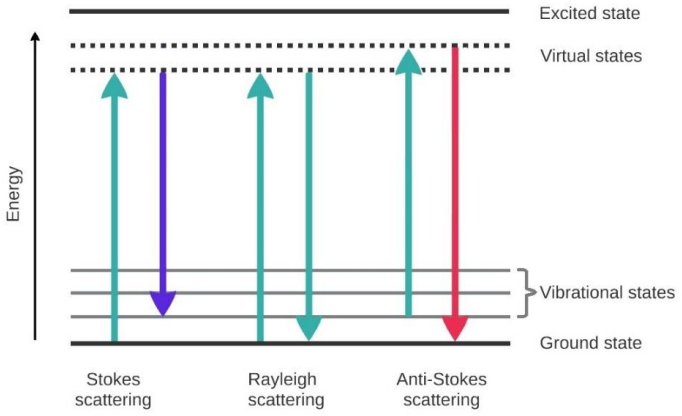


**Figure 4** Raman and Rayleigh scattering processes (adapted from Smith and Dent, 2013).

Vibrational energy transitions detected in Raman spectroscopy correspond to the wavenumber or energy difference between the incident and scattered light (Smith and Dent, 2013). These vibrational energy levels are unique for each different molecule and solid-state form. Atomic masses and the strength of the chemical bond affect the frequency of the vibration. Lower frequencies are caused by heavy atoms and weak bonds, whereas the higher frequencies are caused by strong bonds and light atoms.

Raman spectra are obtained by measuring the intensity distribution of Raman scattered photons from a monochromatic light source as a function of wavenumber (Jestel, 2005). Monochromatic light source (i.e. a laser) determines the Raman signal intensity since the intensity is proportional to the fourth power of the inverse of the incident wavelength. The shorter the laser wavelength, the more Raman photons are produced. In order to measure the scattered light from the sample, the light needs to be separated into distinct wavenumbers (Pitt *et al.*, 2005). The scattered light is collected and focused with a device capable of this separation process in order to obtain the Raman spectra.

The intensity of the Raman scattered light is the result of the energy transfer between the scattering system and the incident radiation (Smith and Dent, 2013, Colthup *et al.*, 1990). This phenomenon can be described using classical theory or quantum mechanical treatment (Smith and Dent, 2013). The classical theory takes into account only the induced electric dipole moment; the Rayleigh scattering is caused by the dipole oscillating at the same frequency as induced by the electric field of the incident radiation and Raman scattering is then caused by the dipole moment oscillating at the modified

frequency. The frequency modulation is the result of a polarizability change of the electron cloud of the molecule. With symmetric bonds, the molecules contain polarizing ellipsoids that change shape, size, or orientation causing the Raman scattering. These changes correspond to vibrational or rotational transitions in the molecule known as polarizability tensors.

The quantum mechanical approach for Raman scattering regards the radiation and molecule together as an entity that exists for a short period of time and determines how energy is transferred between the incident radiation and the molecule (Smith and Dent, 2013). The energy of this entity makes an upward or downward transition between two discrete energy levels. The quantum mechanical approach explains the vibrational transitions more profoundly than the classical theory.

### 2.4.2 BASIS FOR QUANTITATIVE ANALYSIS

Raman spectroscopy is widely used for quantitative analysis of pharmaceuticals (Pratiwi *et al.*, 2002, Strachan *et al.*, 2004, Strachan *et al.*, 2007, Pelletier, 2003, Hennigan and Ryder, 2013, Tian *et al.*, 2007, Heinz *et al.*, 2007). The principle of linear superposition applying to Raman spectroscopy implies that reduction of the excitation light intensity does not occur and there is practically no probability of a Raman scattered photon being lost because of another Raman scattering interaction. Yet, the quantitative analysis is done assuming no absorption that would affect the transmission of excitation or Raman scattered light to or from the sample.

Quantitative determination of a sample from the obtained Raman spectra is based on the concentration of the substance of interest being proportional to the integrated intensity of the Raman band (McCreery, 2005). The relation of the intensity of Raman band and concentration of the substance is defined as (**Equation 12**).

$$L = P_D \beta D_0 K \tag{12}$$

Here, $L$ is the specific intensity of the Raman scattering, $P_D$ is he power density of the incident laser light, $\beta$ is the differential Raman cross section, $D_o$ is the number of molecules per cubic centimeter and $K$ is a geometric factor that depends on the observation geometry.

Quantitative analysis is conducted using analytical models that are built based on the information gathered from the spectra (Pelletier, 2003). The system is trained using known samples that relate certain features of their spectra to a known property. The aim of the data analysis is to extract spectral information that quantifies substances of interest, to estimate the uncertainties of the quantification, and to evaluate the performance of the built model.

Several multivariate methods have been established for the interpretation of the Raman spectra (Pelletier, 2003, Strachan *et al.*, 2007). Spectral data often requires reducing the number of variables in the data sets in order to identify the spectral regions that are useful for quantitative analysis. The most commonly used multivariate analysis methods for Raman spectra of pharmaceuticals are principal component regression, and inverse least squares regression, the partial least squares regression (PLS) (Strachan *et al.*, 2007). Principal component analysis identifies the features of the spectra that are responsible for the largest inter-spectral variation by converting the spectral observations of possibly correlated variables into a set of values of linearly uncorrelated variables (Pearson, 1901). PLS regression is based on the conversion executed in principal component analysis but the covariance between the spectral data and the known concentrations are maximized while unrelated data variation is neglected (Haaland and Thomas, 1988).

Additionally, pre-processing of the spectra is often required to improve the signal-to-noise ratio and remove other forms of spectral variation unrelated to the sample property of interest (Pelletier, 2003). For eliminating sources of non-linearity quantitative analysis of pharmaceuticals various algorithms such as standard normal variate (SNV) transformation, second derivative pre-processing, and multiplicative scatter correction have been used (Barnes *et al.*, 1989, Heinz *et al.*, 2007, Hennigan and Ryder, 2013). Selecting pre-processing procedures for the quantitative analysis of pharmaceuticals is essential (Fraser *et al.*, 2013). Values that describe the functionality of the model include the cumulative correlation coefficients ($R^2$(cum) and $R^2Y$(cum)), the cumulative predictive ability of the model ($Q^2$(cum)), and the relative root mean square errors (RMSE) of estimation (RMSEE), prediction (RMSEP), and cross-validation (RMSECV) (Heinz *et al.*, 2007, Wold and Sjöström, 1977).

Comparison of models for the quantitative analysis is often performed by comparing RMSEP values. The following examples illustrate the general level of RMSEs with various pharmaceuticals. Second derivative pre-processing and multiplicative scatter correction combined with PLS model analysis have been applied to Raman spectra of binary mixtures of piracetam resulting in RMSEPs of 1.92 - 2.75% (Hennigan and Ryder, 2013) and, with more optimized methods, an RMSEP of 1.12% (Croker *et al.*, 2012). SNV correction and mean centering of the data followed by PLS model analysis produced RMSEPs for indomethacin ranging from 5.3% to 6.5% for indomethacin solid-state mixtures (Heinz *et al.*, 2007). Comparison of PLS models using transmission and backscatter Raman setups in evaluation of propranolol chloride tablets and acetylic acid capsules resulted in RMSEPs of 2.2% and 2.9% (Johansson *et al.*, 2007). Quantification has been successful from intact multi-component pharmaceutical capsules (Hargreaves *et al.*, 2011, Johansson *et al.*, 2007) and tablets (Xie *et al.*, 2008).

Raman spectroscopy permits analysis of complex samples (Kudelski, 2008). The spectra can be measured through container walls, blisters, plastic bags, and in an aqueous environment since Raman spectroscopy has low

sensitivity for water (Jestel, 2005). The form of the sample is flexible; powders, slurries, pellets, emulsions, films are all suitable for Raman spectroscopy. The samples can be in any state of matter and made of transparent, scattering, and opaque material (Pelletier, 2003). Raman spectroscopy is applicable to samples with high water content, such as biological and biochemical samples. Raman spectroscopy allows rapid, nondestructive robust *in situ* analysis with no sample preparation needed (Smith and Dent, 2013, Tian *et al.*, 2007, Jestel, 2005).

Error sources in the quantitative analysis of powder mixtures using Raman spectroscopy include variance in intra- and inter-day reproducibility of the Raman instrument, changes in room temperature and humidity, sample fluorescence, mixing, packing and positioning, as well as sample particle size and compactness, random intensity fluctuations and sub-sampling (Heinz *et al.*, 2007, Chen *et al.*, 2012, Pelletier, 2003, Taylor and Langkilde, 2000). Multivariate analysis addresses issues with poor peak resolution, morphology, particle size, and particle density (Rantanen *et al.*, 2005, Tian *et al.*, 2007, Chen *et al.*, 2012, Strachan *et al.*, 2007).

### 2.4.3 SUBTRACTION OF PHOTOLUMINESCENCE IN RAMAN SPECTROSCOPY

The confounding effect of fluorescence in the Raman spectra has been addressed with various methods (Jestel, 2005). Photoluminescence occurs as the molecules of a substance absorb photons and then emit them in with lower energy, with a longer wavelength compared to the incident light (Lakowicz, 2007). After the absorption of an incident photon, several specific molecular relaxation sequences can take place producing subtypes of the photoluminescence phenomenon. Fluorescence is one of these subtypes. The absorption occurs in fluorophores, certain structures in the molecules, such as conjugated double bonds and polycyclic aromatic rings, and the emission spectra vary according to the structure. A typical fluorescence lifetime is near $10^{-8}$ s. This coincides with Raman scattering, having a lifetime of $10^{-12}$ s, and since Raman scattering often occurs more rarely than fluorescence, the Raman signal is often masked by the fluorescence signal (Jestel, 2005, Matousek *et al.*, 2001) (**Figure 5**).

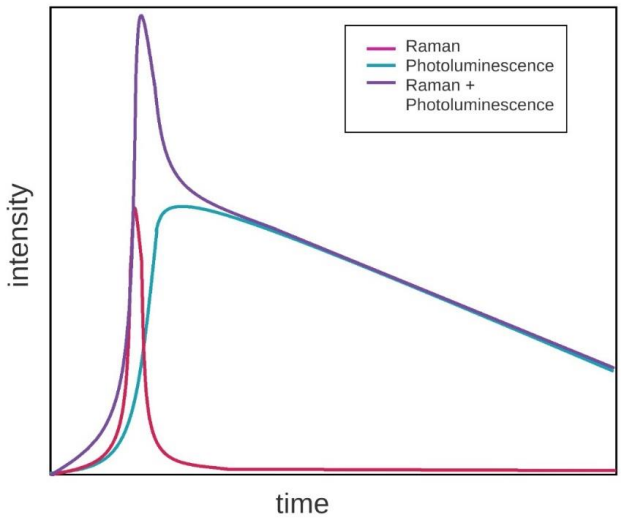


**Figure 5** Relative lifetimes of Raman and fluorescence signals (adapted from Rojalin *et al.*, 2016).

The background spectrum caused by fluorescence is challenging to subtract from the Raman spectrum (Jestel, 2005). The smooth nature of the fluorescence spectrum and the dominance of the photon shot noise reducing the signal-to-noise ratio cause issues with qualitative and quantitative analysis. Automated methods have been developed for the subtraction of fluorescence (Lieber and Mahadevan-Jansen, 2003). Complete subtraction of fluorescence without any instrument-based means is difficult even with sophisticated algorithms.

Fluorescence tends to be higher in the visible wavelength range and thus it can be reduced by using lasers with shorter or longer wavelengths (Lakowicz, 2007). However, since the Raman intensity is proportional to the fourth power of the excitation laser's frequency the use of longer wavelengths of the incident light reduces Raman signal intensity and shorter wavelengths induce damage to the sample (Jestel, 2005).

Fluorescence reduction can be performed by photobleaching, where fluorophores are destroyed by illuminating the sample with the excitation laser over an extended period of time (Golcuk *et al.*, 2006). The bleaching period varies from minutes to hours (Golcuk *et al.*, 2006, Heinz *et al.*, 2007). The use of photobleaching requires assuring that the sample has undergone no chemical or physical changes due to the photobleaching process (Heinz *et al.*, 2007).

Differential techniques can be used to separate fluorescence from Raman signals to some extent (Angel *et al.*, 1984). The differentiation is based on the propensity of the Raman signal to shift with small changes in excitation wavelength, whereas the fluorescence signal is unaffected by such changes (Bell and Bourguignon, 1998). The wavelength differential techniques have

been further developed and currently, the most commonly used of these is the shifted excitation Raman difference spectroscopy (Shreve *et al.*, 1992). The differential methods allow separation of the non-shifted continuous wavelength fluorescence and Raman signals in a quantitative manner. At least two spectra are needed for the separation.

### 2.4.4 TIME-GATED RAMAN SPECTROSCOPY

Complete or partial rejection of the fluorescence signal from the Raman signal is possible with various time-resolved techniques (Fishburn, 2012). The ability to detect the arrival time and energy of each photon allows assessment of the lifetime of both the fluorescence and Raman signals. Due to the lifetime differences discussed earlier, rejecting the fluorescence background is possible. Time-gated devices employ short, intensive laser pulses and the sample response is recorded simultaneously with the pulses (Patounakis *et al.*, 2006).

Time-gating can be realized with detection systems such as time-resolved photomultiplier tubes (Iams and Salzberg, 1935, Van Duyne *et al.*, 1974), high-speed optical shutters based on a Kerr cells (Matousek *et al.*, 2002, Matousek *et al.*, 2001), intensified charge-coupled devices (Efremov *et al.*, 2007), quantum dot resonant tunneling diodes (Blakesley *et al.*, 2005), and complementary metal-oxide semiconductor single-photon avalanche diodes (CMOS SPAD) (Patounakis *et al.*, 2006). One of the essential advantages of CMOS SPADs is the ability to reject both the photoluminescence tail and the photon noise (Kabuss *et al.*, 2010). SPADs are realized in standard CMOS technology and contain a pn junction which is reverse-biased above its breakdown voltage, meaning that entry of even a single photon can trigger avalanche breakdown that can then be recorded (Stoppa *et al.*, 2007, Stoppa *et al.*, 2009, Rochas *et al.*, 2003). The width and position of the time gate need to be properly selected (Nissinen *et al.*, 2017).

Complementary CMOS SPADs are compact and inexpensive and achieve adequate temporal resolutions (sub-nanosecond) (Mosconi *et al.*, 2006, Nissinen *et al.*, 2015, Kostamovaara *et al.*, 2013). CMOS SPAD detectors have been used to evaluate fluorescence lifetime (Schwartz *et al.*, 2007). The applicability of CMOS SPADs for fluorescence rejection in Raman spectroscopy of pharmaceuticals has been shown (Nissinen *et al.*, 2017, Maruyama *et al.*, 2014, Rojalin *et al.*, 2016).

# 3 AIMS OF THE STUDY

The aim of this research was to examine particle formation and analysis with novel technologies (**Figure 6**). The technologies introduced here provide insights into particle formation with two technologies and the improved analytical techniques presented in this study address issues associated with analyzing these particulate systems.

More specifically, the objectives of the research of this dissertation were the following:

- To employ microfluidic technology for engineering droplet-based formulations (I).
- To establish a process employing supercritical carbon dioxide for nanoparticle production (II).
- To develop a dissolution method for powders, nanoparticles, and particulate systems (III).
- To apply time-gated Raman spectroscopy for quantitative analysis of fluorescent powder mixtures (IV).

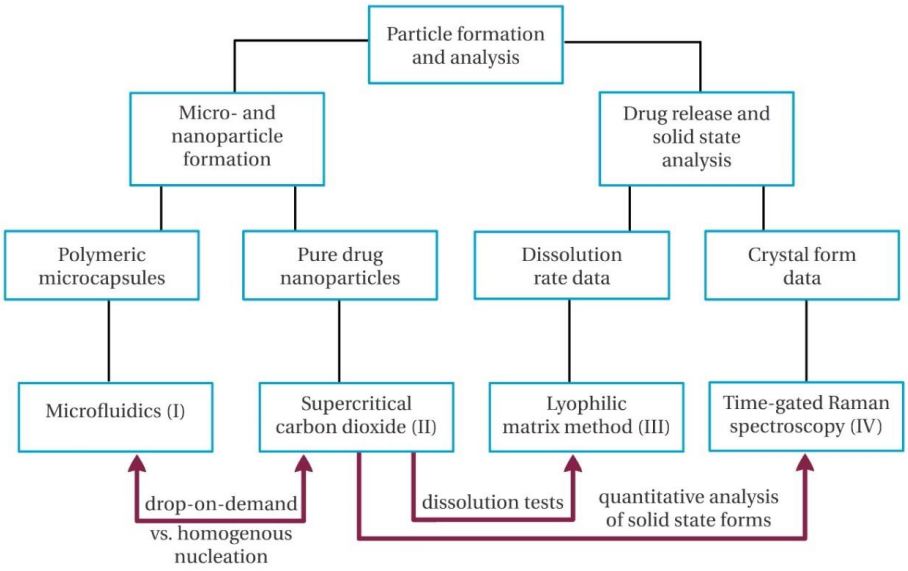


**Figure 6** Content of the particle formation and analysis parts of the thesis.

# 4 EXPERIMENTAL

## 4.1 MATERIALS (I-IV)

Bovine serum albumin (BSA), a model protein, was purchased from Sigma-Aldrich, Germany (I). Piroxicam, a poorly water-soluble non-steroidal anti-inflammatory drug, was purchased from Hawkins Inc., USA (II and IV). Indomethacin, a poorly water-soluble non-steroidal anti-inflammatory drug, was purchased from Hawkins Inc., USA (III). The polymers used were poly(vinyl alcohol) (PVA, 87-89% hydrolyzed, Mw 13,000-23,000; Sigma-Aldrich, USA), polyethylene glycol 6000 (PEG6000, Mw 5,000-7,000; Fluka Analytical, Germany), polycaprolactone (PCL, Mw 70,000-90,0000; Sigma-Aldrich) (I) and poloxamer 188 (BASF Co., Germany) (IV). Hydrophobic and hydrophilic coating agents were trimethoxy(octadecyl)silane (Sigma-Aldrich, USA) and 2-[methoxy(polymethyleneoxy)propyl] 9-12 trimethoxysilane (Gelest Inc., Netherlands) (I). $CO_2$ (≥ 99.8%), used as a supercritical solvent, was purchased from AGA, Finland (II). The chemicals used to prepare media for the dissolution studies were monopotassium phosphate (Riedel-de Haën, Germany), sodium phosphate dibasic (Sigma-Aldrich, USA), 5M sodium hydroxide (VWR Chemicals BDH Prolabo, EC) (III), and Dulbecco's Phosphate Buffered Saline (Sigma Aldrich, USA) (new data). The two fluorescent dyes employed were fluorescein isothiocyanate–dextran (FITC-dextran) (Mw 10,000, Molecular Probes, USA) and 3,4,9,10-perylene-tetracarboxylic dianhydride (Sigma-Aldrich, Germany) (I). Eluents used in the high performance liquid chromatography (HPLC) were acetonitrile (ACN) (I, III), trifluoroacetic acid (TFA)(I), and orthophosphoric acid ($H_3PO_4$) (III). All chemicals in the experiments were of analytical grade and were used as received.

## 4.2 METHODS (I-IV)

### 4.2.1 PRODUCTION OF POLYMERIC MICROPARTICLES WITH MICROFLUIDICS (I)

In this study, the microfluidic technique was employed as a tool for templating and fabricating biocompatible polymeric microcapsules for protein drug delivery. The microcapsules were loaded with bovine serum albumin (BSA) and the properties of the formed microcapsules were evaluated.

All microcapsule formulations were fabricated using glass microcapillary devices (Chu *et al.*, 2007, Duncanson *et al.*, 2012b, Kim and Weitz, 2011, Shum

*et al.*, 2011). Combining co-flow and flow-focusing within the glass capillary device allowed preparation of microcapsules from complex and viscous materials (Utada *et al.*, 2005). Cylindrical capillaries were pulled with a Flaming/Brown micropipette puller (Model P-97, Sutter Instrument Co., USA) to obtain tapered tips and to form tips with diameter of 100 and 150 µm. Cylindrical capillaries were coated with a hydrophilic or hydrophobic coating, trimethoxy(octadecyl)silane or 2-[methoxy(polymethyleneoxy)propyl] 9-12 trimethoxysilane, corresponding to whether they contained water or the oil phase.

The microfluidic device employed a biphasic flow to produce microcapsules from double emulsion droplets with ultrathin shells (**Figure 7**) (Kim *et al.*, 2011). Emulsion phases of the w/o/w emulsion were pumped into the glass capillary devices with syringes using Harvard pumps (Harvard Apparatus Hollston, USA). Syringes were attached to the inlets of the glass capillary device with plastic tubing (PE5 0.86 × 1.32 mm, Scientific Commodities Inc., USA). Microfluidic technology requires specific formulation to successfully produce double emulsion droplets. Formulations prepared with different flow rates were examined during the formulation optimization process. The formulations investigated in the screening study were chosen based on the viscosity and compatibility of the components. The optimized formulation contained 5% (w/w) of PVA in water as the outer phase, 3% (w/w) of PCL in ethyl acetate as the middle phase, and 20% (w/w) of PEG6000 and PVA (1:4) and 1% (w/w) BSA in water as the inner phase. PCL is a semi- crystalline, hydrophobic, biocompatible and biodegradable polymer and it has been widely used for the preparation of microcapsules for drug delivery applications (Chandra and Rustgi, 1998, Pitt, 1990, Chen *et al.*, 2000, Jeong *et al.*, 2003, Natarajan *et al.*, 2011, Scala-Bertola *et al.*, 2012, Somavarapu *et al.*, 2005). The water-solubility of BSA and increase in viscosity limited the maximum amount of BSA used in this formulation to 1% (w/w). The inner and middle phases flowed at the rate of 1000 µL/h and the flow rate of the outer phase was 3000 µL/h, respectively.

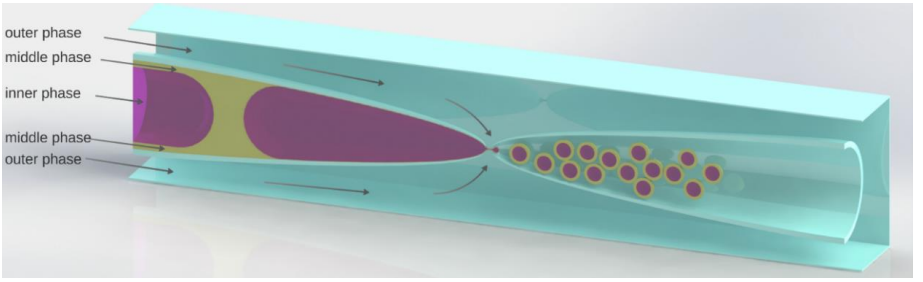


**Figure 7** The inner and middle phases flow in the cylindrical capillary on the left. A stretched capillary is inserted into this cylindrical capillary and the inner phase flows through it, forming large droplets of water phase upon entry into the oil phase. This forms droplets with ultrathin shells as the phases move to the collection capillary (on the right) and form a double emulsion with the outer phase flowing from the square capillary.

#### *4.2.1.1 Characterization of the microparticles*

The morphology and surface properties of the microcapsules were examined by scanning electron microscopy (SEM). SEM images were taken with an environmental SEM microscope (Carl Zeiss AG, EVO 55, Germany) with a wet stage at a chamber pressure of 682 Pa and 26 kV. Samples were placed on wet paper and no further preparation was required. The chamber was cooled down with liquid nitrogen to the water vapor state and the electric beam was run through upper and lower apertures of 100 and 500 μm, respectively.

The particle size was determined by optical microscopy and diameter measurements from 5 batches ($n$ = 100). Diameter measurements were conducted with software for scientific image analysis (ImageJ freeware, National Institutes of Health, USA) and measured according to the 1 mm scale in the optical microscope. Short time stability was examined by monitoring the collapse rate of the particles with optical microscopy. Five batches of particles were observed and the collapse rate of the particles was determined ($n$ = 200). Three batches (batches #1-3) were monitored for 4 weeks the samples were taken when the time elapsed was 0, 1, 3, 7, 14, 21 and 28 days and two batches (batches #4-5) were monitored for 6 weeks and the samples were taken when the time elapsed was 0, 28, 35 and 42 days. Batches for the short time stability tests were stored in the collection media at 8 °C.

The core shell structure of the microcapsules was determined with three parallel tests using a confocal microscope (Leica Microsystems CMS GmbH, Germany), ($n$ = 200). Two fluorescent dyes were employed: FITC-dextran in the inner phase and 3,4,9,10-perylene-tetracarboxylic dianhydride in the middle phase. The labeling agents were chosen based on their solubility in the phases to be stained; as a very hydrophilic compound FITC-dextran was used in the inner water phase, and perylene, a hydrophobic fluorescent agent, was used for the ethylacetate middle phase. As a result, the fluorescent agents remained in their respective phases after preparation. The excitation/emission spectra for FITC-dextran and perylene were 490/525 nm and 410/487 nm, respectively.

The encapsulation efficiency (EE) of BSA into the formed microcapsules was determined from the supernatant of three different batches immediately after the droplet preparation process was completed. The supernatant sample was withdrawn from the particle-free top of the collection vial whereas all microcapsules were settled at the bottom of the vial due to the phase density difference. The EE for BSA was examined by comparing the total quantity of BSA with the quantity of BSA in the supernatant. Samples of BSA were analyzed with HPLC (Thermo System Products, Agilent 1200 Infinity Series, Agilent Technologies, Germany). A Vydac 214MS C4 column (Grace Davison Discovery Science, USA), flow rate of 1 mL/min with a mobile phase consisting of ACN and 0.1% TFA were used operating at 40 °C. The protein analysis required a gradient of TFA and ACN at ratios of 80:20 (v/v) to 35:65 (v/v) within 12 min and reversal back to 80:20 (v/v) within 8 min, with a total run

time of 20 min. The UV detection of BSA was set at 210 nm with a retention time of 8.5 min. A standard curve for BSA quantification was made from BSA concentrations of 5 to 500 μg/mL ($R^2$ = 0.999).

### 4.2.2 NANOPARTICLE PRODUCTION WITH CONTROLLED EXPANSION OF SUPERCRITICAL SOLUTIONS (II)

Nanoscale particles can also be produced in conditions opposite to those in the traditional RESS process: slow depressurization and with a low degree of supersaturation. This can be achieved with a method developed in this research: Controlled Expansion of Supercritical Solution (CESS) (Hæggström *et al.*, 2015). CESS differs from RESS in many essential aspects and employs controlled mass transfer, controlled flow, controlled pressure reduction, and finally particle collection in dry ice (**Table 3**). The core of the technology is to allow large initial nuclei size and particle growth by condensation. This avoids variation in temperature, pressure, and density, as well as particle growth by coagulation.

**Table 3** *Essential differences between RESS and CESS techniques.*

| Feature | RESS | CESS |
|---|---|---|
| Pressure drop | rapid | controlled |
| Ratio of pressure drop | > 10 | < 10 |
| Flow velocities | supersonic | subsonic |
| Degree of supersaturation | high | low |
| Formation of Mach disk | yes | no |
| Particle formation | mainly beyond exit nozzle | mainly prior to exit nozzle |
| Main mechanism for particle growth | coagulation | condensation |

A specific pressure and temperature profile is created with a system consisting of a high pressure pump (SFT-10, Supercritical Fluid Technologies, Inc., USA), a 100 mL custom-made high pressure chamber, a heater/mixer (MR 2002, Heidolph, Germany), needle valve (Swagelok), 40 cm outlet tube (Sandvik, Sweden), a main nozzle and two additional nozzles (Mist&More Inc., USA), and a collection chamber (**Figure 8**). The pressure chamber was loaded at room temperature with a surplus of piroxicam (300 mg), and filled with liquid $CO_2$. Piroxicam was dissolved to saturated concentration as the pressure was increased to 200-350 bar and a temperature of 60-70 °C. A magnetic mixer (1500 rpm) ensured proper mixing. The valve temperature was kept at 40°C with PID-controlled (16S, Meyer) resistors.

**Figure 8** Experimental apparatus used to produce nanoparticles.

The pressure reduction in the system occurs in two steps. The first step takes place along the outlet tube connecting the pressure chamber to the collection chamber. The flow is controlled by a needle valve. At the valve, the pressure decreases from 230-250 bar to 30-45 bar while the temperature is kept constant. The particles are formed as the pressure decreases. The flow rate inside the outlet tube is kept at 24 mL/min. The second pressure reduction step occurs at the exit nozzle as the formed particles are transferred from the outlet tube into the collection chamber. As the volume increases, the pressure drops from 30-45 bar to 4 bar, the counter pressure in the collection chamber (**Figure 9**).

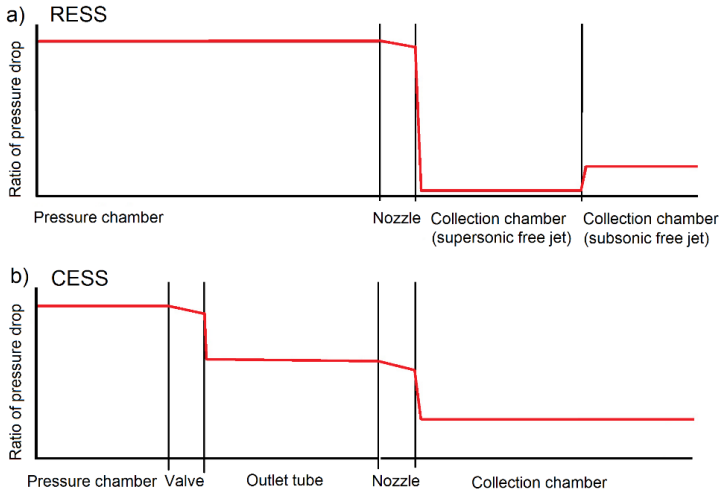


**Figure 9** Schematic picture describing RESS and RESS process. Pressure within a) the RESS and b) the CESS system. Pressure drop in RESS modified from (Martín and Cocero, 2008)

The nozzle at the end of the outlet tube maintains the pressure in the outlet tube and controls the flow. The particles are collected in dry ice formed by the Joule-Thomson effect and enhanced with two additional $CO_2$ sprays (15° angles relative to the main nozzle) (**Figure 10**). A solid dispersion consisting of nanoparticles and dry ice is formed. This further prevents particle growth by coagulation and inhibits aggregation. Collection of the nanoparticles in dry ice has successfully been used for fluoropolymers and explosives (Cortopassi *et al.*, 2008, Khapli and Jagannathan, 2014).

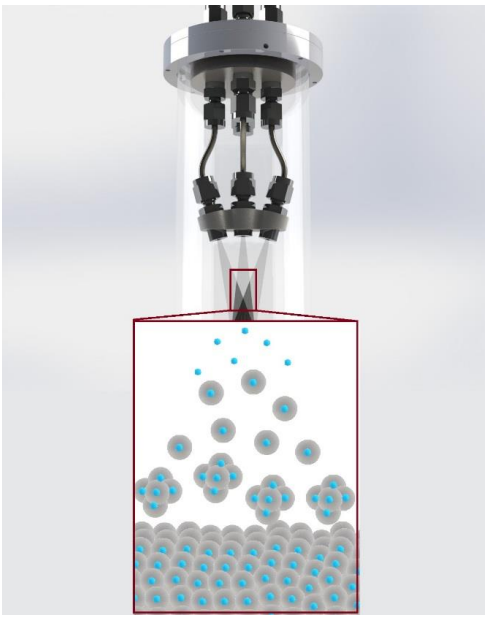

**Figure 10** Collection of the nanoparticles in dry ice. Turquoise dots indicate the nanoparticles formed in the outlet tube and grey circles the dry ice formed around the particles.

The nanoparticles can be stored within the dry ice to increase stability. Alternatively, the dry ice can be sublimated in a nitrogen atmosphere and the particles collected as dry nanoparticle powder. The production rate of the nanoparticles with the small laboratory-scale device is 60 mg/h.

#### *4.2.2.1 Characterization of the nanoparticles*

Particle size and morphology of three nanoparticle batches and bulk piroxicam were examined by SEM (Quanta™250 FEG, FEI Inc., USA). Samples were collected on a generic stainless-steel metal net and sputter-coated with a 5 nm thick platinum layer (Q150T Quomm, China). The particle size was determined by diameter measurements and analysis with the ImageJ freeware (National Institutes of Health, USA).

### 4.2.3 DISSOLUTION TESTING WITH THE LYOPHILIC MATRIX METHOD (III)

The experimental device in the LM method comprised a lyophilic matrix, a cage, a vessel, and a mixing/heating plate (**Figure 11**). The matrix has a core-shell structure comprising a core matrix that contains the particles of the test substance, and a surrounding shell matrix. The matrix material of both core and shell matrices is cotton (100% cotton, Curatex GmbH, Germany). The shell matrix consists of four layers of water jet-pressurized cotton with a dry specific surface weight of 5 ± 0.2 mg/cm². Cotton was selected as matrix material due to its unique properties; hollow cellulose fibers, high wet strength, inert nature, and substantial ability to absorb water-based media. The custom designed stainless steel cages (depth 3 mm x height 26 mm x width 16 mm) were 3D printed with selective laser sintering (Mlab Cusing, Concept Labs, Germany). The cage maintained the desired matrix geometry and provided a fixed diffusion distance.

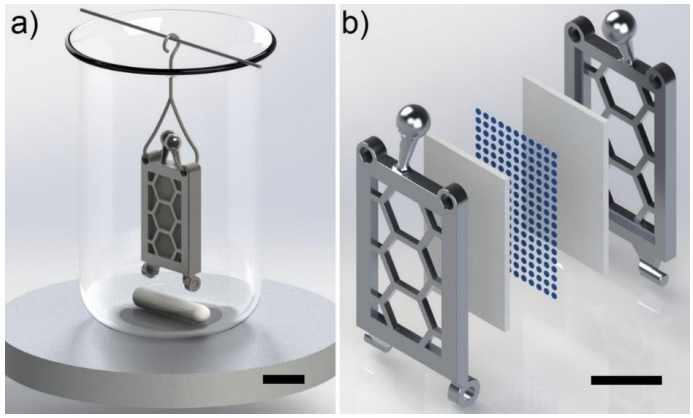


**Figure 11** a) LM method test setup and b) core-shell structure within the LM device, blue dots represent the core matrix containing the particles surrounded on all sides by the shell matrix and cage. Scale bars correspond to 10 mm.

#### *4.2.3.1 Characterization of the matrix*

The cotton matrix was examined prior to, during, and after medium exposure with light microscopy (Leica DMLB, Leica Microsystems Wetzlar, Germany) with a magnification of 200 x, and prior to, and after medium exposure with SEM (Quanta™ 250 FEG, FEI Inc., USA) with a magnification of 500 x, voltage of 5.00 kV, spot size of 3.0, sputter coated with a 5 nm thick platinum layer (Q150T Quomm, Beijing, China). The water intake properties of the matrix were investigated with a fast camera (1200 fps, Casio Exilim High-speed EX-FI1, Casio, Japan) and by weighing the matrix prior to and after exposure to the medium.

The partitioning of the model compound between the matrix and medium was examined by partition coefficient and inverse partitioning coefficient studies. First, the retention of the model compound within the matrix was examined. This was done by partition coefficient tests, where the matrix containing 1 mg of bulk indomethacin was immersed in the medium, and collected after 22 hours. The indomethacin retained in the matrix was determined by immersing the matrix into fresh medium for 22 hours. This procedure was conducted with three parallel experiments in pH 5.5 and pH 7.4 phosphate buffer media prepared according to the instructions in the European Pharmacopoeia (Ph.Eur., 2015) at 37.0 ± 0.5 °C with a stirring rate of 180 rpm (IKA RT 15 P, IKA Werke GmbH & CO. KG, Germany). The concentration of the medium was determined after the first and the second immersion at the 22 h time point. The concentration of the samples was analyzed with HPLC (Thermo System Products, Agilent 1200 Infinity Series, Agilent Technologies, Germany), using a Discovery C18 column (4.6 × 150 mm, 5 µm, Supelco, USA), 1.5 mL/min flow rate with a mobile phase consisting of 60:40 (V/V) ACN and 0.2% $H_3PO_4$ in water (MilliQ), operating at 30 °C with detection at 270 nm. The standard curve for indomethacin quantification was acquired from triplicate samples of indomethacin concentrations between 0.08 mg/L and 500 mg/L ($R^2$ = 0.999).

Second, the partitioning of the dissolved species into the matrix was examined. This was done by inverse partition coefficient tests, where an empty matrix was inserted into a medium with saturated concentration of the model compound. The test was conducted in triplicate in phosphate buffer media with pH of 5.5 and 7.4. The empty matrices were inserted into the medium every 5 minutes and the test lasted 20 minutes. The concentration of the medium was monitored online using *in-situ* fiber-optic UV monitoring (Opt-Diss 410, Distek, Inc., USA) using probes with a path-length of 5 mm, exposure time of 44 ms (4 scans/data point) at an analytical wavelength of 320 nm.

#### *4.2.3.2 Drug release studies*

A nanosized fraction, two sieved particle size fractions, and bulk indomethacin were tested with the LM method. Nanosuspension was prepared by milling with a Fritsch Pulverisette 7 Premium ball mill (Fritsch GmbH, Germany) to obtain particles for the experiments. Nanoparticles for the LM method were prepared of 2 g indomethacin suspended in solution containing 5.0 mL 0.24 g/mL poloxamer 188 solution (60 wt% relative to the drug amount) and 5.0 mL water (MilliQ), and by grinding at 850 rpm in 5 cycles of 3 min using 60 g milling pearls (zirconium oxide, diameter 1 mm). The particle size distribution in the nanosuspension was determined with a Zetasizer Nano SZ (Malvern Instruments Ltd., UK).

The bulk indomethacin was divided into two fractions using a sieve with a 125 µm pore size (Fritsch GmbH, Germany). The particle size of the bulk powder and the two fractions were determined from SEM images (see section 2.3.1.) ($n$ = 300, ImageJ freeware, National Institutes of Health, USA). The

bulk powder and the two fractions were each mixed with poloxamer 188 (60 wt% relative to the drug amount) to achieve physical mixtures with content identical to the nanosuspension.

For dissolution experiments the test substances (corresponding to 0.5 mg of indomethacin) were distributed within the core matrix, the nanosuspension was distributed wet and left to dry. The core matrix was then placed in the matrix holder. Dissolution tests were conducted in triplicate for nanoparticles, bulk powder, and the two particle size fractions in pH 5.5 phosphate buffer medium (Ph.Eur., 2015) and for nanoparticles and bulk powder in pH 7.4 phosphate buffer medium (Ph.Eur., 2015). All tests were performed under sink conditions in 100 mL of dissolution medium at 37.0 ± 0.5 °C using a stirring rate of 180 rpm (IKA RT 15 P, IKA Werke GmbH & CO. KG, Germany). The stirring rate and the matrix geometry were optimized with preliminary experiments. Aliquots of 1 mL, subsequently replaced with the same volume of fresh medium, were taken at 12 timepoints: 30 s, 1 min, 2 min, 5 min, 10 min, 30 min, 1 h, 2 h, 3 h, 4 h, 6 h, and 22 h. The samples were analyzed with HPLC as described in section 2.3.2. The cumulative release of indomethacin and standard deviation in three parallel samples were determined for each experiment.

Drug release tests with the LM method for piroxicam nanoparticles, prepared with the CESS technology described above, and bulk piroxicam were performed to investigate the effect of reduction of particle size on the dissolution rate (new data). Drug release tests of piroxicam nanoparticles and bulk piroxicam were conducted in glass vials under heating (37.0 ± 0.5 °C) and stirring (180 rpm) in 100 ml of phosphate buffer media at pH 6.8 (Dulbecco's Phosphate Buffered Saline, Sigma Aldrich). The concentration of the media was measured online every 2 seconds for 2 hours, and again at 14 hours to measure the concentration at equilibrium (μDISS Profiler, Pion Inc., USA).

### 4.2.4 QUANTITATIVE ANALYSIS WITH TIME-GATED RAMAN SPECTROSCOPY (IV)

#### *4.2.4.1 Mixture design*

Piroxicam has six reported polymorphs β (I), α1 and α2 (both also referred as form II), III, IV, and V) and one hydrated form (monohydrate, MH) (Lavrič *et al.*, 2015, Naelapää *et al.*, 2012, Sheth *et al.*, 2004, Upadhyay and Bond, 2015, Vrečer *et al.*, 2003, Thomas *et al.*, 2016). Ternary powder mixtures used in this study consisted of the most commonly observed forms: β, α2 and MH.

Piroxicam form α2 was prepared by recrystallization from a saturated solution of form β (bulk) in absolute ethanol (Vrečer *et al.*, 2003). Piroxicam MH was prepared by recrystallization from a saturated aqueous solution of form β (bulk) (Kogermann *et al.*, 2008). The aqueous solution was heated to

80 °C, the ethanol solution to 70 °C and then the solutions slowly cooled to room temperature before vacuum filtration.

Particle size and morphology of the piroxicam solid-state forms were examined by SEM with a Quanta™ 250 FEG instrument (FEI Inc., U.S.). Samples for SEM were mounted on a carbon-coated double-sided tape (Agar Scientific, Germany) and sputter-coated with a 5 nm thin layer of platinum (Q150T Quomm, Turbo-Pumped Sputter Coater, China). X-ray powder diffractometry (XRPD) analysis was performed using a Bruker D8 Advance diffractometer (Bruker, Germany) with a Cu Kα radiation source (λ = 1.5418 Å) over a 2θ range between 5° to 40°, using a step size of 0.01°, a step time of 0.5 s, voltage of 40 kV, and current of 40 mA. The results were compared to the patterns in the Cambridge Structural Database (CSD). Fourier transform infrared spectroscopy (FTIR) measurements were performed with a Bruker Vertex 70 spectrometer (Bruker Optik, Germany) with an ATR accessory with a single reflection diamond crystal (MIRacle, Pike Technologies, Madison, WI, USA). The obtained spectra were the mean of 64 scans and have a spectral range from 650 to 4000 $cm^{-1}$ with a resolution of 4 $cm^{-1}$. The ATR spectra were converted to absorbance spectra with OPUS software (v. 5.0, Bruker Optik, Ettlingen, Germany). Differential scanning calorimetry (DSC) was performed with differential scanning calorimeter (DSC821e, Mettler Toledo AG) in sealed perforated aluminum pans under dry nitrogen purge (50 mL/min) at a heating rate of 10 °C/min from 30 to 210 °C.

The powder mixtures were prepared according to a special cubic mixture design (Eriksson *et al.*, 1998) (**Figure 12**). The solid-state forms of piroxicam were carefully mixed using geometric dilution with a card to avoid inducing changes in the solid state. Thirteen mixtures were used in the study, the mixtures contained mass ratios (m/m/m) of form β, form α2 and MH as follows: (1 : 0 : 0), (0 : 1 : 0), (0 : 0 : 1), (2/3 : 1/3 : 0), (2/3 : 0 : 1/3), (0 : 2/3 : 1/3), (0 : 1/3 : 2/3), (1/3 : 0 : 2/3), (1/3 : 2/3 : 0), (1/3 : 1/3 : 1/3), (2/3 : 1/6 : 1/6), (1/6 : 2/3 : 1/6), (1/6 : 1/6 : 2/3). The mixture of (1/3 : 1/3 : 1/3) (β : α2 : MH) was prepared in triplicate.

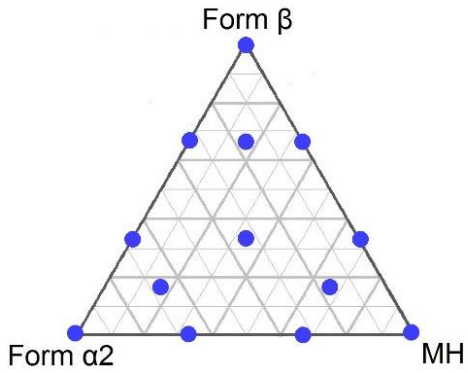


**Figure 12** Mixture design employed in the experiments.

#### *4.2.4.2 Time-gated Raman measurements*

Raman spectra of the mixtures of different solid-state forms of piroxicam were collected with a TimeGated® TG532 M1 Raman spectrometer (TimeGate Instruments Oy, Finland) coupled with a BWTek sampling probe with a focal spot size of approximately 85 µm (**Figure 13**). The Raman instrument was equipped with a picosecond pulsed laser, a CMOS SPAD array detector, and the sampling probe. The excitation source was a 532 nm Nd:YVO microchip pulsed laser, the average power used was 14 mW, repetition rate 40 kHz, pulse width 150 ps, focus diameter 50 µm, pulse energy 0.35 µJ, peak power (after the probe) 35 mW, and maximum irradiance 28 MW $cm^{-2}$.

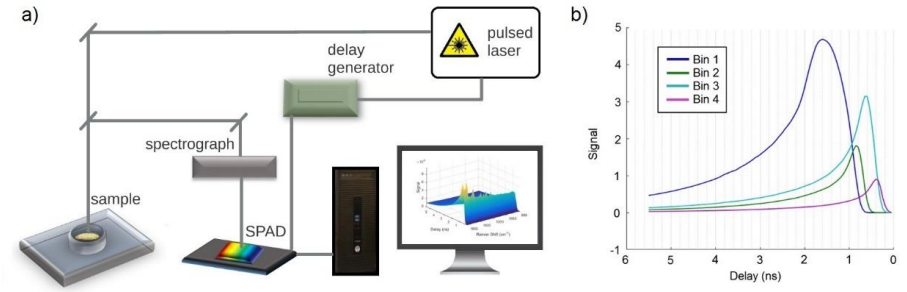


**Figure 13** a) The time-gated Raman instrument used for obtaining the Raman spectra and performing the fluorescence rejection, and b) basis for bin 3 selection; the 4 bins collect the scattered photons with different delays and intensity of the obtained signal varies. Bin 3 provided the strongest signal at the optimal time-frame for detection of Raman scattered photons for piroxicam.

The detector used was a 128 × (2) × 4 CMOS SPAD matrix detector (Kostamovaara *et al.*, 2013). An internal time histogram consisting of four bins accumulating single-photon arrivals. Bin 3 provided the strongest Raman signal. The signals collected in bin 3 were used for the data analysis. The time-resolved spectral datasets were collected by sequentially moving the gate in 50 ps steps using the electronic delay generator. Raman spectra with fluorescence rejection and time-resolved fluorescence spectra were acquired simultaneously. The spectra were obtained from the Raman shift range of 700 $cm^{-1}$ to 1700 $cm^{-1}$ up to 5 ns. For the chemometric data analysis, the time-frame was selected by choosing the location of the Raman peaks from the time-domain (at 0.4 - 0.8 ns).

The measurements were conducted in triplicate and the focal point was moved between each measurement to acquire a more representative signal over a larger area of the sample. The measurements were carried out at ambient temperature, lighting, and humidity. Cyclohexane was used as a reference standard to monitor wavenumber accuracy. Data acquisition software and setup control were carried out by the software provided with the instrument (TimeGated® Model 1).

The applicability of time-gated Raman spectroscopy for particles produced with CESS process was investigated. The crystal form of piroxicam produced with the CESS process can be modified by changing the process parameters (new data). Particles produced with modified parameters (60 °C, 210 bar, and 80 bar) were imaged with SEM and were investigated with the time-gated Raman analysis described above.

#### *4.2.4.3 Data analysis*

Part of the fluorescence was rejected from the signal by the time-gated detection system using the data obtained from bin 3 data. Residual photoluminescence signal was removed using the software provided with the instrument (TimeGated® Model 1). This was performed by selecting a time-frame by manually choosing the location of the Raman peaks from the time-domain (at 0.4 - 0.8 ns) and carrying out baseline correction. The baseline correction was performed using adaptive iteratively reweighted penalized least squares and local minima fitting algorithms and the model parameters being selected based on visual appearance. Through these procedures, the recorded 3D data was transformed into conventional 2D Raman spectra, which could then be analyzed with established PLS analysis.

Multivariate data analysis was carried out using SIMCA-P multivariate data analysis software (v. 13.0.3, Umetrics AB, Sweden). Principal component analysis was used for qualitative analysis and standard PLS regression for quantitative modeling (Martens and Naes, 1992). PLS maximizes the covariance between the information variation in two data matrices, X (here, the spectral variation) and Y (here, the sample composition), by a multivariate model (Wold and Sjöström, 1977). The performance of the models was evaluated by $R^2X(cum)$, $R^2Y(cum)$, $Q^2(cum)$, and mean RMSE obtained by leave-one-out cross validation. SNV (Barnes *et al.*, 1989) was used to pre-treat the data. SNV removes spectral features uncorrelated with the chemical composition of the sample, such as baseline shifts, resulting in more coherent spectra. Additionally, spectroscopic data were subjected to mean centering prior to PLS analysis.

# 5 RESULTS AND DISCUSSION

## 5.1 PROPERTIES OF MICROPARTICLES PRODUCED WITH MICROFLUIDICS (I)

The morphology studies with SEM indicated that the PCL microcapsules were spherical, intact, and monodisperse in size (**Figure 14**). Furthermore, the microcapsules appeared to have non-porous structure and smooth surface. Non-porous structure inhibits a fast release of the drug from the microcapsules (Scala-Bertola *et al.*, 2012); PCL particles prepared in other studies also had similar surface properties and intact form (Bolzinger *et al.*, 2007, Hnaien *et al.*, 2011, Jeong *et al.*, 2003, Somavarapu *et al.*, 2005).

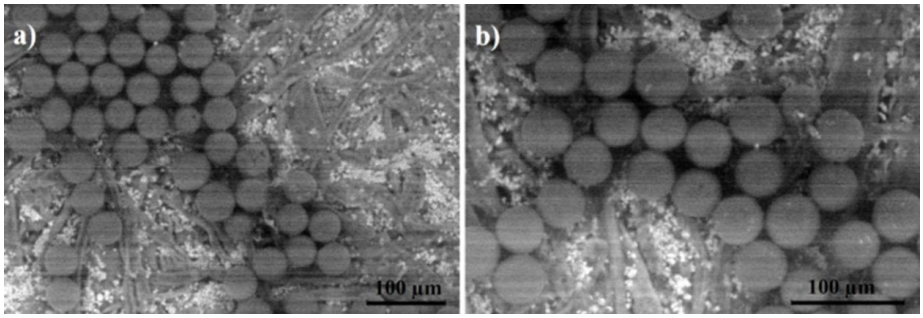


**Figure 14** SEM images of PCL microcapsules: a) 506x magnification taken at chamber pressure of 682 Pa with 26 kV; and b) 735x magnification of different particles of the same batch with the same pressure and voltage. The microparticles appeared to have a non-porous structure, smooth surface and were monodisperse in size.

The particle size of the microcapsules produced by microfluidics varied from 23 - 47 µm depending on the device used for the preparation of the batch. The average diameter of the microcapsules was 39 ± 10 µm ($n$ = 100, 5 batches), the particle size variation within each batch was moderate. The short time stability tests indicated that the particles were stable up to 4 weeks. The collapse rate of the particles after that was approximately 15% per week.

All microcapsules produced and collected contained the inner phase and the middle phase. **Figure 15** shows the confocal fluorescence microscopy images of the microcapsules showing the presence of the inner phase stained in green with FITC-dextran and the middle phase stained in red by perylene. By employing two different dyes, the inner phase and the middle phase were clearly distinguished in the confocal images. The confocal images indicate that all the content of the inner phase, FITC-dextran or BSA, is located within the microcapsule structure. The middle phases of the particles were evenly distributed along the inner phases, and the particles prepared were fairly monodisperse. Thus, monodisperse microcapsules were successfully prepared

using this methodology and effective formation of a double emulsion structure was also an indication of high EE and precision of the preparation process.

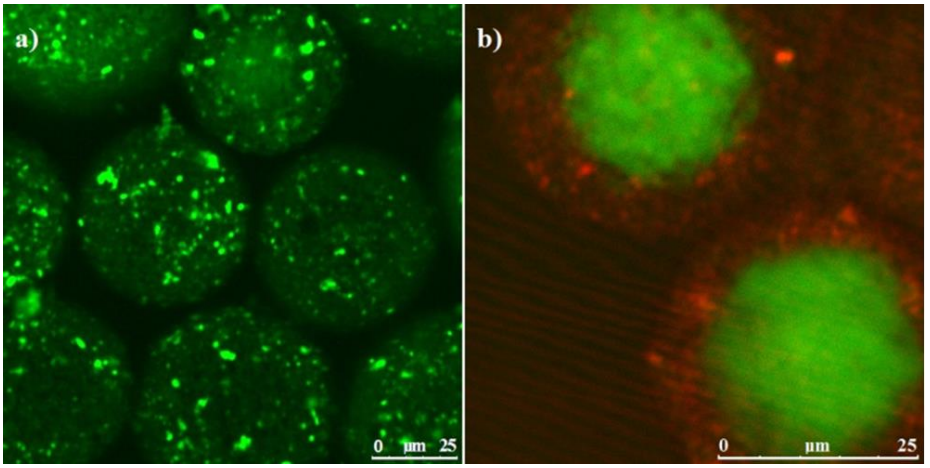


**Figure 15** Confocal fluorescence microscopy images of a) PCL microcapsules encapsulating FITC-dextran (green), and b) PCL particles with FITC-dextran (green) in the inner phase and perylene (red) in the middle phase.

The average EE for BSA was 84.0 ± 10.5% ($n$ = 3). The results of the EE experiment were reproducible and the variation between the parallel tests was moderate. EE is often dependent on the particle size and for the size range of the microcapsules prepared in this study, an EE of 84% is difficult to achieve. In several previous studies the EE for similar or smaller particle size ranges were at the highest approximately ca. 40 - 60% (Bolzinger *et al.*, 2007, Hnaien *et al.*, 2011, Scala-Bertola *et al.*, 2012, Somavarapu *et al.*, 2005). Other studies indicated poorer EE with the highest being barely ca. 40% (Hnaien *et al.*, 2011). Generally, an EE of 70% is considered high, even for significantly larger particles. For example, PCL particles prepared with a flow-focused jetting cell achieved an EE of 42 - 79% (Cheng *et al.*, 2010). Thus, PCL microcapsules produced here with microfluidics were superior to previously reported particles in terms of EE.

These results indicate that the microfluidic preparation method is very efficient and additional energy input is not necessary in order to achieve excellent EE. Thus, this method is therefore potentially suitable for protein encapsulation. Furthermore, when using expensive therapeutics, such as protein and peptide drugs, high EE may minimize material loss during the preparation process and create cost-effective manufacturing. However, the process requires using organic solvents for the polymers in the oil phase. Production of a microcapsule structure for poorly water-soluble molecules requires an o/w/o/w emulsion, which complicates the structure of the microfluidic device. Furthermore, the process is not optimal for upscaling, since the drops are formed one by one and thus the only upscaling option is contructing parallel microfluidic devices.

## 5.2 PROPERTIES OF NANOPARTICLES PRODUCED WITH CONTROLLED EXPANSION OF SUPERCRITICAL SOLUTIONS (II)

In the nanoparticle production with CESS, the pressure, flow, and rate of solid dispersion formation within the collection chamber were successfully kept constant. Hence the collection and particle production processes were stable. The robustness, stability, and reproducibility of the process were proven by preparing three batches of similar product. The SEM images obtained from different parts of each sample indicate that the nanoparticles prepared from piroxicam were monodisperse in size and shape. The average nanoparticle diameter was 176 nm ± 53 nm, the batches 169 ± 48 nm ($n$=300), 179 nm ± 54 nm ($n$=300), and 179 nm ± 67 nm ($n$=300) (**Figure 16**). The particle size of the bulk was 7106 ± 5639 nm ($n$=300). The nanoparticles were significantly smaller than the particles in the bulk. The size distribution was narrow and the formed particles were slightly elongated. In the literature, piroxicam has been micronized with RESS, resulting in particles with Ø=1.52 – 8.78 μm (Hezave and Esmaeilzadeh, 2012).

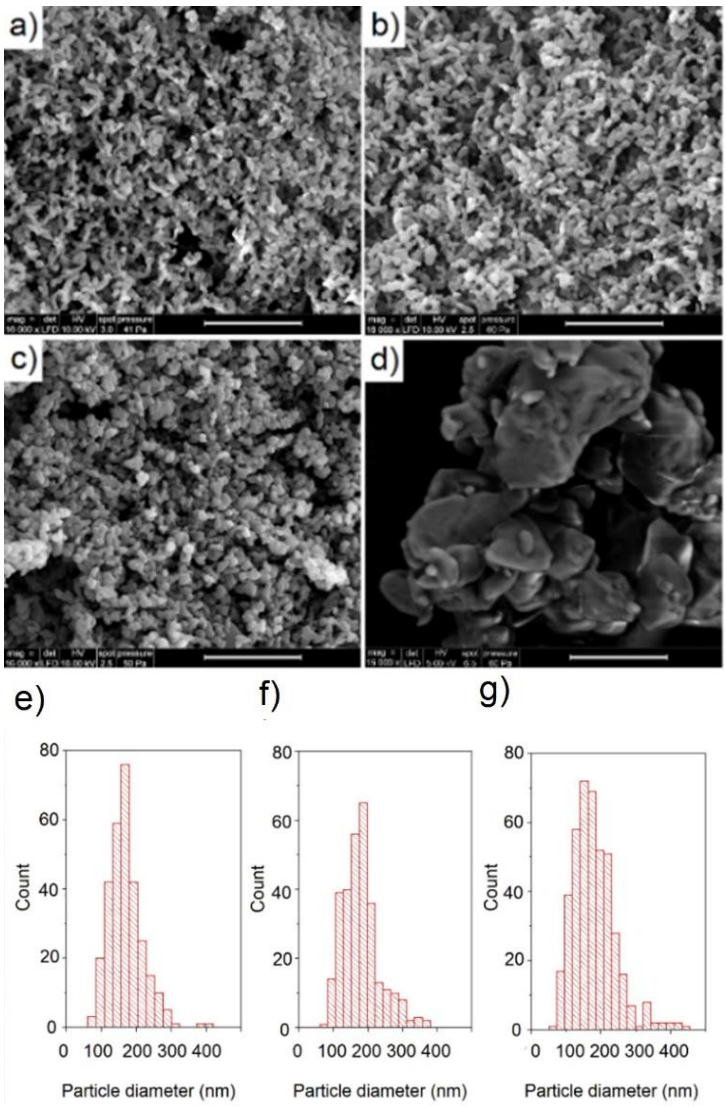


**Figure 16** Nanoparticles and bulk piroxicam: a) batch 1, b) batch 2, c) batch 3, and d) bulk piroxicam. The size bar is 5 µm. Particle size distributions with mean particle size and standard deviations for a) batch 1, b) batch 2, and c) batch 3.

In RESS, the rapid $scCO_2$ expansion is considered essential for producing small particles (Keshavarz *et al.*, 2012, Pathak *et al.*, 2004, Huang and Moriyoshi, 2006, Türk, 2014). The nanoparticles prepared in this research suggest otherwise. The precipitation process does not have to be fast to produce small, monodisperse particles; neither does the pressure decrease need to be rapid, nor is there a need to use ultra-high pressures.

### 5.2.1 PRINCIPLE OF THE CONTROLLED EXPANSION OF SUPERCRITICAL SOLUTIONS

The decrease in the solvent power of $CO_2$, caused by the pressure drop, initiates nucleation at the needle valve and particle formation occurs in the outlet tube. The limited outlet tube volume, 1 mL, inhibits expansion $scCO_2$ which keeps the degree of supersaturation moderate. The size of the initial nuclei is larger, and the number of nuclei is lower than in the RESS process. Condensation is the main mechanism for particle growth within the outlet tube. In the outlet tube there are the formed nuclei and free piroxicam molecules. As the generated nuclei are transported through the outlet tube, piroxicam molecules precipitating out of the $scCO_2$ phase are deposited onto the nuclei, and the particles grow. The condensation step in the CESS system is optimized by keeping the outlet tube short while securing the ability to maintain the desired pressure.

In CESS, the focus is on achieving slower mass flow than in RESS and limited mass transfer. The ratio of pressure before and after each pressure drop is kept below ten. This prevents the flow speed beyond the nozzle from reaching sonic velocity, and thus there is neither a Mach disk nor density differences in the collection chamber as in the RESS process. Consequently, particle growth by coagulation is reduced. Particles form under milder conditions than in most particle technologies, and particle formation and growth is thus much slower than in RESS, and the particles form in a controlled environment.

The CESS process itself is more robust, stable, and reproducible than the RESS process; the pressure and flow, as well as the production rate, are constant, and the environment for particle formation between processes is identical. In contrast to RESS, small changes in initial pressure and temperature do not affect the end-product (Huang *et al.*, 2014). The CESS process produces small particles without use of co-solvents, excipients, and collection into aqueous media.

A disadvantage of the CESS approach is the larger initial nuclei size. This can be addressed for example by altering the thermodynamics of the process by laser ultrasound. Furthermore, additional pressure drop steps, other supercritical solvents, and alternative collection methods can be introduced to the process. The production and the production rate can be increased. The process itself permits up-scaling. The advantage in upscaling of the CESS process, when compared to for example the microfluidic technology, is that all the nuclei are formed at once and the quantity of forming nuclei can be increased by increasing the size of features of the device used.

## 5.3 DISSOLUTION TESTING WITH THE LYOPHILIC MATRIX METHOD (III)

### 5.3.1 PROPERTIES OF THE MATRIX

No visual changes were detected in the size, topology, and morphology of the cotton fibers as the matrix was exposed to dissolution medium, nor did the structure of the cotton change after drying (**Figure 17**). When immersed into the medium, the cotton matrix was wetted in 0.31 s ± 0.10 s. The matrix withdrew medium approximately 23 times its weight. The matrix volume increased when exposed to the medium. However, microscope studies indicated that the single fibers do not swell when immersed into the medium.

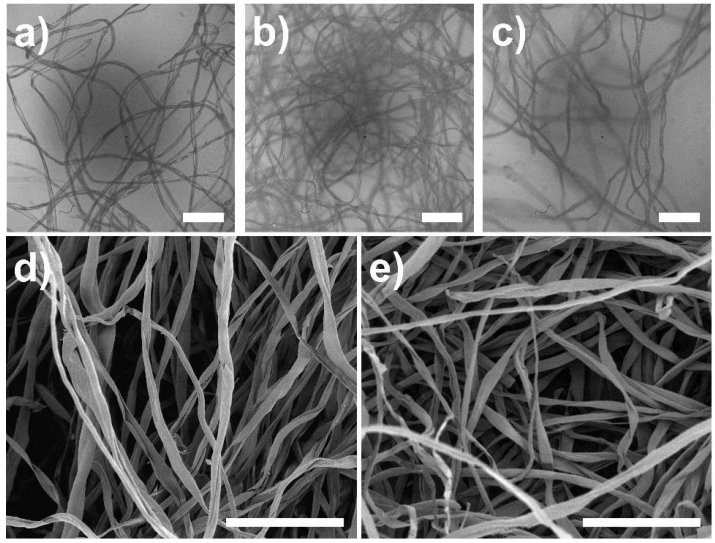


**Figure 17** Light microscope images of the cotton matrix a) prior to dissolution medium exposure, b) exposed to the medium, and c) after medium exposure. SEM images of the cotton d) prior to medium exposure, and e) after medium exposure. Scale bars correspond to 200 µm.

No retained indomethacin was found in the matrix at 22 hours in the partition coefficient tests. The concentrations obtained were below the detection limit (0.08 mg/L) of the HPLC method. This indicates that > 99.2% of indomethacin is released from the matrix and that the dissolved species is not significantly retained within the matrix. The inverse partition coefficient test showed no detectable change in concentration when the matrix was immersed into the medium with dissolved indomethacin. Based on the detection limit of the online measurement device, the possible undetected change in the concentration is < 2.3%. This indicates that > 97.7% of the dissolved species is

not affected by the immersion of the matrix and that the matrix does not significantly absorb dissolved indomethacin from the dissolution medium.

As shown in the characterization tests, the matrix is practically inert and has little effect on the total quantity of indomethacin released, and the particles within the matrix are exposed to the medium immediately after immersion (**Table 4**). As the pH has no effect on the partition coefficient, we conclude that at least with indomethacin - a weak acid ($pK_a$ 4.5) - the change in the pH of the medium causes no adsorption onto the fibers. The partitioning coefficient studies were conducted only in regard to the dissolved species. The possible adhesion is not considered to be an issue since the non-dissolved particles should remain within the matrix.

**Table 4** *Investigated matrix properties.*

| Property | Experiment | Result |
|---|---|---|
| Intake of medium | Weighing | 23 x mass of the matrix |
| Wetting time of the matrix | Fast camera tests | 0.31 ± 0.10 s |
| Impact of medium on morphology | Imaging | No impact |
| Adsorption of dissolved species to matrix (from particles) | Partition coefficient | Less than 0.8% |
| Adsorption of dissolved species to matrix (from media) | Inverse partition coefficient | Less than 2.3% |

### 5.3.2 DRUG RELEASE

The average size of the nanoparticles was 424 nm ± 236 nm, and of the bulk powder 20.3 µm ± 30.0 µm, featuring a size range of 1 µm - 272 µm. The average size of the small fraction was 17.4 µm ± 11.6 µm, while that of the large fraction was 22.1 µm ± 21.8 µm.

Differences in dissolution rate as a function of particle size and pH were evident in the dissolution profiles obtained with the LM method. **Figure 18** shows the cumulative release of the small and large size fractions of indomethacin nanoparticles in pH 5.5, as well as nanoparticles and bulk indomethacin in pH 7.4, up to 30 min. The short lag times of less than 1 minute indicated rapid wetting of the samples and absence of any significant membrane effect caused by a diffusion barrier. Monotonously increasing dissolution profiles and constant standard deviations indicate that the variation between aliquots is moderate, i.e. that no substantial withdrawal of particles occurred during sampling. The method was accurate with small sample quantities, and differences between the dissolution rates were detected within 5 minutes from the start of the experiment as seen in the dissolution profiles.

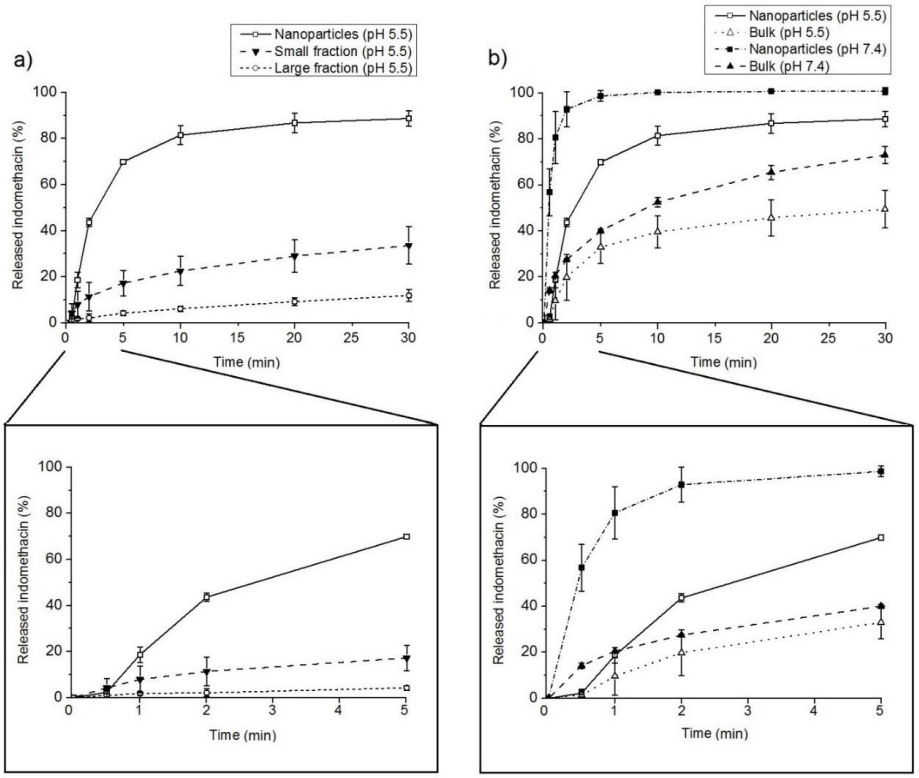


**Figure 18** Cumulative release (%) of indomethacin a) nanoparticles, small fractions and large fraction in pH 5.5 up to 30 min and 5 min at 37.0 ± 0.5 °C, b) nanoparticles and bulk in pH 5.5 and 7.4 up to 30 min and 5 min at 37.0 ± 0.5 °C. Error bars are standard deviations of three parallel measurements.

The LM method distinguished the dissolution rates of bulk piroxicam and the nanoparticles (**Figure 19**) (new data). Processing piroxicam with CESS significantly increases the dissolution rate due to increased surface area.

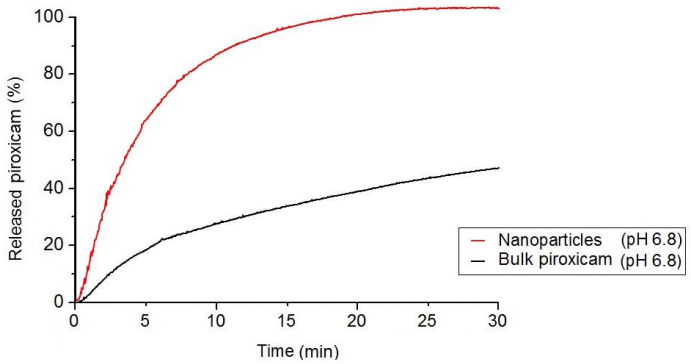


**Figure 19** The dissolution rates of the bulk piroxicam and the nanoparticles in phosphate buffer at pH 6.8 up to 30 min.

### 5.3.3 PRINCIPLE OF THE LYOPHILIC MATRIX METHOD

The key factor of the LM method is its ability to separate non-dissolved particles from dissolved species and its ability to prevent dispersion of the particulates without presenting a significant membrane effect. The dissolved species exit the matrix, whereas the non-dissolved particles remain within the matrix (**Figure 20**).

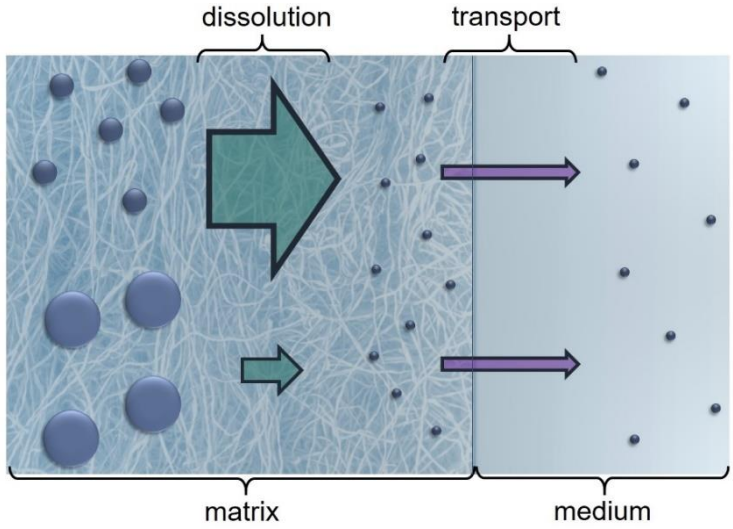


**Figure 20** Dissolved species (small spheres) diffuse promptly into the medium, whereas the non-dissolved particles remain in the matrix (medium size and large spheres). Smaller particles (medium size spheres) dissolve to faster than larger particles (large spheres).

Instead of dispersing the particles into the dissolution medium or exchanging the medium through a barrier, the matrix fixes the position of the non-dissolved particles and brings the medium to the particles. In the LM method, the particles are dissolved from a stationary point in a semi 2-dimensional system under sink conditions. The efficient intake of the medium, the concentration gradient, and the mild convection induced in the vessel drive the dissolved species out of the matrix. The matrix forms no separate compartment in the dissolution vessel, and the lack of interaction between the cotton fibers and the model compound ensures that the dissolved species is not trapped in the matrix.

The dissolution of the particles within the matrix is initiated as the matrix absorbs medium. The whole particle population is wetted nearly simultaneously. The dissolution rate depends on the active surface area of the particles as described by the Nernst-Brunner equation and the radius and particle curvature as described by the Gibbs-Kelvin equation (Nernst, 1904, Thomson, 1871, Brunner, 1904). The equations predict that small particles dissolve faster than large ones.

The results demonstrate that the LM method neither overestimates the dissolution rates due to particle dispersion, nor induces substantial lag times. The ability to produce realistic dissolution data supports early formulation development, which is valuable for evaluation of advantages gained by particle size reduction. Small sample-to-sample variation produces reliable results with small inter- or intra-laboratory variation. Consequently, dissolution testing with lyophilic matrices produces realistic estimates of dissolution rates of nanoscale particles. Further studies are needed to determine whether the LM method is universally applicable as well as assess the dissolution rate for different substances and investigate the degree of IVIV-correlation.

## 5.4 QUANTITATIVE ANALYSIS WITH TIME-GATED RAMAN SPECTROSCOPY (IV)

### 5.4.1 TERTIARY MIXTURES

XRPD, FTIR, and DSC analyses confirmed complete polymorph conversion of piroxicam form β (BIYSEH13) (Shi *et al.*, 2016) to form α2 (BIYSEH06) (Vrečer *et al.*, 2003) and MH (CIDYAP02) (Shi *et al.*, 2016). No impurities were detected. SEM images show clear differences between the solid-state forms (**Figure 21**). Additionally, principal component analysis (**Figure 24**) of the Raman data showed clear differences for all mixtures with no overlap of the sample clusters observed.

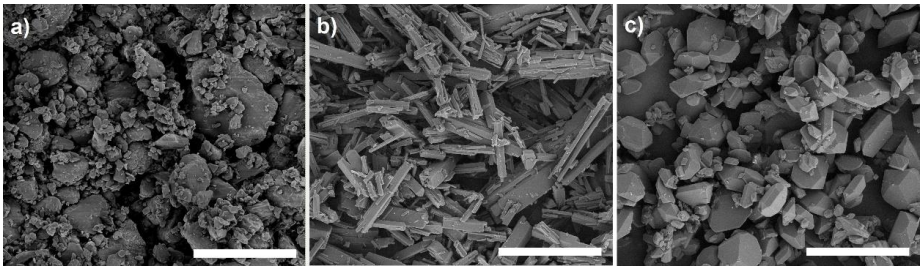


**Figure 21** SEM images of the piroxicam crystal form used in this study, a) form β, b) form α2, and c) MH. Scale bars correspond to 40 µm.

### 5.4.2 RAMAN SPECTRA AND FLUORESCENCE REJECTION

The fluorescence rejection with the time-gated Raman spectroscopy resulted in 2D spectra with fluorescence-free baselines (**Figure 22**). Prior to the fluorescence rejection, the peaks characteristic to piroxicam were not shown and the intensity fluctuation was significantly greater. The characteristic peaks of the solid-state forms of piroxicam have previously been predicted with

density functional theory calculations and match those observed in previous experimentally recorded spectra (Redenti *et al.*, 1999, Suresh *et al.*, 2015).

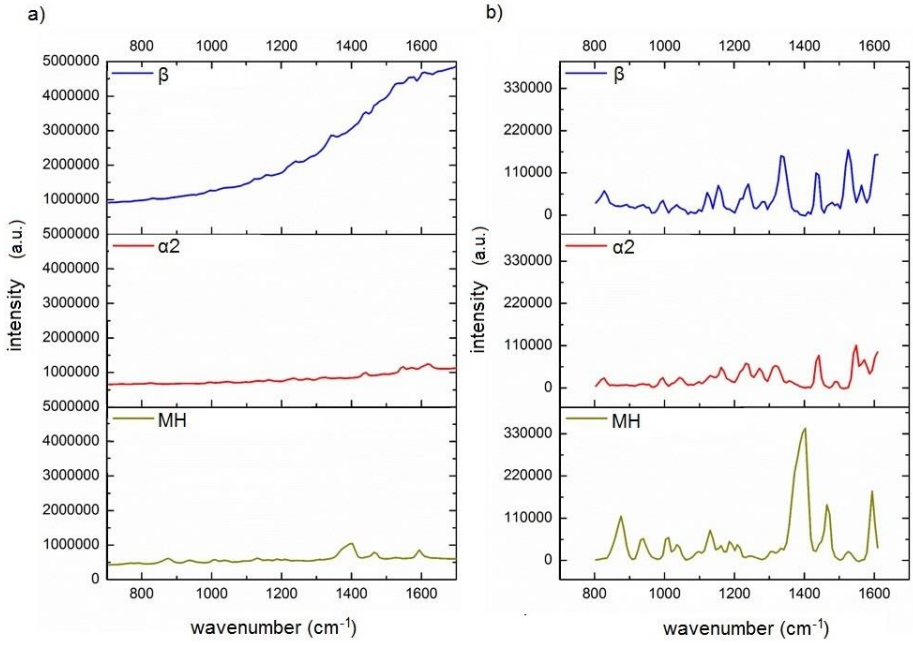


**Figure 22** 2D spectra obtained with time-gated Raman setup as a) sum spectra containing the fluorescence signal, and b) spectra after fluorescence rejection.

The raw 3D spectra recorded with the time-gated instrument, the subtracted 3D fluorescence spectra and the 3D Raman spectra after fluorescence rejection from piroxicam form β, form α2 and the MH are presented in **Figure 23**. The three solid-state forms of piroxicam fluoresced to varying degrees. After subtracting the fluorescence spectra from the Raman spectra, very little fluorescence signal was observed. The 3D data indicates the starting point of the Raman signal immediately after the laser pulse, as well as the fluorescence starting-point and the fluorescence tail.

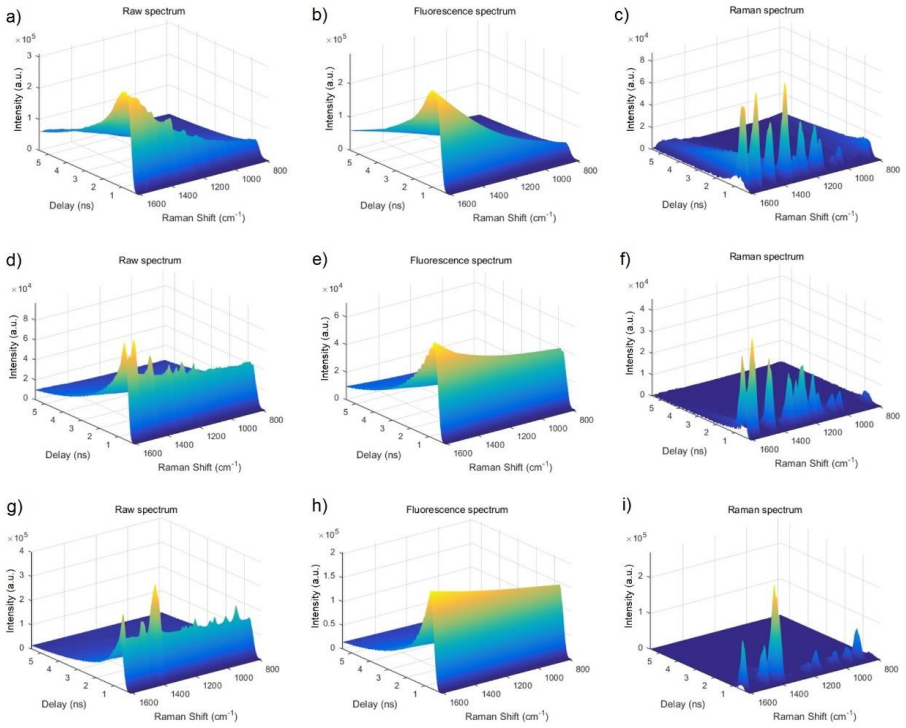


**Figure 23** 3D spectra obtained with time-gated Raman: a) raw 3D spectrum (form β), b) subtracted baseline spectrum (form β), c) Raman spectrum (form β), d) raw 3D spectrum (form α2), e) subtracted baseline spectrum (form α2), f) Raman spectrum (form α2), g) raw 3D spectrum (MH), h) subtracted baseline spectrum (MH), and i) Raman spectrum (MH).

### 5.4.3 QUANTITATIVE ANALYSIS OF THE TERTIARY MIXTURES

Traditional PLS models with two factors based on the SNV transformed Raman shift (2D) data resulted in an overall RMSE value of 4.1%, consisting of mean RMSEs of 4.1% (form β), 4.5% (form α2) and 3.8% (MH) (**Table 5**).

**Table 5** *Pre-treatment methods, PLS factors, $R^2X$(cum), $R^2Y$(cum), $Q^2$(cum), and mean RMSE values data analysis performed with conventional PLS using SIMCA software.*

| Solid-state form | Pre-treatment | PLS factors | $R^2X$ (cum) | $R^2Y$ (cum) | $Q^2$ (cum) | Mean RMSECV (%) |
|---|---|---|---|---|---|---|
| Form β | SNV, mean centering | 4 | 0.997 | 0.982 | 0.977 | 4.1 |
| Form α2 | | | | | | 4.5 |
| MH | | | | | | 3.8 |

Time-gated Raman was found applicable for investigating the crystal form of piroxicam particles produced with CESS (new data). SEM images of the particles produced with modified process parameters clearly indicate changed morphology of the particles compared to **Figure 16** and principal component analysis indicated that the CESS particles produced with altered parameters were a mix of form β and form α2 (**Figure 24**).

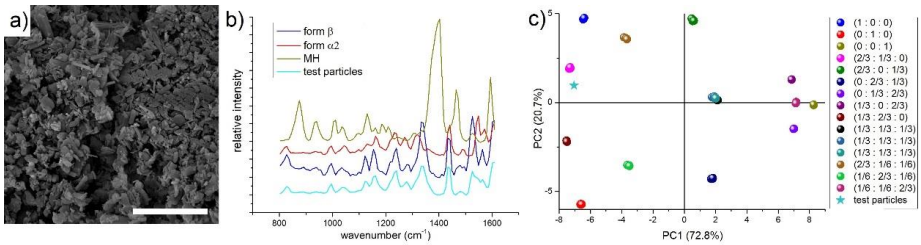


**Figure 24** a) Effect of parameter modification on the CESS particles, size bar corresponds to 5 µm, b) spectra of piroxicam form β, form α2, MH, and the CESS particles produced with modified parameters, and c) principal component analysis of the CESS particles produced with modified parameters, mixture ratios of (β : α2 : MH).

The time-gated Raman instrument enabled robust fluorescence rejection that does not require substance specific calibration or suppression methods. Accurate quantitative analysis with algorithm-treated data is useful for relatively routine solid-state analysis of photoluminescent pharmaceuticals during drug development and manufacturing. Raman spectroscopy is suitable for focusing on the properties of the API in mixtures and pharmaceutical products. This is because the functional moieties present in common APIs typically produce stronger Raman signals than the structures in common excipients (Smith and Dent, 2013). Furthermore, many excipients (e.g. cellulose-based polymers) can also fluoresce, which would restrict conventional Raman analysis of dosage forms containing such excipients. The time-gated measurement can be performed in ambient lighting, enabling analysis during pharmaceutical processing. Thus, the time-gated Raman spectroscopy approach used in this study provides a feasible system for process monitoring in pharmaceutical manufacturing. Even though the piroxicam Raman bands were observable without the fluorescence rejection, the quality of the analysis was significantly improved by the fluorescence rejection. Furthermore, the quantitative analysis system established in this study is applicable to more strongly fluorescing systems, as well as, for example, samples with high water contents, such as proteins, biological and biochemical samples.

Altogether, the capability of the time-resolved Raman and fluorescence measurements with a CMOS SPAD detector for quantitative analysis shows promise in diverse areas, including fundamental chemical research, the pharmaceutical setting, process analytical technology, and the life sciences.

# 6 CONCLUSIONS

Controlled particle formation investigated in this thesis work created opportunities for sophisticated formulation development. The drop-by-drop microfluidic technique has potential for engineering and manufacturing drug delivery systems for therapeutic proteins (I) whereas increased control implemented to expansion of supercritical solutions produced nanoparticles with narrow size distribution (II). The dissolution rates (III) and solid-state properties (IV) of the nanoparticles produced were investigated with the lyophilic matrix method developed in this research and time-gated Raman spectroscopy, respectively.

A novel crystallization process that employs $scCO_2$ and offers significant advantages compared to existing $scCO_2$ techniques was established. Controlled Expansion of Supercritical Solutions (CESS) with two-step gradient pressure reduction permits production of pure drug nanoparticles with a narrow size distribution. CESS is a method to produce nanoparticles that contain no excipients or organic solvents. Whereas the aim of the Rapid Expansion of Supercritical Solutions (RESS) process is to produce a rapid pressure drop and particle formation, CESS forms particles in a controlled manner. Uniform nanoparticles are produced and collected efficiently, and the process is robust and up-scalable (II).

Dissolution rates of particulate systems were investigated by the Lyophilic Matrix (LM) method developed in this research. The method features a short lag time, small sample-to-sample variation, and monotonously increasing dissolution profiles. The LM method discriminated between the dissolution rates of the tested particle size fractions. The inert cotton matrix permitted release studies without a substantial diffusion barrier, it avoided dispersion of the non-dissolved particles and rapidly wetted the sample (III).

Time-gated Raman spectroscopy was found to be a useful tool for quantifying powder mixtures of fluorescent materials. Standard multivariate analysis techniques allowed precise quantitative analysis after the rejection of fluorescence. Time-gated Raman spectroscopy shows potential for relatively routine quantitative solid-state analysis of photoluminescent pharmaceuticals during drug development and manufacturing (IV).

# REFERENCES


Abbaspourrad, A., Datta, S. S. & Weitz, D. A. (2013) Controlling release from pH-responsive microcapsules. *Langmuir,* **29** (41), 12697-12702.

Abdel-Mottaleb, M. M. & Lamprecht, A. (2011) Standardized in vitro drug release test for colloidal drug carriers using modified USP dissolution apparatus I. *Drug Development and Industrial Pharmacy,* **37** (2), 178-184.

Abouelmagd, S. A., Sun, B., Chang, A. C., Ku, Y. J. & Yeo, Y. (2015) Release kinetics study of poorly water-soluble drugs from nanoparticles: are we doing it right? *Molecular Pharmaceutics,* **12** (3), 997-1003.

Adams, L., Kodger, T. E., Kim, S.-H., Shum, H. C., Franke, T. & Weitz, D. A. (2012) Single step emulsification for the generation of multi-component double emulsions. *Soft Matter,* **8** (41), 10719-10724.

Amidon, G. L., Lennernäs, H., Shah, V. P. & Crison, J. R. (1995) A theoretical basis for a biopharmaceutic drug classification: the correlation of in vitro drug product dissolution and in vivo bioavailability. *Pharmaceutical Research,* **12** (3), 413-420.

Amstad, E., Kim, S. H. & Weitz, D. A. (2012) Photo-and thermoresponsive polymersomes for triggered release. *Angewandte Chemie,* **124** (50), 12667-12671.

Angel, S., DeArmond, M., Hanck, K. & Wertz, D. (1984) Computer-controlled instrument for the recovery of a resonance Raman spectrum in the presence of strong luminescence. *Analytical Chemistry,* **56** (14), 3000-3001.

Anhalt, K., Geissler, S., Harms, M., Weigandt, M. & Fricker, G. (2012) Development of a new method to assess nanocrystal dissolution based on light scattering. *Pharmaceutical Research,* **29** (10), 2887-2901.

Arriaga, L., Amstad, E. & Weitz, D. (2015) Scalable single-step microfluidic production of single-core double emulsions with ultra-thin shells. *Lab on a Chip,* **15** (16), 3335-3340.

Arriaga, L. R., Datta, S. S., Kim, S. H., Amstad, E., Kodger, T. E., Monroy, F. & Weitz, D. A. (2014) Ultrathin shell double emulsion templated giant unilamellar lipid vesicles with controlled microdomain formation. *Small,* **10** (5), 950-956.

Asghari, I. & Esmaeilzadeh, F. (2012) Formation of ultrafine deferasirox particles via rapid expansion of supercritical solution (RESS process) using Taguchi approach. *International Journal of Pharmaceutics,* **433** (1), 149-156.

Atila, C., Yıldız, N. & Çalımlı, A. (2010) Particle size design of digitoxin in supercritical fluids. *The Journal of Supercritical Fluids,* **51** (3), 404-411.

Azarmi, S., Roa, W. & Löbenberg, R. (2007) Current perspectives in dissolution testing of conventional and novel dosage forms. *International Journal of Pharmaceutics,* **328** (1), 12-21.

Barnes, R., Dhanoa, M. S. & Lister, S. J. (1989) Standard normal variate transformation and de-trending of near-infrared diffuse reflectance spectra. *Applied Spectroscopy,* **43** (5), 772-777.

Baseri, H. & Lotfollahi, M. N. (2013) Formation of gemfibrozil with narrow particle size distribution via rapid expansion of supercritical solution process (RESS). *Powder Technology,* **235**, 677-684.

Baxter, J. L., Kukura, J. & Muzzio, F. J. (2005) Hydrodynamics-induced variability in the USP apparatus II dissolution test. *International Journal of Pharmaceutics,* **292** (1), 17-28.

Bell, S. J. & Bourguignon, E. O. (1998) Analysis of luminescent samples using subtracted shifted Raman spectroscopy. *Analyst,* **123** (8), 1729-1734.
Bhardwaj, U. & Burgess, D. J. (2010) A novel USP apparatus 4 based release testing method for dispersed systems. *International Journal of Pharmaceutics,* **388** (1), 287-294.
Bhattachar, S. N., Wesley, J. A., Fioritto, A., Martin, P. J. & Babu, S. R. (2002) Dissolution testing of a poorly soluble compound using the flow-through cell dissolution apparatus. *International Journal of Pharmaceutics,* **236** (1), 135-143.
Blakesley, J., See, P., Shields, A., Kardynał, B., Atkinson, P., Farrer, I. & Ritchie, D. (2005) Efficient single photon detection by quantum dot resonant tunneling diodes. *Physical Review Letters,* **94** (6), 067401.
Bleich, J., Müller, B. & Wassmus, W. (1993) Aerosol solvent extraction system—a new microparticle production technique. *International Journal of Pharmaceutics,* **97** (1-3), 111-117.
Bocanegra, L., Morris, G., Jurewicz, J. & Mauger, J. (1990) Fluid and particle laser Doppler velocity measurements and mass transfer predictions for the USP paddle method dissolution apparatus. *Drug Development and Industrial Pharmacy,* **16** (9), 1441-1464.
Bolten, D. & Türk, M. (2012) Micronisation of carbamazepine through rapid expansion of supercritical solution (RESS). *The Journal of Supercritical Fluids,* **62,** 32-40.
Bolzinger, M., Bordes, C., Gauvrit, J. & Briançon, S. (2007) Improvement of a bovine serum albumin microencapsulation process by screening design. *International Journal of Pharmaceutics,* **344** (1), 16-25.
Brittain, H. G. (1997) Spectral methods for the characterization of polymorphs and solvates. *Journal of Pharmaceutical Sciences,* **86** (4), 405-412.
Brown, C. K., Chokshi, H. P., Nickerson, B., Reed, R. A., Rohrs, B. R. & Shah, P. A. (2004) Dissolution testing of poorly soluble compounds. *Pharmceutical Technology,* **28,** 56-43.
Brunner, E. (1904) Reaktionsgeschwindigkeit in heterogenen Systemen. *Zeitschrift für Physikalische Chemie,* **43,** 56–102.
Calvo, P., Vila-Jato, J. L. & Alonso, M. J. (1996) Comparative in vitro evaluation of several colloidal systems, nanoparticles, nanocapsules, and nanoemulsions, as ocular drug carriers. *Journal of Pharmaceutical Sciences,* **85** (5), 530-536.
Campardelli, R., Adami, R., Della Porta, G. & Reverchon, E. (2012) Nanoparticle precipitation by supercritical assisted injection in a liquid antisolvent. *Chemical Engineering Journal,* **192,** 246-251.
Chandra, R. & Rustgi, R. (1998) Biodegradable polymers. *Progress in Polymer Science,* **23** (7), 1273-1335.
Chang, C. & Randolph, A. (1989) Precipitation of microsize organic particles from supercritical fluids. *AIChE Journal,* **35** (11), 1876-1882.
Chattopadhyay, P., Huff, R. & Shekunov, B. Y. (2006) Drug encapsulation using supercritical fluid extraction of emulsions. *Journal of Pharmaceutical Sciences,* **95** (3), 667-679.
Chauhan, B., Shimpi, S. & Paradkar, A. (2005) Preparation and characterization of etoricoxib solid dispersions using lipid carriers by spray drying technique. *AAPS PharmSciTech,* **6** (3), E405-E409.
Chen, D., Chen, H., Bei, J. & Wang, S. (2000) Morphology and biodegradation of microspheres of polyester–polyether block copolymer based on polycaprolactone/polylactide/poly (ethylene oxide). *Polymer International,* **49** (3), 269-276.
Chen, Z.-P., Li, L.-M., Jin, J.-W., Nordon, A., Littlejohn, D., Yang, J., Zhang, J. & Yu, R.-Q. (2012) Quantitative analysis of powder mixtures by

Raman spectrometry: the influence of particle size and its correction. *Analytical Chemistry,* **84** (9), 4088-4094.
Cheng, X., Liu, R. & He, Y. (2010) A simple method for the preparation of monodisperse protein-loaded microspheres with high encapsulation efficiencies. *European Journal of Pharmaceutics and Biopharmaceutics,* **76** (3), 336-341.
Chidambaram, N. & Burgess, D. (1999) A novel in vitro release method for submicron-sized dispersed systems. *The AAPS Journal,* **1** (3), 32-40.
Cho, E. J., Holback, H., Liu, K. C., Abouelmagd, S. A., Park, J. & Yeo, Y. (2013) Nanoparticle characterization: state of the art, challenges, and emerging technologies. *Molecular Pharmaceutics,* **10** (6), 2093.
Choi, C. H., Lee, H., Abbaspourrad, A., Kim, J. H., Fan, J., Caggioni, M., Wesner, C., Zhu, T. & Weitz, D. A. (2016) Triple Emulsion Drops with An Ultrathin Water Layer: High Encapsulation Efficiency and Enhanced Cargo Retention in Microcapsules. *Advanced Materials*.
Chu, L. Y., Utada, A. S., Shah, R. K., Kim, J. W. & Weitz, D. A. (2007) Controllable monodisperse multiple emulsions. *Angewandte Chemie International Edition,* **46** (47), 8970-8974.
Cohen, J. L., Hubert, B. B., Leeson, L. J., Rhodes, C. T., Robinson, J. R., Roseman, T. J. & Shefter, E. (1990) The development of USP dissolution and drug release standards. *Pharmaceutical Research,* **7** (10), 983-987.
Colthup, N., Daly, L. & Wiberley, S. (1990) *Introduction to Infrared and Raman Spectroscopy*. Academic Press, Inc., San Diego.
Cooper, E. R. (2010) Nanoparticles: a personal experience for formulating poorly water soluble drugs. *Journal of Controlled Release,* **141** (3), 300-302.
Cortopassi, A., Ferrara, P. J., Wawiernia, T. M. & Essel, J. T. (2008) Synthesis of nano-sized rdx using an ultra-high-pressure RESS system. *International Journal of Energetic Materials and Chemical Propulsion,* **7** (1), 39-54.
Cox, D. C. & Furman, W. B. (1984) Collaborative study of the USP dissolution test for prednisone tablets with apparatus 2. *Journal of Pharmaceutical Sciences,* **73** (5), 670-676.
Cox, D. C., Wells, C. E., Furman, W. B., Savage, T. S. & King, A. C. (1982) Systematic error associated with apparatus 2 of the USP dissolution test II: effects of deviations in vessel curvature from that of a sphere. *Journal of Pharmaceutical Sciences,* **71** (4), 395-399.
Croker, D. M., Hennigan, M. C., Maher, A., Hu, Y., Ryder, A. G. & Hodnett, B. K. (2012) A comparative study of the use of powder X-ray diffraction, Raman and near infrared spectroscopy for quantification of binary polymorphic mixtures of piracetam. *Journal ofPharmaceutical and Biomedical Analysis,* **63**, 80-86.
D'Arcy, D., Corrigan, O. & Healy, A. (2005) Hydrodynamic simulation (computational fluid dynamics) of asymmetrically positioned tablets in the paddle dissolution apparatus: impact on dissolution rate and variability. *Journal of Pharmacy and Pharmacology,* **57** (10), 1243-1250.
D'souza, S. S. & DeLuca, P. P. (2006) Methods to assess in vitro drug release from injectable polymeric particulate systems. *Pharmaceutical Research,* **23** (3), 460-474.
D'Arcy, D. M., Corrigan, O. I. & Healy, A. M. (2006) Evaluation of hydrodynamics in the basket dissolution apparatus using computational fluid dynamics—dissolution rate implications. *European Journal of Pharmaceutical Sciences,* **27** (2), 259-267.

Dalvi, S. V., Azad, M. A. & Dave, R. (2013) Precipitation and stabilization of ultrafine particles of Fenofibrate in aqueous suspensions by RESOLV. *Powder Technology,* **236,** 75-84.
Das, R. S. & Agrawal, Y. (2011) Raman spectroscopy: recent advancements, techniques and applications. *Vibrational Spectroscopy,* **57** (2), 163-176.
Datta, S. S., Abbaspourrad, A., Amstad, E., Fan, J., Kim, S. H., Romanowsky, M., Shum, H. C., Sun, B., Utada, A. S. & Windbergs, M. (2014) 25th anniversary article: double emulsion templated solid microcapsules: mechanics and controlled release. *Advanced Materials,* **26** (14), 2205-2218.
Datta, S. S., Kim, S.-H., Paulose, J., Abbaspourrad, A., Nelson, D. R. & Weitz, D. A. (2012) Delayed buckling and guided folding of inhomogeneous capsules. *Physical Review Letters,* **109** (13), 134301-134304.
Debenedetti, P. & Kumar, S. (1986) Infinite dilution fugacity coefficients and the general behavior of dilute binary systems. *AIChE Journal,* **32** (8), 1253-1262.
Debenedetti, P. G. (1990) Homogeneous nucleation in supercritical fluids. *AIChE Journal,* **36** (9), 1289-1298.
Debenedetti, P. G., Lim, G.-B. & Prud'Homme, R. K. (2000) Preparation of protein microparticles by supercritical fluid precipitation. WO 1985000993 A1.
Debenedetti, P. G., Tom, J. W., Kwauk, X. & Yeo, S.-D. (1993) Rapid expansion of supercritical solutions (RESS): fundamentals and applications. *Fluid Phase Equilibria,* **82,** 311-321.
DiLauro, A. M., Abbaspourrad, A., Weitz, D. A. & Phillips, S. T. (2013) Stimuli-responsive core–shell microcapsules with tunable rates of release by using a depolymerizable poly (phthalaldehyde) membrane. *Macromolecules,* **46** (9), 3309-3313.
Discher, B. M., Won, Y.-Y., Ege, D. S., Lee, J. C., Bates, F. S., Discher, D. E. & Hammer, D. A. (1999) Polymersomes: tough vesicles made from diblock copolymers. *Science,* **284** (5417), 1143-1146.
Dixon, D. J., Johnston, K. P. & Bodmeier, R. A. (1993) Polymeric materials formed by precipitation with a compressed fluid antisolvent. *AIChE Journal,* **39** (1), 127-139.
Dokoumetzidis, A. & Macheras, P. (2006) A century of dissolution research: from Noyes and Whitney to the biopharmaceutics classification system. *International Journal of Pharmaceutics,* **321** (1), 1-11.
Domingo, C., Berends, E. & van Rosmalen, G. M. (1997) Precipitation of ultrafine organic crystals from the rapid expansion of supercritical solutions over a capillary and a frit nozzle. *The Journal of Supercritical Fluids,* **10** (1), 39-55.
Duncanson, W. J., Abbaspourrad, A., Shum, H. C., Kim, S.-H., Adams, L. L. & Weitz, D. A. (2012a) Monodisperse gas-filled microparticles from reactions in double emulsions. *Langmuir,* **28** (17), 6742-6745.
Duncanson, W. J., Arriaga, L. R., Ung, W. L., Kopechek, J. A., Porter, T. M. & Weitz, D. A. (2014) Microfluidic fabrication of perfluorohexane-shelled double emulsions for controlled loading and acoustic-triggered release of hydrophilic agents. *Langmuir,* **30** (46), 13765-13770.
Duncanson, W. J., Lin, T., Abate, A. R., Seiffert, S., Shah, R. K. & Weitz, D. A. (2012b) Microfluidic synthesis of advanced microparticles for encapsulation and controlled release. *Lab on a Chip,* **12** (12), 2135-2145.
Duncanson, W. J., Zieringer, M., Wagner, O., Wilking, J. N., Abbaspourrad, A., Haag, R. & Weitz, D. A. (2012c) Microfluidic synthesis of

monodisperse porous microspheres with size-tunable pores. *Soft Matter,* **8** (41), 10636-10640.
Edwards, L. (1951) The dissolution and diffusion of aspirin in aqueous media. *Transactions of the Faraday Society,* **47**, 1191-1210.
Efremov, E. V., Buijs, J. B., Gooijer, C. & Ariese, F. (2007) Fluorescence rejection in resonance Raman spectroscopy using a picosecond-gated intensified charge-coupled device camera. *Applied Spectroscopy,* **61** (6), 571-578.
Eriksson, L., Johansson, E. & Wikström, C. (1998) Mixture design—design generation, PLS analysis, and model usage. *Chemometrics and Intelligent Laboratory Systems,* **43** (1), 1-24.
Fages, J., Lochard, H., Letourneau, J.-J., Sauceau, M. & Rodier, E. (2004) Particle generation for pharmaceutical applications using supercritical fluid technology. *Powder Technology,* **141** (3), 219-226.
Fischer, W. & Muller, B. W. (1991) Method and apparatus for the manufacture of a product having a substance embedded in a carrier. US 5043280 A.
Fishburn, M. W. (2012) *Fundamentals of CMOS Single-Photon Avalanche Diodes*. Google Books Inc.
Florence, A. & Attwood, D. (2006) *Physicochemical Principles of Pharmacy*. Pharmaceutical Press, London.
Franklin, R. K., Edwards, J. R., Chernyak, Y., Gould, R. D., Henon, F. & Carbonell, R. G. (2001) Formation of perfluoropolyether coatings by the rapid expansion of supercritical solutions (RESS) process. Part 2: Numerical modeling. *Industrial & Engineering Chemistry Research,* **40** (26), 6127-6139.
Fraser, S. J., Oughton, J., Batten, W. A., Clark, A. S., Schmierer, D. M., Gordon, K. C. & Strachan, C. J. (2013) Simultaneous qualitative and quantitative analysis of counterfeit and unregistered medicines using Raman spectroscopy. *Journal of Raman Spectroscopy,* **44** (8), 1172-1180.
Freiberg, S. & Zhu, X. (2004) Polymer microspheres for controlled drug release. *International Journal of Pharmaceutics,* **282** (1), 1-18.
Gañán-Calvo, A. M. & Gordillo, J. M. (2001) Perfectly monodisperse microbubbling by capillary flow focusing. *Physical Review Letters,* **87** (27), 274501.
Gao, Z. (2009) In vitro dissolution testing with flow-through method: a technical note. *AAPS PharmSciTech,* **10** (4), 1401-1405.
Girotra, P., Singh, S. K. & Nagpal, K. (2013) Supercritical fluid technology: a promising approach in Pharmaceutical Research. *Pharmaceutical Development and Technology,* **18** (1), 22-38.
Golcuk, K., Mandair, G. S., Callender, A. F., Sahar, N., Kohn, D. H. & Morris, M. D. (2006) Is photobleaching necessary for Raman imaging of bone tissue using a green laser? *Biochimica et Biophysica Acta (BBA)-Biomembranes,* **1758** (7), 868-873.
Graser, F. & Wickenhaeuser, G. (1984) Conditioning of finely divided crude organic pigments. US 4451654 A.
Gupta, R. (2006) *Supercritical Fluid Technology for Particle Engineering*. Taylor & Francis Group, New York.
Gupta, R. B. & Kompella, U. B. (2006) *Nanoparticle Technology for Drug Delivery*. CRC Press.
Gupta, R. B. & Shim, J. J. (2006) *Solubility in Supercritical Carbon Dioxide*. Taylor & Francis, Florida.
Haaland, D. M. & Thomas, E. V. (1988) Partial least-squares methods for spectral analyses. 1. Relation to other quantitative calibration methods and the extraction of qualitative information. *Analytical Chemistry,* **60** (11), 1193-1202.

Hæggström, E., Yliruusi, J., Falk, K., Räikkönen, H., Pessi, J., Lassila, I. & Meriläinen, A. (2015) A method and a device for producing nanoparticles. WO 2016055696 A1.
Haleblian, J. & McCrone, W. (1969) Pharmaceutical applications of polymorphism. *Journal of Pharmaceutical Sciences,* **58** (8)**,** 911-929.
Hamlin, W., Nelson, E., Ballard, B. & Wagner, J. (1962) Loss of sensitivity in distinguishing real differences in dissolution rates due to increasing intensity of agitation. *Journal of Pharmaceutical Sciences,* **51** (5)**,** 432-435.
Hanna, M. & York, P. (1993) Methods and apparatus for the formation of particles. US 5851453.
Hanna, M. & York, P. (2000) Method and apparatus for the formation of particles. US 6063138 A.
Hannay, J. & Hogarth, J. (1879) On the solubility of solids in gases. *Proceedings of the Royal Society of London,* **30** (200-205)**,** 178-188.
Hargreaves, M. D., Macleod, N. A., Smith, M. R., Andrews, D., Hammond, S. V. & Matousek, P. (2011) Characterisation of transmission Raman spectroscopy for rapid quantitative analysis of intact multi-component pharmaceutical capsules. *Journal ofPharmaceutical and Biomedical Analysis,* **54** (3)**,** 463-468.
Healy, A., McCarthy, L., Gallagher, K. & Corrigan, O. (2002) Sensitivity of dissolution rate to location in the paddle dissolution apparatus. *Journal of Pharmacy and Pharmacology,* **54** (3)**,** 441-444.
Heinz, A., Savolainen, M., Rades, T. & Strachan, C. J. (2007) Quantifying ternary mixtures of different solid-state forms of indomethacin by Raman and near-infrared spectroscopy. *European Journal of Pharmaceutical Sciences,* **32** (3)**,** 182-192.
Helfgen, B., Hils, P., Holzknecht, C., Türk, M. & Schaber, K. (2001) Simulation of particle formation during the rapid expansion of supercritical solutions. *Journal of Aerosol Science,* **32** (3)**,** 295-319.
Helfgen, B., Türk, M. & Schaber, K. (2000) Theoretical and experimental investigations of the micronization of organic solids by rapid expansion of supercritical solutions. *Powder Technology,* **110** (1)**,** 22-28.
Helfgen, B., Türk, M. & Schaber, K. (2003) Hydrodynamic and aerosol modelling of the rapid expansion of supercritical solutions (RESS-process). *The Journal of Supercritical Fluids,* **26** (3)**,** 225-242.
Heng, D., Cutler, D. J., Chan, H.-K., Yun, J. & Raper, J. A. (2008) What is a suitable dissolution method for drug nanoparticles? *Pharmaceutical Research,* **25** (7)**,** 1696-1701.
Hennigan, M. C. & Ryder, A. G. (2013) Quantitative polymorph contaminant analysis in tablets using Raman and near infra-red spectroscopies. *Journal ofPharmaceutical and Biomedical Analysis,* **72,** 163-171.
Henriksen, I., Sande, S. A., Smistad, G., Ågren, T. & Karlsen, J. (1995) In vitro evaluation of drug release kinetics from liposomes by fractional dialysis. *International Journal of Pharmaceutics,* **119** (2)**,** 231-238.
Hermsdorf, D., Jauer, S. & Signorell, R. (2007) Formation and stabilization of ibuprofen nanoparticles by pulsed rapid expansion of supercritical solutions. *Molecular Physics,* **105** (8)**,** 951-959.
Herranz-Blanco, B., Arriaga, L. R., Mäkilä, E., Correia, A., Shrestha, N., Mirza, S., Weitz, D. A., Salonen, J., Hirvonen, J. & Santos, H. A. (2014) Microfluidic assembly of multistage porous silicon–lipid vesicles for controlled drug release. *Lab on a Chip,* **14** (6)**,** 1083-1086.
Hezave, A. Z., Aftab, S. & Esmaeilzadeh, F. (2010) Micronization of ketoprofen by the rapid expansion of supercritical solution process. *Journal of Aerosol Science,* **41** (8)**,** 821-833.

Hezave, A. Z. & Esmaeilzadeh, F. (2012) Precipitation of micronized piroxicam particles via RESS. *Journal of Dispersion Science and Technology,* **33** (7), 990-999.
Hirunsit, P., Huang, Z., Srinophakun, T., Charoenchaitrakool, M. & Kawi, S. (2005) Particle formation of ibuprofen–supercritical $CO_2$ system from rapid expansion of supercritical solutions (RESS): A mathematical model. *Powder Technology,* **154** (2), 83-94.
Hnaien, M., Ruffin, E., Bordes, C., Marcillat, O., Lagarde, F., Jaffrezic-Renault, N. & Briançon, S. (2011) Integrity characterization of myoglobin released from poly (ε-caprolactone) microspheres using two analytical methods: UV/Vis spectrometry and conductometric bi-enzymatic biosensor. *European Journal of Pharmaceutics and Biopharmaceutics,* **78** (2), 298-305.
Huang, J. & Moriyoshi, T. (2006) Fabrication of fine powders by RESS with a clearance nozzle. *The Journal of Supercritical Fluids,* **37** (3), 292-297.
Huang, Z., Guo, Y.-h., Miao, H. & Teng, L.-j. (2014) Solubility of progesterone in supercritical carbon dioxide and its micronization through RESS. *Powder Technology,* **258,** 66-77.
Huang, Z., Sun, G.-B., Chiew, Y. C. & Kawi, S. (2005) Formation of ultrafine aspirin particles through rapid expansion of supercritical solutions (RESS). *Powder Technology,* **160** (2), 127-134.
Iams, H. & Salzberg, B. (1935) The secondary emission phototube. *Proceedings of the Institute of Radio Engineers,* **23** (1), 55-64.
Jeong, J.-C., Lee, J. & Cho, K. (2003) Effects of crystalline microstructure on drug release behavior of poly (ε-caprolactone) microspheres. *Journal of Controlled Release,* **92** (3), 249-258.
Jestel, N. L. (2005) Process Raman spectroscopy. In Bakeev, K. A. (Ed.) *Process Analytical Technology Spectroscopic Tools and Implementation Strategies for the Chemical and Pharmaceutical Industries.* Oxford, Blackwell Publishing Ltd.
Johansson, J., Sparén, A., Svensson, O., Folestad, S. & Claybourn, M. (2007) Quantitative transmission Raman spectroscopy of pharmaceutical tablets and capsules. *Applied Spectroscopy,* **61** (11), 1211-1218.
Jung, J. & Perrut, M. (2001) Particle design using supercritical fluids: literature and patent survey. *The Journal of Supercritical Fluids,* **20** (3), 179-219.
Jünemann, D. & Dressman, J. (2012) Analytical methods for dissolution testing of nanosized drugs. *Journal of Pharmacy and Pharmacology,* **64** (7), 931-943.
Kabuss, J., Werner, S., Hoffmann, A., Hildebrandt, P., Knorr, A. & Richter, M. (2010) Theory of time-resolved Raman scattering and fluorescence emission from semiconductor quantum dots. *Physical Review B,* **81** (7), 075314 075311-075318.
Keshavarz, A., Karimi-Sabet, J., Fattahi, A., Golzary, A., Rafiee-Tehrani, M. & Dorkoosh, F. A. (2012) Preparation and characterization of raloxifene nanoparticles using rapid expansion of supercritical solution (RESS). *The Journal of Supercritical Fluids,* **63,** 169-179.
Keshmiri, K., Vatanara, A., Tavakoli, O. & Manafi, N. (2015) Production of ultrafine clobetasol propionate via rapid expansion of supercritical solution (RESS): Full factorial approach. *The Journal of Supercritical Fluids,* **101,** 176-183.
Khalil, I. & Miller, D. R. (2004) The structure of supercritical fluid free-jet expansions. *AIChE Journal,* **50** (11), 2697-2704.
Khapli, S. & Jagannathan, R. (2014) Supercritical $CO_2$ based processing of amorphous fluoropolymer Teflon-AF: Surfactant-free dispersions and

superhydrophobic films. *The Journal of Supercritical Fluids,* **85,** 49-56.
Kim, J.-T., Kim, H.-L. & Ju, C.-S. (2010) Micronization and characterization of drug substances by RESS with supercritical CO 2. *Korean Journal of Chemical Engineering,* **27** (4), 1139-1144.
Kim, S.-H., Kim, J. W., Cho, J.-C. & Weitz, D. A. (2011) Double-emulsion drops with ultra-thin shells for capsule templates. *Lab on a Chip,* **11** (18), 3162-3166.
Kim, S.-H., Kim, J. W., Kim, D. H., Han, S. H. & Weitz, D. A. (2013) Polymersomes containing a hydrogel network for high stability and controlled release. *Small,* **9** (1), 124-131.
Kim, S. H. & Weitz, D. A. (2011) One-Step Emulsification of Multiple Concentric Shells with Capillary Microfluidic Devices. *Angewandte Chemie International Edition,* **50** (37), 8731-8734.
Knez, Z. & Weidner, E. (2003) Particles formation and particle design using supercritical fluids. *Current Opinion in Solid State and Materials Science,* **7** (4), 353-361.
Kogermann, K., Aaltonen, J., Strachan, C. J., Pöllänen, K., Heinämäki, J., Yliruusi, J. & Rantanen, J. (2008) Establishing quantitative in-line analysis of multiple solid-state transformations during dehydration. *Journal of Pharmaceutical Sciences,* **97** (11), 4983-4999.
Kostamovaara, J., Tenhunen, J., Kögler, M., Nissinen, I., Nissinen, J. & Keränen, P. (2013) Fluorescence suppression in Raman spectroscopy using a time-gated CMOS SPAD. *Optics Express,* **21** (25), 31632-31645.
Krukonis, V. J., Gallagher, P. & Coffey, M. (1994) Gas anti-solvent recrystallization process. US 5360478 A.
Kudelski, A. (2008) Analytical applications of Raman spectroscopy. *Talanta,* **76** (1), 1-8.
Kuentz, M. (2015) Analytical technologies for real-time drug dissolution and precipitation testing on a small scale. *Journal of Pharmacy and Pharmacology,* **67** (2), 143-159.
Kwauk, X. & Debenedetti, P. G. (1993) Mathematical modeling of aerosol formation by rapid expansion of supercritical solutions in a converging nozzle. *Journal of Aerosol Science,* **24** (4), 445-469.
Lakowicz, J. R. (2007) Introduction to Fluorescence. *Principles of Fluorescence Spectroscopy*. Baltimore, Springer US.
Langer, R. (1998) Drug deliveryand targeting. *Nature,* **392** (6679), 5-10.
Lavrič, Z., Pirnat, J., Lužnik, J., Puc, U., Trontelj, Z. & Srčič, S. (2015) 14N Nuclear Quadrupole Resonance Study of Piroxicam: Confirmation of New Polymorphic Form V. *Journal of Pharmaceutical Sciences,* **104** (6), 1909-1918.
Lee, J. N., Park, C. & Whitesides, G. M. (2003) Solvent compatibility of poly (dimethylsiloxane)-based microfluidic devices. *Analytical Chemistry,* **75** (23), 6544-6554.
Lele, A. K. & Shine, A. D. (1992) Morphology of polymers precipitated from a supercritical solvent. *AIChE Journal,* **38** (5), 742-752.
Levy, G., Leonards, J. R. & Procknal, J. A. (1965) Development of in vitro dissolution tests which correlate quantitatively with dissolution rate-limited drug absorption in man. *Journal of Pharmaceutical Sciences,* **54** (12), 1719-1722.
Lieber, C. A. & Mahadevan-Jansen, A. (2003) Automated method for subtraction of fluorescence from biological Raman spectra. *Applied Spectroscopy,* **57** (11), 1363-1367.
Lipinski, C. (2002) Poor aqueous solubility—an industry wide problem in drug discovery. *American Pharmaceutical Review,* **5** (3), 82-85.

Liu, J., Amberg, G. & Do-Quang, M. (2014) Numerical simulation of particle formation in the rapid expansion of supercritical solution process. *The Journal of Supercritical Fluids*.
Liu, L., Yang, J.-P., Ju, X.-J., Xie, R., Yang, L., Liang, B. & Chu, L.-Y. (2009) Microfluidic preparation of monodisperse ethyl cellulose hollow microcapsules with non-toxic solvent. *Journal of Colloid and Interface Science,* **336** (1), 100-106.
Martens, H. & Naes, T. (1992) *Multivariate Calibration*. John Wiley & Sons.
Martín, A. & Cocero, M. J. (2008) Micronization processes with supercritical fluids: fundamentals and mechanisms. *Advanced Drug Delivery Reviews,* **60** (3), 339-350.
Maruyama, Y., Blacksberg, J. & Charbon, E. (2014) A 1024 x 8, 700-ps Time-Gated SPAD Line Sensor for Planetary Surface Exploration With Laser Raman Spectroscopy and LIBS. *IEEE Journal of Solid-state Circuits,* **49** (1), 179-189.
Matousek, P., Towrie, M., Ma, C., Kwok, W., Phillips, D., Toner, W. & Parker, A. (2001) Fluorescence suppression in resonance Raman spectroscopy using a high-performance picosecond Kerr gate. *Journal of Raman Spectroscopy,* **32** (12), 983-988.
Matousek, P., Towrie, M. & Parker, A. (2002) Fluorescence background suppression in Raman spectroscopy using combined Kerr gated and shifted excitation Raman difference techniques. *Journal of Raman Spectroscopy,* **33** (4), 238-242.
Matson, D. W., Petersen, R. C. & Smith, R. D. (1987) Production of powders and films by the rapid expansion of supercritical solutions. *Journal of Materials Science,* **22** (6), 1919-1928.
Matsuyama, K., Mishima, K., Umemoto, H. & Yamaguchi, S. (2001) Environmentally benign formation of polymeric microspheres by rapid expansion of supercritical carbon dioxide solution with a nonsolvent. *Environmental Science & Technology,* **35** (20), 4149-4155.
McCreery, R. L. (2005) Magnitude of Raman scattering. *Raman Spectroscopy for Chemical Analysis*. Wiley.
McHugh, M. A. & Krukonis, V. J. (1986) *Supercritical Fluid Extraction: Principles and Practice*. Butterworths.
Meister, B. J. & Scheele, G. F. (1969) Drop formation from cylindrical jets in immiscible liquid systems. *AIChE Journal,* **15** (5), 700-706.
Merisko-Liversidge, E., Liversidge, G. G. & Cooper, E. R. (2003) Nanosizing: a formulation approach for poorly-water-soluble compounds. *European Journal of Pharmaceutical Sciences,* **18** (2), 113-120.
Merisko-Liversidge, E. M. & Liversidge, G. G. (2008) Drug nanoparticles: formulating poorly water-soluble compounds. *Toxicologic Pathology,* **36** (1), 43-48.
Meziani, M., Pathak, P. & Sun, Y. P. (2008) Supercritical Fluid Technology for Nanotechnology in Drug Delivery. In de Villiers, M., Aramwit, P. & Kwon, G. (Eds.) *Nanotechnology in Drug Delivery*. New York, Springer.
Michalowski, C., Guterres, S. & Dalla Costa, T. (2004) Microdialysis for evaluating the entrapment and release of a lipophilic drug from nanoparticles. *Journal of Pharmaceutical and Biomedical Analysis,* **35** (5), 1093-1100.
Mitsana-Papazoglou, A., Christopoulos, T. K., Diamandis, E. P. & Koupparis, M. A. (1987) Dissolution studies of drug formulations using ion-selective electrodes as sensors in an air-segmented continuous flow analyzer. *Journal of Pharmaceutical Sciences,* **76** (9), 724-730.

Modi, S. & Anderson, B. D. (2013) Determination of drug release kinetics from nanoparticles: overcoming pitfalls of the dynamic dialysis method. *Molecular Pharmaceutics,* **10** (8), 3076-3089.
Montes, A., Bendel, A., Kürti, R., Gordillo, M., Pereyra, C. & Martínez de la Ossa, E. (2013) Processing naproxen with supercritical $CO_2$. *The Journal of Supercritical Fluids,* **75,** 21-29.
Moreno-Bautista, G. & Tam, K. C. (2011) Evaluation of dialysis membrane process for quantifying the in vitro drug-release from colloidal drug carriers. *Colloids and Surfaces A: Physicochemical and Engineering Aspects,* **389** (1), 299-303.
Moribe, K., Tozuka, Y. & Yamamoto, K. (2008) Supercritical carbon dioxide processing of active pharmaceutical ingredients for polymorphic control and for complex formation. *Advanced Drug Delivery Reviews,* **60** (3), 328-338.
Morihara, M., Aoyagi, N., Kaniwa, N., Katori, N. & Kojim, S. (2002) Hydrodynamic flows around tablets in different pharmacopeial dissolution tests. *Drug Development and Industrial Pharmacy,* **28** (6), 655-662.
Mosconi, D., Stoppa, D., Pancheri, L., Gonzo, L. & Simoni, A. (2006) CMOS single-photon avalanche diode array for time-resolved fluorescence detection. *ESSCIRC 2006*. IEEE.
Moussa, A. B. & Ksibi, H. (2010) A review of numerical investigations regarding the supercritical fluid expansion in the RESS process. *International Journal of Emerging Multidisciplinary Fluid Sciences,* **2** (1), 45-58.
Moussa, A. B., Ksibi, H. & Baccar, M. (2008) Simulation of particles transport and coagulation during the RESS process. *The European Physical Journal Applied Physics,* **43** (2), 253-261.
Müllers, K. C., Paisana, M. & Wahl, M. A. (2015) Simultaneous formation and micronization of pharmaceutical cocrystals by rapid expansion of supercritical solutions (RESS). *Pharmaceutical Research,* **32** (2), 702-713.
Nabavi, S. A., Vladisavljević, G. T., Gu, S. & Ekanem, E. E. (2015) Double emulsion production in glass capillary microfluidic device: Parametric investigation of droplet generation behaviour. *Chemical Engineering Science,* **130,** 183-196.
Naelapää, K., van de Streek, J., Rantanen, J. & Bond, A. D. (2012) Complementing high-throughput X-ray powder diffraction data with quantum–chemical calculations: Application to piroxicam form III. *Journal of Pharmaceutical Sciences,* **101** (11), 4214-4219.
Natarajan, V., Krithica, N., Madhan, B. & Sehgal, P. K. (2011) Formulation and evaluation of quercetin polycaprolactone microspheres for the treatment of rheumatoid arthritis. *Journal of Pharmaceutical Sciences,* **100** (1), 195-205.
Nelson, E. (1957) Solution rate of theophylline salts and effects from oral administration. *Journal of Pharmaceutical Sciences,* **46** (10), 607-614.
Nernst, W. (1904) Theorie der Reaktionsgeschwindigkeit in heterogenen Systemen. *Zeitschrift für Physikalische Chemie, Stöchiometrie und Verwandtschaftslehre,* **47,** 52-55.
Nicklasson, M., Orbe, A., Lindberg, J., Borgå, B., Magnusson, A.-B., Nilsson, G., Ahlgren, R. & Jacobsen, L. (1991) A collaborative study of the in vitro dissolution of phenacetin crystals comparing the flow through method with the USP Paddle method. *International Journal of Pharmaceutics,* **69** (3), 255-264.
Nissinen, I., Nissinen, J., Keränen, P. & Kostamovaara, J. (2017) On the effects of the time gate position and width on the signal-to-noise ratio for

detection of Raman spectrum in a time-gated CMOS single-photon avalanche diode based sensor. *Sensors and Actuators B: Chemical,* **241,** 1145-1152.
Nissinen, I., Nissinen, J., Keränen, P., Länsman, A.-K., Holma, J. & Kostamovaara, J. (2015) A 2 x (4) x 128 Multitime-Gated SPAD Line Detector for Pulsed Raman Spectroscopy. *IEEE Sensors Journal,* **15** (3)**,** 1358-1365.
Noyes, A. A. & Whitney, W. R. (1897) The rate of solution of solid substances in their own solutions. *Journal of the American Chemical Society,* **19** (12)**,** 930-934.
Paisana, M. C., Müllers, K. C., Wahl, M. A. & Pinto, J. F. (2016) Production and stabilization of olanzapine nanoparticles by rapid expansion of supercritical solutions (RESS). *The Journal of Supercritical Fluids,* **109,** 124-133.
Palakodaty, S. & York, P. (1999) Phase behavioral effects on particle formation processes using supercritical fluids. *Pharmaceutical Research,* **16** (7)**,** 976-985.
Panza, J. & Beckman, E. (2004) Chemistry and Material Design for $CO_2$. In P., Y., U., K. & Shekunov, B. (Eds.) *Supercritical fluid Technology for Drug Product Development*. New York, Taylor & Francis Group.
Pasquali, I., Bettini, R. & Giordano, F. (2008) Supercritical fluid technologies: an innovative approach for manipulating the solid-state of pharmaceuticals. *Advanced Drug Delivery Reviews,* **60** (3)**,** 399-410.
Pathak, P., Meziani, M. J., Desai, T. & Sun, Y.-P. (2004) Nanosizing drug particles in supercritical fluid processing. *Journal of the American Chemical Society,* **126** (35)**,** 10842-10843.
Pathak, P., Meziani, M. J., Desai, T. & Sun, Y.-P. (2006) Formation and stabilization of ibuprofen nanoparticles in supercritical fluid processing. *The Journal of Supercritical Fluids,* **37** (3)**,** 279-286.
Pathak, P., Prasad, G. L., Meziani, M. J., Joudeh, A. A. & Sun, Y.-P. (2007) Nanosized paclitaxel particles from supercritical carbon dioxide processing and their biological evaluation. *Langmuir,* **23** (5)**,** 2674-2679.
Patounakis, G., Shepard, K. L. & Levicky, R. (2006) Active CMOS array sensor for time-resolved fluorescence detection. *IEEE Journal of Solid-state Circuits,* **41** (11)**,** 2521-2530.
Pearson, K. (1901) LIII. On lines and planes of closest fit to systems of points in space. *The London, Edinburgh, and Dublin Philosophical Magazine and Journal of Science,* **2** (11)**,** 559-572.
Pelletier, M. (2003) Quantitative analysis using Raman spectrometry. *Applied Spectroscopy,* **57** (1)**,** 20-42.
Peng, D.-Y. & Robinson, D. B. (1976) A new two-constant equation of state. *Industrial & Engineering Chemistry Fundamentals,* **15** (1)**,** 59-64.
Pereda, S., Bottini, S. & Brignole, E. (2008) *Fundamentals of Supercritical Fluid Technology*. Taylor & Francis Group, New York.
Pernarowski, M., Woo, W. & Searl, R. (1968) Continuous flow apparatus for the determination of the dissolution characteristics of tablets and capsules. *Journal of Pharmaceutical Sciences,* **57** (8)**,** 1419-1421.
Peschka, R., Dennehy, C. & Szoka Jr, F. C. (1998) A simple in vitro model to study the release kinetics of liposome encapsulated material. *Journal of Controlled Release,* **56** (1)**,** 41-51.
Ph.Eur. (2015) 4.01.03 Buffer solutions. *Eur. Pharmacopoeia Online 8.8. Available at:* http://online6.edqm.eu/ep808/ *[Accessed August 16th, 2016].*
Pillay, V. & Fassihi, R. (1999) Unconventional dissolution methodologies. *Journal of Pharmaceutical Sciences,* **88** (9)**,** 843-851.

Pitt, C. G. (1990) Poly-ε-Caprolactone and Its Copolymers. In Chasin M. & Langer M. (Eds.) *Biodegradable Polymers as Drug Delivery Systems.* Marcel Dekker, New York.
Pitt, G., Batchelder, D., Bennett, R., Bormett, R., Hayward, I., Smith, B., Williams, K., Yang, Y., Baldwin, K. & Webster, S. (2005) Engineering aspects and applications of the new Raman instrumentation. *IEE Proceedings-Science, Measurement and Technology,* **152** (6)**,** 241-318.
Plateau, J. A. F. (1873) *Statique Expérimentale et Théorique des Liquides Soumis aux Seules Forces Moléculaires*. Gauthier-Villars.
Poliakoff, M. & King, P. (2001) Phenomenal fluids. *Nature,* **412** (6843)**,** 125-125.
Pourasghar, M., Fatemi, S., Vatanara, A. & Najafabadi, A. R. (2012) Production of ultrafine drug particles through rapid expansion of supercritical solution; a statistical approach. *Powder Technology,* **225,** 21-26.
Powers, T. R., Zhang, D., Goldstein, R. E. & Stone, H. A. (1998) Propagation of a topological transition: The Rayleigh instability. *Physics of Fluids (1994-present),* **10** (5)**,** 1052-1057.
Pratiwi, D., Fawcett, J. P., Gordon, K. C. & Rades, T. (2002) Quantitative analysis of polymorphic mixtures of ranitidine hydrochloride by Raman spectroscopy and principal components analysis. *European Journal of Pharmaceutics and Biopharmaceutics,* **54** (3)**,** 337-341.
Pratsinis, S. E. (1988) Simultaneous nucleation, condensation, and coagulation in aerosol reactors. *Journal of Colloid and Interface Science,* **124** (2)**,** 416-427.
Qureshi, S. A. & Shabnam, J. (2001) Cause of high variability in drug dissolution testing and its impact on setting tolerances. *European Journal of Pharmaceutical Sciences,* **12** (3)**,** 271-276.
Raman, C. V. & Krishnan, K. S. (1928) A new type of secondary radiation. *Nature,* **121,** 501-502.
Rantanen, J., Wikström, H., Rhea, F. E. & Taylor, L. S. (2005) Improved understanding of factors contributing to quantification of anhydrate/hydrate powder mixtures. *Applied Spectroscopy,* **59** (7)**,** 942-951.
Rayleigh, L. (1879) On the capillary phenomena of jets. *Proceedings of the Royal Society of London,* **29,** 71-97.
Redenti, E., Zanol, M., Ventura, P., Fronza, G., Comotti, A., Taddei, P. & Bertoluzza, A. (1999) Raman and solid state 13C-NMR investigation of the structure of the 1: 1 amorphous piroxicam: β-cyclodextrin inclusion compound. *Biospectroscopy,* **5** (4)**,** 243-251.
Reverchon, E. (2002) Supercritical-assisted atomization to produce micro- and/or nanoparticles of controlled size and distribution. *Industrial & Engineering Chemistry Research,* **41** (10)**,** 2405-2411.
Reverchon, E. & Adami, R. (2006) Nanomaterials and supercritical fluids. *The Journal of Supercritical Fluids,* **37** (1)**,** 1-22.
Reverchon, E. & Della Porta, G. (2014) Continuous process for microspheres production by using expanded fluids. US 8628802 B2 / WO 2009016677 A2.
Reverchon, E. & Pallado, P. (1996) Hydrodynamic modeling of the RESS process. *The Journal of Supercritical Fluids,* **9** (4)**,** 216-221.
Rochas, A., Gani, M., Furrer, B., Besse, P., Popovic, R., Ribordy, G. & Gisin, N. (2003) Single photon detector fabricated in a complementary metal–oxide–semiconductor high-voltage technology. *Review of Scientific Instruments,* **74** (7)**,** 3263-3270.
Rojalin, T., Kurki, L., Laaksonen, T., Viitala, T., Kostamovaara, J., Gordon, K. C., Galvis, L., Wachsmann-Hogiu, S., Strachan, C. J. & Yliperttula, M. (2016) Fluorescence-suppressed time-resolved Raman spectroscopy of

pharmaceuticals using complementary metal-oxide semiconductor (CMOS) single-photon avalanche diode (SPAD) detector. *Analytical and bioAnalytical Chemistry,* **408** (3), 761-774.
Sabet, J. K., Ghotbi, C. & Dorkoosh, F. (2012) Application of response surface methodology for optimization of paracetamol particles formation by RESS method. *Journal of Nanomaterials,* **2012,** 43.
Saeki, D., Sugiura, S., Kanamori, T., Sato, S. & Ichikawa, S. (2010) Microfluidic preparation of water-in-oil-in-water emulsions with an ultra-thin oil phase layer. *Lab on a Chip,* **10** (3), 357-362.
Samei, M., Vatanara, A., Fatemi, S. & Najafabadi, A. R. (2012) Process variables in the formation of nanoparticles of megestrol acetate through rapid expansion of supercritical CO 2. *The Journal of Supercritical Fluids,* **70,** 1-7.
Sarnes, A., Østergaard, J., Jensen, S. S., Aaltonen, J., Rantanen, J., Hirvonen, J. & Peltonen, L. (2013) Dissolution study of nanocrystal powders of a poorly soluble drug by UV imaging and channel flow methods. *European Journal of Pharmaceutical Sciences,* **50** (3), 511-519.
Scala-Bertola, J., Javot, L., Camargo, J., Bonneaux, F., Lecompte, T., Maincent, P. & Sapin, A. (2012) Evaluation of subcutaneous forms in the improvement of pharmacokinetic profile of warfarin. *International Journal of Pharmaceutics,* **431** (1), 33-38.
Scheele, G. F. & Meister, B. J. (1968) Drop formation at low velocities in liquid-liquid systems: Part I. Prediction of drop volume. *AIChE Journal,* **14** (1), 9-15.
Schwartz, D. E., Charbon, E. & Shepard, K. L. (2007) A single-photon avalanche diode imager for fluorescence lifetime applications. *VLSI Circuits, 2007 IEEE Symposium on* IEEE.
Shah, R. K., Shum, H. C., Rowat, A. C., Lee, D., Agresti, J. J., Utada, A. S., Chu, L.-Y., Kim, J.-W., Fernandez-Nieves, A. & Martinez, C. J. (2008) Designer emulsions using microfluidics. *Materials Today,* **11** (4), 18-27.
Sharma, S. K. & Jagannathan, R. (2016) High throughput RESS processing of sub-10nm ibuprofen nanoparticles. *The Journal of Supercritical Fluids,* **109,** 74-79.
Shaw, L. R., Irwin, W. J., Grattan, T. J. & Conway, B. R. (2002) The development of a modified dissolution method suitable for investigating powder mixtures. *Drug Development and Industrial Pharmacy,* **28** (9), 1147-1153.
Shen, J. & Burgess, D. J. (2013) In vitro dissolution testing strategies for nanoparticulate drug delivery systems: recent developments and challenges. *Drug Delivery and Translational Research,* **3** (5), 409-415.
Sheng, J. J., Sirois, P. J., Dressman, J. B. & Amidon, G. L. (2008) Particle diffusional layer thickness in a USP dissolution apparatus II: a combined function of particle size and paddle speed. *Journal of Pharmaceutical Sciences,* **97** (11), 4815-4829.
Sheth, A. R., Bates, S., Muller, F. X. & Grant, D. J. (2004) Polymorphism in piroxicam. *Crystal Growth & Design,* **4** (6), 1091-1098.
Shi, X., El Hassan, N., Ikni, A., Li, W., Guiblin, N., de-Biré, A. S. & Ghermani, N. (2016) Experimental electron densities of neutral and zwitterionic forms of the drug piroxicam. *CrystEngComm,* **18** (18), 3289-3299.
Shimpi, S. L., Chauhan, B., Mahadik, K. & Paradkar, A. (2005) Stabilization and improved in vivo performance of amorphous etoricoxib using Gelucire 50/13. *Pharmaceutical Research,* **22** (10), 1727-1734.
Shreve, A. P., Cherepy, N. J. & Mathies, R. A. (1992) Effective rejection of fluorescence interference in Raman spectroscopy using a shifted excitation difference technique. *Applied Spectroscopy,* **46** (4), 707-711.

Shum, H. C., Zhao, Y. j., Kim, S. H. & Weitz, D. A. (2011) Multicompartment polymersomes from double emulsions. *Angewandte Chemie,* **123** (7), 1686-1689.
Sievers, R., Huang, E., Villa, J., Engling, G. & Brauer, P. (2003) Micronization of water-soluble or alcohol-soluble pharmaceuticals and model compounds with a low-temperature Bubble Dryer®. *The Journal of Supercritical Fluids,* **26** (1), 9-16.
Sievers, R. E. & Karst, U. (1997) Methods for fine particle formation. US 5639441 A.
Siewert, M., Dressman, J., Brown, C. K., Shah, V. P., Aiache, J.-M., Aoyagi, N., Bashaw, D., Brown, C., Brown, W. & Burgess, D. (2003) FIP/AAPS guidelines to dissolution/in vitro release testing of novel/special dosage forms. *AAPS PharmSciTech,* **4** (1), 43-52.
Siewert, M., Weinandy, L., Whiteman, D. & Judkins, C. (2002) Typical variability and evaluation of sources of variability in drug dissolution testing. *European Journal of Pharmaceutics and Biopharmaceutics,* **53** (1), 9-14.
Smekal, A. (1923) Zur quantentheorie der dispersion. *Naturwissenschaften,* **11** (43), 873-875.
Smith, E. & Dent, G. (2013) *Modern Raman Spectroscopy: A Practical Approach*. Wiley.
Smith, R., Inomata, H. & Peters, C. (2013) *Introduction to Supercritical Fluids: A Spreadsheet-based Approach*. Elsevier, Amsterdam.
Smith, R. & Wash, R. (1986) Supercritical fluid molecular spray film deposition and powder formation. US 4582731.
Somavarapu, S., Pandit, S., Gradassi, G., Bandera, M., Ravichandran, E. & Alpar, O. H. (2005) Effect of vitamin E TPGS on immune response to nasally delivered diphtheria toxoid loaded poly (caprolactone) microparticles. *International Journal of Pharmaceutics,* **298** (2), 344-347.
Span, R. & Wagner, W. (1996) A new equation of state for carbon dioxide covering the fluid region from the triple-point temperature to 1100 K at pressures up to 800 MPa. *Journal of physical and chemical reference data,* **25** (6), 1509-1596.
Springer, G. S. (1978) Homogeneous nucleation. *Advances in Heat Transfer,* **14**, 281-346.
Squires, T. M. & Quake, S. R. (2005) Microfluidics: Fluid physics at the nanoliter scale. *Reviews of Modern Physics,* 77 (3), 977.
Stoppa, D., Mosconi, D., Pancheri, L. & Gonzo, L. (2009) Single-photon avalanche diode CMOS sensor for time-resolved fluorescence measurements. *IEEE Sensors Journal,* **9** (9), 1084-1090.
Stoppa, D., Pancheri, L., Scandiuzzo, M., Gonzo, L., Dalla Betta, G.-F. & Simoni, A. (2007) A CMOS 3-D imager based on single photon avalanche diode. *IEEE Transactions on Circuits and Systems I: Regular Papers,* **54** (1), 4-12.
Strachan, C. J., Pratiwi, D., Gordon, K. C. & Rades, T. (2004) Quantitative analysis of polymorphic mixtures of carbamazepine by Raman spectroscopy and principal components analysis. *Journal of Raman Spectroscopy,* **35** (5), 347-352.
Strachan, C. J., Rades, T., Gordon, K. C. & Rantanen, J. (2007) Raman spectroscopy for quantitative analysis of pharmaceutical solids. *Journal of Pharmacy and Pharmacology,* **59** (2), 179-192.
Sun, Y. P. (2002) *Supercritical Fluid Technology in Materials Science and Engineering*. Marcel Dekker, Inc, New York.
Suresh, S., Gunasekaran, S. & Srinivasan, S. (2015) Vibrational spectra (FT-IR, FT-Raman), frontier molecular orbital, first hyperpolarizability,

NBO analysis and thermodynamics properties of Piroxicam by HF and DFT methods. *Spectrochimica Acta Part A: Molecular and Biomolecular Spectroscopy,* **138,** 447-459.
Taylor, L. S. & Langkilde, F. W. (2000) Evaluation of solid-state forms present in tablets by Raman spectroscopy. *Journal of Pharmaceutical Sciences,* **89** (10), 1342-1353.
Thakur, R. & Gupta, R. B. (2005) Rapid expansion of supercritical solution with solid cosolvent (RESS–SC) process: formation of griseofulvin nanoparticles. *Industrial & Engineering Chemistry Research,* **44** (19), 7380-7387.
Thakur, R. & Gupta, R. B. (2006) Formation of phenytoin nanoparticles using rapid expansion of supercritical solution with solid cosolvent (RESS-SC) process. *International Journal of Pharmaceutics,* **308** (1), 190-199.
Thomas, L. H., Wales, C. & Wilson, C. C. (2016) Selective preparation of elusive and alternative single component polymorphic solid forms through multi-component crystallisation routes. *Chemical Communications,* **52** (46), 7372-7375.
Thomson, W. (1871) LX. On the equilibrium of vapour at a curved surface of liquid. *The London, Edinburgh, and Dublin Philosophical Magazine and Journal of Science,* **42** (282), 448-452.
Tian, F., Zhang, F., Sandler, N., Gordon, K., McGoverin, C., Strachan, C., Saville, D. & Rades, T. (2007) Influence of sample characteristics on quantification of carbamazepine hydrate formation by X-ray powder diffraction and Raman spectroscopy. *European Journal of Pharmaceutics and Biopharmaceutics,* **66** (3), 466-474.
Tom, J. W. & Debenedetti, P. G. (1991) Particle formation with supercritical fluids—a review. *Journal of Aerosol Science,* **22** (5), 555-584.
Tyler, E. (1933) XL. Instability of liquid jets. *The London, Edinburgh, and Dublin Philosophical Magazine and Journal of Science,* **16** (105), 504-518.
Türk, M. (1999) Formation of small organic particles by RESS: experimental and theoretical investigations. *The Journal of Supercritical Fluids,* **15** (1), 79-89.
Türk, M. (2000) Influence of thermodynamic behaviour and solute properties on homogeneous nucleation in supercritical solutions. *The Journal of Supercritical Fluids,* **18** (3), 169-184.
Türk, M. (2014) *Particle Formation with Supercritical Fluids: Challenges and Limitations*. Elsevier, Amsterdam.
Türk, M. & Bolten, D. (2010) Formation of submicron poorly water-soluble drugs by rapid expansion of supercritical solution (RESS): results for naproxen. *The Journal of Supercritical Fluids,* **55** (2), 778-785.
Türk, M., Hils, P., Helfgen, B., Schaber, K., Martin, H.-J. & Wahl, M. A. (2002) Micronization of pharmaceutical substances by the rapid expansion of supercritical solutions (RESS): a promising method to improve bioavailability of poorly soluble pharmaceutical agents. *The Journal of Supercritical Fluids,* **22** (1), 75-84.
Türk, M. & Lietzow, R. (2008) Formation and stabilization of submicron particles via rapid expansion processes. *The Journal of Supercritical Fluids,* **45** (3), 346-355.
Uchida, H., Nishijima, M., Sano, K., Demoto, K., Sakabe, J. & Shimoyama, Y. (2015) Production of theophylline nanoparticles using rapid expansion of supercritical solutions with a solid cosolvent (RESS-SC) technique. *The Journal of Supercritical Fluids,* **105,** 128-135.

Umbanhowar, P., Prasad, V. & Weitz, D. (2000) Monodisperse emulsion generation via drop break off in a coflowing stream. *Langmuir,* **16** (2), 347-351.
Underwood, F. L. & Cadwallader, D. E. (1976) Effects of various hydrodynamic conditions on dissolution rate determinations. *Journal of Pharmaceutical Sciences,* **65** (5), 697-700.
Upadhyay, P. P. & Bond, A. D. (2015) Crystallization and disorder of the polytypic α1 and α2 polymorphs of piroxicam. *CrystEngComm,* **17** (28), 5266-5272.
USP (2015) United States Pharmacopoeia XXIV Pharmacopoeia XXIV. *US Pharmacopeia Convention, Inc., Rockville*.
Utada, A., Chu, L.-Y., Fernandez-Nieves, A., Link, D., Holtze, C. & Weitz, D. (2007a) Dripping, jetting, drops, and wetting: the magic of microfluidics. *Mrs Bulletin,* **32** (09), 702-708.
Utada, A., Lorenceau, E., Link, D., Kaplan, P., Stone, H. & Weitz, D. (2005) Monodisperse double emulsions generated from a microcapillary device. *Science,* **308** (5721), 537-541.
Utada, A. S., Fernandez-Nieves, A., Stone, H. A. & Weitz, D. A. (2007b) Dripping to jetting transitions in coflowing liquid streams. *Physical Review Letters,* **99** (9), 094502.
Valizadeh, H., Nokhodchi, A., Qarakhani, N., Zakeri-Milani, P., Azarmi, S., Hassanzadeh, D. & Löbenberg, R. (2004) Physicochemical characterization of solid dispersions of indomethacin with PEG 6000, Myrj 52, lactose, sorbitol, dextrin, and Eudragit® E100. *Drug Development and Industrial Pharmacy,* **30** (3), 303-317.
Wallace, S. J., Li, J., Nation, R. L. & Boyd, B. J. (2012) Drug release from nanomedicines: selection of appropriate encapsulation and release methodology. *Drug Delivery and Translational Research,* **2** (4), 284-292.
Van Duyne, R. P., Jeanmaire, D. L. & Shriver, D. (1974) Mode-locked Laser Raman spectroscopy—A new technique for the rejection of interfering background luminescence signals. *Analytical Chemistry,* **46** (2), 213-222.
Wang, W., Xie, R., Ju, X.-J., Luo, T., Liu, L., Weitz, D. A. & Chu, L.-Y. (2011) Controllable microfluidic production of multicomponent multiple emulsions. *Lab on a Chip,* **11** (9), 1587-1592.
Wang, W., Zhang, M.-J. & Chu, L.-Y. (2014) Microfluidic approach for encapsulation via double emulsions. *Current Opinion in Pharmacology,* **18,** 35-41.
Wartewig, S. & Neubert, R. H. (2005) Pharmaceutical applications of Mid-IR and Raman spectroscopy. *Advanced Drug Delivery Reviews,* **57** (8), 1144-1170.
Washington, C. (1990) Drug release from microdisperse systems: a critical review. *International Journal of Pharmaceutics,* **58** (1), 1-12.
Weber, M., Russell, L. M. & Debenedetti, P. G. (2002) Mathematical modeling of nucleation and growth of particles formed by the rapid expansion of a supercritical solution under subsonic conditions. *The Journal of Supercritical Fluids,* **23** (1), 65-80.
Weber, M. & Thies, M. C. (2007) A simplified and generalized model for the rapid expansion of supercritical solutions. *The Journal of Supercritical Fluids,* **40** (3), 402-419.
Wennergren, B., Lindberg, J., Nicklasson, M., Nilsson, G., Nyberg, G., Ahlgren, R., Persson, C. & Palm, B. (1989) A collaborative in vitro dissolution study: comparing the flow-through method with the USP paddle method using USP prednisone calibrator tablets. *International Journal of Pharmaceutics,* **53** (1), 35-41.

Ventosa, N., Sala, S., Veciana, J., Torres, J. & Llibre, J. (2001) Depressurization of an expanded liquid organic solution (DELOS): a new procedure for obtaining submicron-or micron-sized crystalline particles. *Crystal Growth & Design,* **1** (4), 299-303.
Whitesides, G. M. & Stroock, A. D. (2001) Flexible methods for microfluidics. *Phys. Today,* **54** (6), 42-48.
Vippagunta, S. R., Brittain, H. G. & Grant, D. J. (2001) Crystalline solids. *Advanced Drug Delivery Reviews,* **48** (1), 3-26.
Vladisavljevic´, G. T., Duncanson, W. J., Shum, H. C. & Weitz, D. A. (2012) Emulsion templating of poly (lactic acid) particles: droplet formation behavior. *Langmuir,* **28** (36), 12948-12954.
Vladisavljević, G. T., Shahmohamadi, H., Das, D. B., Ekanem, E. E., Tauanov, Z. & Sharma, L. (2014) Glass capillary microfluidics for production of monodispersed poly (DL-lactic acid) and polycaprolactone microparticles: Experiments and numerical simulations. *Journal of Colloid and Interface Science,* **418,** 163-170.
Wold, S. & Sjöström, M. (1977) SIMCA: a Method for Analyzing Chemical Data in Terms of Similarity and Analogy. ACS Publications.
von Helmholtz, R. (1886) Untersuchungen über Dämpfe und Nebel, besonders über solche von Lösungen. *Annalen der Physik,* **263** (4), 508-543.
Vrečer, F., Vrbinc, M. & Meden, A. (2003) Characterization of piroxicam crystal modifications. *International Journal of Pharmaceutics,* **256** (1), 3-15.
Xia, Y. & Whitesides, G. M. (1998) Soft lithography. *Annual Review of Materials Science,* **28** (1), 153-184.
Xie, L., Beyer, S., Vogel, V., Wacker, M. G. & Mäntele, W. (2015) Assessing the drug release from nanoparticles: Overcoming the shortcomings of dialysis by using novel optical techniques and a mathematical model. *International Journal of Pharmaceutics,* **488** (1), 108-119.
Xie, Y., Tao, W., Morrison, H., Chiu, R., Jona, J., Fang, J. & Cauchon, N. (2008) Quantitative determination of solid-state forms of a pharmaceutical development compound in drug substance and tablets. *International Journal of Pharmaceutics,* **362** (1), 29-36.
Xu, X., Khan, M. A. & Burgess, D. J. (2012) A two-stage reverse dialysis in vitro dissolution testing method for passive targeted liposomes. *International Journal of Pharmaceutics,* **426** (1), 211-218.
Yamamoto, S. & Furusawa, T. (2015) Thermophysical flow simulations of rapid expansion of supercritical solutions (RESS). *The Journal of Supercritical Fluids,* **97,** 192-201.
Yasuji, T., Takeuchi, H. & Kawashima, Y. (2008) Particle design of poorly water-soluble drug substances using supercritical fluid technologies. *Advanced Drug Delivery Reviews,* **60** (3), 388-398.
Yeo, S.-D. & Kiran, E. (2005) Formation of polymer particles with supercritical fluids: a review. *The Journal of Supercritical Fluids,* **34** (3), 287-308.
York, P. (1999) Strategies for particle design using supercritical fluid technologies. *Pharmaceutical Science & Technology Today,* **2** (11), 430-440.
Young, T. J., Mawson, S., Johnston, K. P., Henriksen, I. B., Pace, G. W. & Mishra, A. K. (2000) Rapid Expansion from Supercritical to Aqueous Solution to Produce Submicron Suspensions of Water-Insoluble Drugs. *Biotechnology Progress,* **16** (3), 402-407.
Zabihi, F., Akbarnejad, M. M., Vaziri Yazdi, A., Arjomand, M. & Safekordi, A. A. (2011) Drug nano-particles formation by supercritical rapid expansion method; Operational condition effects investigation. *Iranian Journal of Chemistry and Chemical Engineering,* **30** (1), 7-15.

Zambito, Y., Pedreschi, E. & Di Colo, G. (2012) Is dialysis a reliable method for studying drug release from nanoparticulate systems?—A case study. *International Journal of Pharmaceutics,* **434** (1), 28-34.
Zhang, G., Vadino, W., Yang, T., Cho, W. & Chaudry, I. (1994) Evaluation of the flow-through cell dissolution apparatus: effects of flow rate, glass beads and tablet position on drug release from different type of tablets. *Drug Development and Industrial Pharmacy,* **20** (13), 2063-2078.
Zhang, Y. & Liu, H. (2012) Physics of Multiphase Microflows and Microdroplets. In Day, P., Manz, A. & Zhang, Y. (Eds.) *Microdroplet Technology: Principles and Emerging Applications in Biology and Chemistry*. New York, Springer.
Zhao, C.-X., Chen, D., Hui, Y., Weitz, D. A. & Middelberg, A. P. (2017) Controlled generation of ultra-thin-shell double emulsions and their stability study. *ChemPhysChem*. **18**, 1-8.
Zhao, Y., Shum, H. C., Chen, H., Adams, L. L., Gu, Z. & Weitz, D. A. (2011) Microfluidic generation of multifunctional quantum dot barcode particles. *Journal of the American Chemical Society,* **133** (23), 8790-8793.
Zhou, X. H. (1994) Overcoming enzymatic and absorption barriers to non-parenterally administered protein and peptide drugs. *Journal of Controlled Release,* **29** (3), 239-252.